Thermodynamics of water adsorption in model structured molecular systems including analogues of hemicelluloses, crystalline cellulose and lignin

Aurelio Barbetta

THÈSE POUR OBTENIR LE GRADE DE DOCTEUR DE L'UNIVERSITÉ DE MONTPELLIER

En Chimie et Physico-Chimie des Matériaux

École doctorale Sciences Chimiques Balard - ED 459

Unité de recherche UMR 5257 - ICSM - Institut de Chimie Séparative de Marcoule

Thermodynamics of water adsorption in model structured molecular systems including analogues of hemicelluloses, crystalline cellulose and lignin

Présentée par Aurelio BARBETTA

Le 20 Novembre 2017

Sous la direction de Thomas ZEMB et Helmuth MÖHWALD

Devant le jury composé de

M. Thomas ZEMB, Professeur, ICSM Marcoule	Directeur de these
M. Helmuth MÖHWALD, Professeur, Max Planck Institute of Colloids and Interfaces	CoDirecteur de these
M. Francesco DI RENZO, Directeur de recherche, ENSCM	Examinateur
Mme Anne-Karine FROMENT, Ingénieur, Aro-nucleart	Rapporteur
M. Emanuel SCHNECK, Group Leader, Max Planck Institute of Colloids and Interfaces	Rapporteur
M.Luca BERTINETTI, Group Leader, Max Planck Institute of Colloids and Interfaces	Invité

UNIVERSITÉ DE MONTPELLIER

THERMODYNAMICS OF WATER ADSORPTION IN MODEL STRUCTURED MOLECULAR SYSTEMS INCLUDING ANALOGUES OF HEMICELLULOSES, CRYSTALLINE CELLULOSE AND LIGNIN.

PRESENTED BY **AURELIO BARBETTA**

Delivered by **UNIVERSITE de MONTPELLIER**

and the **Institute of Chemistry - University of Potsdam**

In the researcher units of **ICSM Marcoule**

and **Max Planck Institute of Colloids and Interface**

within the frameworks of **L.I.A. Recycling CNRS-MPG**

Abstract

Wood is a complex and hierarchically organized material. It is characterized by an architecture of stiff crystalline cellulose fibrils, parallel to each other, and surrounded by a soft matrix made of hemicelluloses, lignin and water. When adsorbing water, the matrix swells and provides a source of internal stress for the stiff cellulose fibre, which are winding with a spiral angle around a central lumen. According to this angle, the material exhibit a wide range of behaviors and mechanical properties, being able to act as a stiff material to bear load, or shrink or expand.

Results of theoretical calculations on all the forces playing a role during water adsorption bring to the formulation of an Equation of State, that considers entropic, chemical, colloidal and mechanical terms to predict with an analytical expression the water absorption of untreated wood as a function of humidity changes.

The aim of the thesis is to extend the equation of state to the case of wood treated with electrolytes. The experimental part is performed using specific sorption devices as well as X-Ray scattering techniques. The theoretical part is developed extending the established master equation linking molecular level chemical forces, colloidal interactions and mechanics. The results of the model are tested against experimental data of electrolytes adsorption and compared with their chaotropic/kosmotropic character according to the Hofmeister series, which classifies ions according to their hydration properties.

Nowadays, several wood treatments have been developed to reduce the water uptake by wood, in order to confer higher resistance to moist to low-quality wood materials. The final aim of the project is to test the prediction of the model against these known treatments and to develop a general model to describe the behaviour of the wood under different chemical and physical environments. This way, new treatments can be conceptually designed and pre-existing treatments (as for instance the patented "woodprotect" one) improved.

Resume

Le bois est un matériau nanocomposite complex, fortement anisotrope et hiérarchiquement organisé. La micro-structure à l'échelle nanométrique est caractérisée par des nanofibres rigides de cellulose cristalline parallèles les unes aux autres et noyées dans un matrice plus molle et moins anisotrope. Cette matrice est composée par hémicelluloses et lignine, avec une absorption contrôlée par l'entropie et les liasons hydrogène entre hémicelluloses, lignine, et la surface de micro-cristaux de cellulose. La matrice est hygroscopique et se gonfle avec les changements de l'humidité relative, en fournissant une source de stress interne, tandis que les fibrilles de cellulose s'enroulent en spirale autour de la lumière centrale à un angle précis, qui est appellè AMF, angle des micro-fibrilles. Les micro-fibrilles se réorganisent passivement selone les contraintes osmotique appliquéees. Selon l'AMF, le positionnement et les propriétés mécaniques des fibres de bois varient considérablement: le matériau rigide se rétrécit ou il s'alloonge dans le sens de la longeur lors du gonflement, en générant de cette façon une grande déformation anisotrope.

Une première forme d'équation d'état comprenant entropie et termes chimiques, colloïdaux (comme la force d'hydratation) et termes mécaniques macroscopiques a été établie et permet de prédire sans paramétres l'absorption d'eau en fonction de l'humidité relative du composite de bois pas traité.

Le but de la thèse est d'étendre cette équation d'état au bois traité par absorption d'électrolytes en conditions hydrotermales, en intégrant l'équation avec des termes chimiques lié à la presence d'électrolytes. Les résultats du modéle sont comparés avec les données experimentales de sorption d'électrolytes formulés en fonction de la balance entr chaotropes et kosmotropes de l'échelle de Hofmeister. Les données expérimentales sont produit à partir des isothermes de sorption et des mécanismes moteurs pour tester la prédiction de la théorie en explorant l'effet du soluté (introduit dans le bois par mise en équilibre avec une solution utilisée comme une réservoir osmotique) sur la structure et les dimensions du materiau.

Zusammenfassung

Holz ist ein komplexes, hoch anisotropes und hierarchisch organisiertes Nanokompositmaterial. Die nanoskalige Mikrostruktur zeichnet sich durch starre, parallele, kristalline Cellulose-Nanofasern aus, die in eine weichere, weniger anisotrope Matrix eingebettet sind. Diese Matrix besteht aus Hemizellulosen und Lignin, mit kontrollierter Absorption durch Entropie und Wasserstoffbrücken zwischen Hemizellulosen, Lignin und der Oberfläche von Cellulose-Mikrokristallen. Die Matrix ist hygroskopisch und quillt mit Veränderungen der relativen Luftfeuchtigkeit auf, wodurch ein innerer Stressfaktor entsteht, während Zellulosefibrillen sich in einem präzisen Winkel um das zentrale Licht winden, der als AMF bezeichnet wird. Die Mikrofibrillen reorganisieren sich passiv zu den osmotischen Zwängen. Je nach AMF variieren die Positionier- und mechanischen Eigenschaften der Holzfasern erheblich: Das starre Material schwindet oder legiert sich beim Quellen in Längsrichtung und erzeugt so eine große anisotrope Verformung.

Eine erste Zustandsgleichungsform, die Entropie und chemische, kolloidale (wie z. B. Hydratationskraft) und makroskopische mechanische Begriffe umfasst, wurde etabliert und erlaubt die Vorhersage der Wasseraufnahme in Abhängigkeit von der relativen Luftfeuchtigkeit eines unbehandelten Holzwerkstoffes ohne Parameter.

Das Ziel der Dissertation ist es, diese Gleichung Zustand zu erweitern, um Holz behandelt durch Absorption von Elektrolyten unter hydroterminalen Bedingungen, die Integration der Gleichung mit chemischen Begriffen im Zusammenhang mit dem Vorhandensein von Elektrolyten. Die Ergebnisse des Modells werden mit experimentellen Daten der Elektrolytsorption verglichen, die entsprechend dem chaotropen und kosmotropen Gleichgewicht der Hofmeister-Skala formuliert wurden. Experimentelle Daten werden von Sorptionsisothermen und motorischen Mechanismen erzeugt, um die Vorhersage der Theorie zu testen, indem die Wirkung des gelösten Stoffes (eingeführt in Holz durch Auswuchten mit einer Lösung als osmotisches Reservoir) auf die Struktur und Dimension des Materials untersucht wird.

Contents

1. Introduction

The aim of this work is to contribute to investigations on the thermodynamic aspects of the interactions occurring between water and cell wall material in the presence of electrolytes in the impregnating aqueous solutions, when wood cell wall is exposed to different environmental conditions linked to the water activity (i.e. relative humidity changes).

This introductory literature section gives an overview of the current knowledge of these interactions and is organized in different sub-topics, which are: interactions of wood materials with water, salted water at interfaces, and salted water in wood. This latter topic will be studied via an Equation of State (EOS) approach, as in the case of hybrid solids in contact with structured colloidal fluids. Historically, studies on real gases (Nobel prize for Physics in 1910) have identified co-volume and attraction between atomic gases (Van der Waals 1910). This equation of state approach was then extended to the case of emulsions by Jean Perrin (Perrin 1926), and the comparison with gravity allowed to measure Avogadro's number and the Boltzmann constant. Later, the Equation of State was elaborated for lecithin multilayered vesicles, and led to the identification of the hydration force (LeNeveu et al. 1977). Afterwards, the Equation of State of DNA was experimentally established, and the role of hexatic phases and cationic species understood (Podgornik et al. 1998), with a high impact on compaction in cell nucleus and transfection techniques (Knobler et al. 2009). The biological role of cholesterol (Mouritsen 2004) and charged head-groups interacting with salts in stacked membranes was also understood via an Equation of State (Andelman 1995). In that case, two terms were recognized as fundamental: the perpendicular and lateral components of the Equation of State. Finally, the Equation of State has been qualitatively used also as an efficient unified guide-line to develop innovative preservation methods in the case of meat (Puolanne and Halonen 2010).

Using this approach, the core of this work is therefore to develop an Equation of State that can describe the effects of the colloidal interactions, due to added electrolytes, between water and cell walls polymeric components, in order to understand the impregnation of wood by electrolytes.

At first, a brief introduction on the wide varieties of mechanisms developed by plants when interacting with water is reported. A deep understanding of the topic strongly depends on an accurate knowledge of the physical-chemical phenomena regulating water adsorption, transport, and consequent water-actuated movements of plants.

The interest of the current work particularly concerns the adsorption of water and salt solutions within wood materials. Wood materials' compositional and structural changes are investigated at macroscopic scale (with micromechanical tensile devices), at microscopic scale (electron microscopy) and at nanometric scale (X-ray scattering) to develop a model that takes into account structure and composition of wood and that is able to predict and therefore enable the control of water and electrolyte sorption.

*The initial goal set for this work was to investigate if the master equation approach to the wood swelling had first to be extended to the case of impregnation of wood with salts: as a matter of fact, all published sorption models, used at industrial scale as starting point to perform chemical and thermal treatments capable to increase wood durability, are developed from parameter fitting of experimental sorption isotherms, (Volkova et al. 2012) and should be rationalized in terms of an Equation of State (see **1.3**), i.e. a minimal parameter-free model representing the water sorption isotherm in wood and osmotic pressure variations versus anisotropic swelling. As we will see, the EOS approach is expressed in physical chemistry as a pressure versus distance relation, while chemical engineering expresses the same relation by the mass water uptake versus relative humidity: in order to make results accessible to both communities, we will express most of the main results of this work in the two languages.*

1.1 Interaction of wood with water

Living organisms are made of molecular building blocks, assembled at several hierarchical levels, from supra-molecular to macroscopic: their individual components show poor mechanical qualities, but they form nano-composite tissues. Reinforcement of soft materials with complex architectures of stiff fibers allows them to show a great variety of structural and functional properties (see **Fig 1.1.1**), *e.g.* materials are tailored to bear and distribute loads (*Fratzl and Weinkamer 2007*).

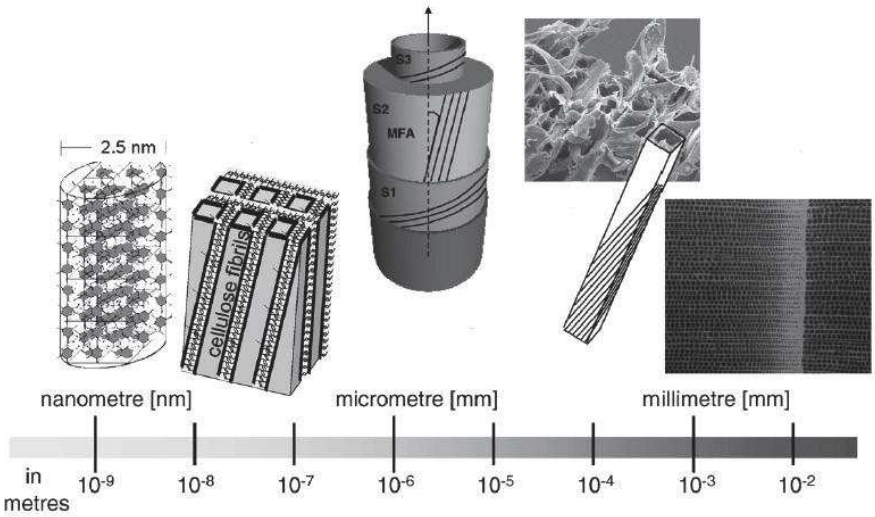

Fig 1.1.1: *Hierarchical structure of wood. From left to right: the crystalline part of a cellulose micro-fibril, the model of the arrangement of cellulose fibrils in a matrix of hemicelluloses and lignin, the structure of the cell-wall of a softwood, broken tracheids within a fracture surface of spruce wood, the cross-section through the stem (Weinkamer and Fratzl 2011).*

As water is an ubiquitous element in nature, a large variety of material's mechanisms in response to water absorption and changes in moisture content and environmental humidity can be observed. A fascinating example is the sophisticated hydration-dependent unfolding of ice plant seed capsules (*Harrington et al. 2010*). These mechanisms, often found in plants, are passive: it means they involve only dead cells, such as in the case of the scales of seed-bearing pine cones, and determine macroscopic structure changes with changes in environmental humidity (*Ibrîm et*

al. 1997). With time, biological organisms' evolution leads to optimization of interactions of their components with water, in order to obtain desired properties and behaviors on which they rely to accomplish their vital functions, such as seed dispersal, spatial re-orientation, organ locomotion and so on (*Fratzl and Barth 2009*).

First evidence of water uptake, studied using typical sorption models, such as BET (*Brunauer et al. 1938*), GAB (*de Boer 1955*), Dent (*Dent 1980*)... (see section **1.1.1**), is that it is accompanied by volume changes (*Elbaum et al. 2008*). These volume changes can induce passive hydro-actuated swelling or shrinkage, which organisms' sensors and actuators translate into movements, or stress generation. In this sense, organisms developed tissues tailored to give extremely specific responses to environmental condition changes, even in relative humidity ranges of a few percent (*e.g.* ice plants seed capsules undergo a reversible unfolding in the presence of liquid water, but do not give any response to RH changes up to 90%, *Razghandi et al. 2014*).

Besides volume changes, and consequent dimensional deformations (*Goswami et al. 2008*), which are the main experimentally observed phenomena in the current work, water absorption can induce drastic changes in the mechanical properties of the materials. The hydrogen-bonding network becomes looser and this is associated with large changes in mechanical performance, as shown in the case of wood cell wall materials in **Fig 1.1.2** (*Bertinetti et al. 2015*). It can trigger a phase separation by changing the mobility of the ionic species (*Ihli et al. 2014*), or lead to remarkable conformational differences between hydrated and non-hydrated conditions. This can occur not only in the material, as the example of collagen based rat tail tendon shows (*Masic et al. 2015*), but also in the orientation of water itself when it is perturbed in the presence of interfaces and solutes (see **1.2**, *Parsegian and Zemb 2011*).

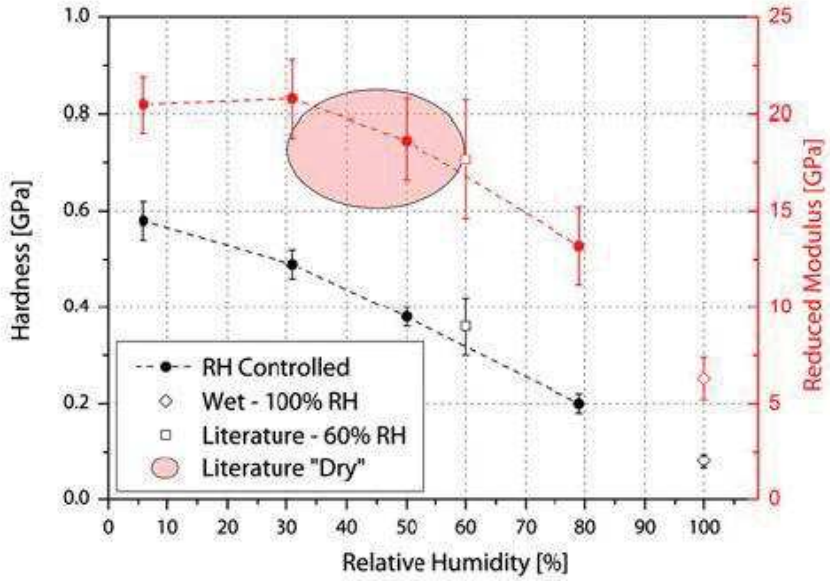

Fig 1.1.2: *Mechanical properties of the secondary wood cell wall in P.abies: the average hardness and reduced modulus are measured in a static indentation mode for different RH values. The reduced Yung modulus represents the elastic deformation that occurs in both sample and indenter tip and it is calculated from the elastic modulus and the Poisson's ratio (i.e. the signed ratio of transverse strain to axial strain) of both the material and the indenter (Bertinetti et al. 2015).*

Within this framework, processes in which movements are actuated by passive water adsorption/desorption, and without the need of any metabolic intervention, can be studied by combining mechano-chemical experiments and theoretical studies of the different hierarchical levels at which geometrical constraints and polymeric composition control organ deformations due to water uptake, and subsequently might suggest new paths for bio-mimetic material research (*Burgert and Fratzl 2009*). In this sense, the principle of the dynamic interconnection between osmotically driven water influx/efflux, material swelling/shrinking, mechanical energy storing and effecting of movement can be inspiring for design of bio-mimetic complex nano-architectures of stiff fibers embedded in a swellable, elastic matrix, as it is the case for example for wood cell wall materials, whose functionality is potentially controlled by the regulation of one single physical-chemical parameter (the water chemical potential). A remarkable variety of reversibly-actuated patterns has been already investigated in the case of hydrogels (*Sidorenko et al. 2007*).

Wood is a very important example case, when considered as made of nano-composites assembled at different hierarchical levels (**Fig 1.1.1**): at the nanometric scale, wood cell walls are organized into stiff crystalline cellulose nano-fibrils (35-50%, light grey in **Fig 1.1.3**, *Nishiyama 2009*), of a typical thickness of 2.5 nm, and parallel to each others, with a typical spacing distance between 1 and 4 nm, and the inter-crystalline gap is filled by a less anisotropic and much softer matrix (*McNeil et al. 1984*) constituting of an aqueous solution of hemicelluloses (20-35%) and lignin (10-25%). The detailed nano-structure of cellulose in wood is not yet fully known (*Fernandes et al. 2011)*, and neither is the distribution of the matrix polymers between the crystalline cellulose, even if their natural affinity to create nano-composites has been already proved (**Fig 1.1.3**, *Eronen et al. 2011*).

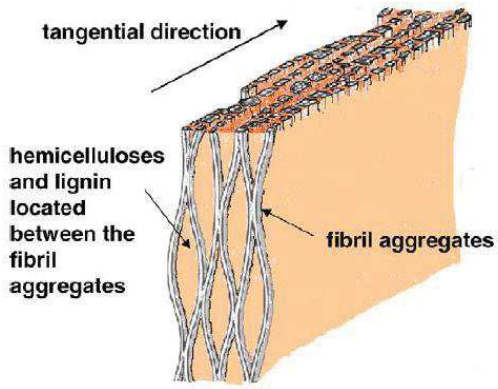

Fig 1.1.3*: Schematic drawing of the cellulose aggregate structure (Salmén 2004).*

Nonetheless, it is clear that this particular inter-linked structure allows the cell wall to perform several vital functions, such as cell membrane support and protection, and cell expansion during plant growth (*Cosgrove 2005, Jarvis 2011*). From a macroscopic point of view, wood cell wall can be described with a mechanical model based on a matrix that without any constraint would swell isotropically, and without any elastic energy being stored, but because of the presence of the stiff fibers that act as rigid elements and counteract this swelling, inducing significant anisotropic elastic strain. This is strongly dependent on the winding angle of the cellulose micro-fibrils (the so called *microfibrillar angle*, MFA, *Salmén 2004, Fratzl et. al 2008*), that regulates tensile and compressive stress generation (*Burgert and Fratzl 2009 II*).

In "normal" wood, tracheids have a rectangular shape and the cellulose fibrils are almost parallel to the cell axis (the MFA is rather low, ranging from 5° to 20°), while in the so-called "compression" wood tracheids are round in cross section with a higher MFA, up to 45°. In this way, cell wall architecture controls material's stress generation capabilities, as shown in **Fig 1.1.4**. For large angles, the cell expands longitudinally on swelling, while for lower angles (less than 45°) they contract. The combination of different types of cells cause differential expansion and can result in organ actuation (as observed for instance in trees` branches, where compression/reaction wood is deposited alongside to normal wood to withstand stresses).

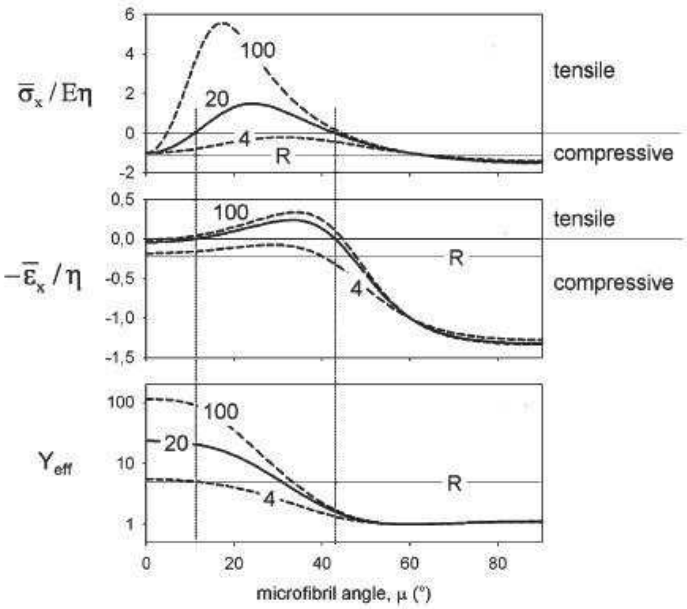

Fig 1.1.4: *Mechanical effects due to swelling of the cell wall as a function of the micro-fibril angle MFA. From top to bottom: stress generated by swelling when the cell is not allowed to change length, strain generated without any stress applied, and effective Young's modulus of the cell wall material (Fratzl et al. 2008).*

Freshly cut wood ("green") holds water in several states: liquid, liquid-vapor mixtures, and vapor inside the cell lumens. Water is absorbed in wood porous structure, which results in phase transition from vapor to liquid water (capillary condensation) when it enters in nano-pores (with a typical diameter of 2 nm). This phenomenon depends on the capillary size and the relative vapor pressure, whose relationship is described by the Kelvin equation, based on the molecular interactions at the liquid/vapor interfaces. Based on the Kelvin equation, and considering 2 nm diameter pores, capillary condensation would take place at nanopores in wood as low as at 40%

RH, and at bordered pits of tracheids at 95% RH. However, it was suggested that the equation should not be used when RH is below 80%, that is when the corresponding pore diameters are less than 10 nm, as the surface-tension-related theories assume large numbers of molecules (*Popper et al. 2009, Wang et al. 2014*)

Green wood moisture states range approximately from 100% to 170%, with variations according to the species, and to the environmental conditions (*Engelund et al. 2013*). Studies on never-dried wood show how the material has better qualities in terms of flexibility and ability of absorbing chemicals (*Gerber et al. 1999*). The difference with dried wood mainly consists in a shrinkage of the internal volume of the fibers, which causes difficulties for the pores to open again after rewetting, resulting in a decrease of water retention capacity (*Keckes et al. 2003, Spinu et al. 2011*). During drying, material's moisture content is reduced, until the point it reaches a transition state called *fiber saturation point*, FSP (*Berry and Roderick 2005*), between 38% and 43% MC (moisture content) for different softwood species, below which it turns into an unsaturated state. Water interacts in different ways with wood tissues (*Araujo et al. 1992*): differential scanning calorimetry shows that "free capillary water" is retained within the cell lumen, while "bound water" interacts with the hydrophilic components of the inter-crystalline matrix (*Nakamura et al. 1981*), *i.e.* accessible hydroxyl groups (*Sumi et al. 1963*) of the hemicelluloses identified via infrared spectroscopy, that are proved to be the active chemical moieties responsible for building hydrogen-bonds with water molecules.

Analysis of sorption isotherms proves that the dynamic equilibrium established during the continuous moisture exchanges shows several irreversible aspects, (**Fig 1.1.5**, *Derome et al. 2011, Patera et al. 2013*), that are due to glass transitions of hemicelluloses, whose mobility is moisture content dependent (*Downes and MacKay 1958*).

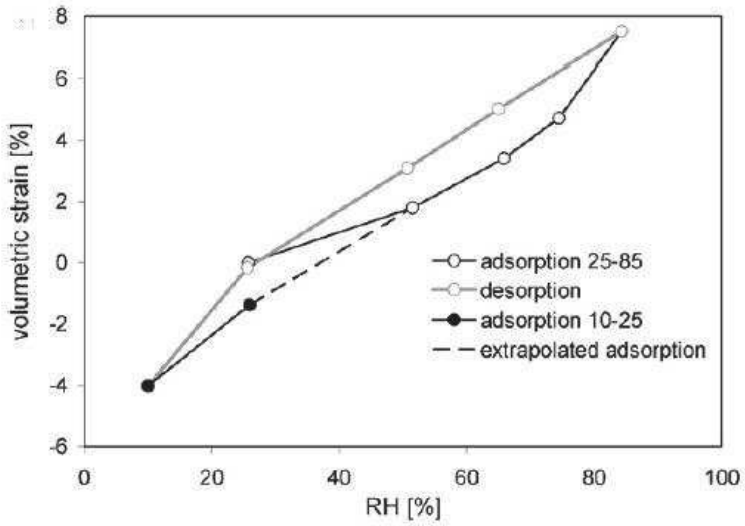

Fig 1.1.5: *Wood cell wall volumetric strain, with respect to the initial volume at RH=25%, versus RH, for a latewood sample (Derome et al. 2011).*

1.1.1 Sorption models

A sorption isotherm represents the relationship occurring between equilibrium moisture content and relative humidity, at constant temperature. Among all types of sorption described in literature (*Limousin 2007*), the most suitable curve to describe water uptake by wood materials and other natural hygroscopic polymers has a sigmoidal shape, and it can be considered as an intermediate between a model considering a single layer of sorbent on the substrate and a multilayered sorption (*Skaar 1988*). A list of empirical and semi-empirical sorption models available in literature counts 77 equations that have been applied to the case of wood, mostly based on parameter fitting of sorption experiments (*van der Berg and Bruin 1981*), even if many of them can be rearranged in mathematically equivalent forms (*Boquet et al. 1980*). The two main approaches consist in considering sorption as a surface phenomenon (*e.g.* BET, Dent theories) or a solution phenomenon (*e.g.* Hailwood-Horrobin model).

BET (1938) and Dent (1977) models assume that adsorbed water is present in two forms: primary molecules, that are directly adsorbed on wood cell wall sorption sites (*i.e.* hydroxyl groups), and secondary molecules on secondary sites with lower binding energy. Both equations are defined from the equilibrium of condensation and evaporation of water at each layer. The difference between the two theories is that in case of the thermodynamic properties of the secondary layers

are considered to be the same as liquid water in the case of the BET model, and differ in the case of the Dent model. Since BET theory (and Dent's modification as well) is based on gas adsorption studies, and therefore do not take into account swelling, it has limited applicability (*Simpson 1980*).

On the other hand, the Hailwood-Horrobin theory (1946) considers that part of the adsorbed water forms a hydrate with the wood and the balance forms a solid solution in the cell wall: the dominant processes are assumed to be the formation of the solid solution of water in the polymer and the formation of hydrates between water and defined units of the polymer molecules. Thus, water exists in two forms: in solution with the polymer, and combined with polymers to form hydrates. Two equilibria are therefore taken into account: the one between the dissolved water and the water vapor of the surroundings, and the one between the hydrated water and the dissolved water.

The isotherm equation predicted by Hailwood-Horrobin and Dent models can be written in the same form (**Eq. 1.1**):

$$MC = \frac{RH}{A+Bh-Ch^2} \qquad \textbf{Eq 1.1}$$

where $h = RH/100$, and A, B and C are three constants dependent on type of wood, initial moisture content, and two different equilibrium constants K_1 and K_2 describing the mentioned equilibria. These values are tabulated in literature (*Okoh and Skaar 1980*). In this Equation, the moisture content MC indicates the water content in terms of normalized mass difference of the sample between wet and dry, while the relative humidity RH is an index of water activity in terms of ration between the partial pressure of water vapor to the equilibrium vapor pressure of water.

In all cases, comparison with predicted and experimentally calculated heat of adsorption, which is a good index of model reliability, give errors of ca. 50%. Nonetheless, they can be fitted with non-linear regression techniques to experimental data with excellent results (*Simpson 1973*).

1.2 Salted water at interfaces

Fig 1.2.1 describes the electrostatic double layer with a model that involves the diffuse part of the double layer extending into the solution. Coulomb attraction by the charged groups on the surface attracts the counterions, but the osmotic pressure forces the counterions away from the interface. This results in a diffuse double layer. The double layer very near to the interface includes counterions specifically adsorbed on the interface of the inner part of the so-called Stern layer, and non-specifically adsorbed ions, where the diffuse layer begins. A sharp linear potential drop is observed in these regions. The diffuse part of the electrostatic double layer is known as Gouy-Chapman layer. In this model, ions are assumed of a finite size.

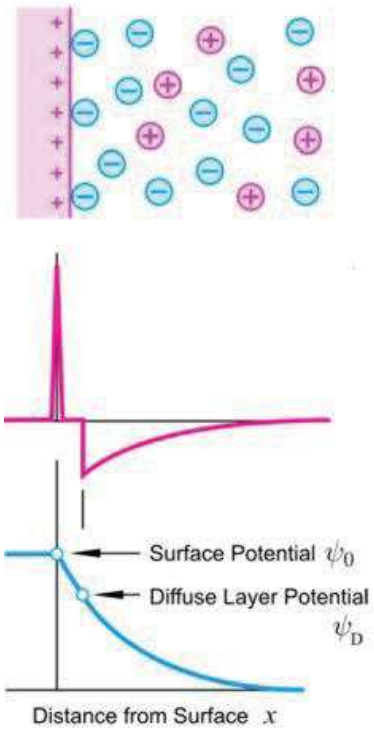

Fig 1.2.1: *Diffuse Stern model for ions at interface. From top to bottom: pictorial representation, charge density profile, electric potential profile.*

The introduction of the idea of three "competing" typical length scales relevant to ions at interfaces (*Netz 2004*) allowed an efficient classification, depending on the dominating mechanism. The three lengths to be considered are:

- Debye screening length (*i.e.* a value of how far electrostatic effects due to the presence of a charge carrier in solution persist), whose values, obtained by the classic formula, for monovalent salt and considering the concentration as that of a saturated NaCl solution (6.70 M) and a relative permittivity of 80, are calculated to be on the order of 0.1 nm;
- the Gouy-Chapman length describing relative influence of thermal and electrostatic energy, in the diffuse part of the electrostatic double layer, defined in analogy to the Bjerrum length (*i.e.* the separation at which the electrostatic interaction between two elementary charges is comparable in magnitude to the thermal energy scale), with values of less than 1 nm;
- the square root of the charge per unit surface, noted as Σ, indicating the distance between charges on the surface of the low charge density cellulose crystals, in the order of 2-4 nm considering the distance between the reducing aldehyde hydrate end group and the non-reducing alcoholic hydroxyl end group at the borders of a cellulose chain in a elementary fibril.

This allowed us to simplify the problem of the mixed effects of long-range Coulomb interactions with other range interactions (LRI). These LRI extend beyond the first neighbour that are classically treated as chemical equilibria and with the mass action law, but are despite their names - LRI or colloidal, molecular forces – nevertheless "short range" when compared to distances between crystalline cellulose fibrils (*Xiao and Song 2011*).

In the case of water-ion interactions in solution, it is intuitive to think that in the presence of water, or other polar solvents, the electric field generated by electrolytes induces the permanent dipoles of water to reorient around the ions. Moreover, it is possible to distinguish between water molecules that are strongly bound to ions (first neighbor ion-water distances) and water molecules whose interactions with ions are weak. The discrimination between physisorbed species (water, hydrated ions) and chemisorbed species (water, protons, ions), according to the Stern definition, is that the effective potential of a hydrated ion at the interface is more or less higher than $1K_BT$ respectively for "bound" and "free" counter-ions.

The ion-solvent interaction strength influences the hydrodynamic radius of the hydrated species, and their mobility in solution: different ions, even if they carry the same charge, have different size and different polarizability, and this also influences the availability of water itself (*Zavitsas 2001*). Therefore, ions will be differently hydrated. Properties of electrolytes in solution strongly depend

on their hydration and can be investigated with different experimental techniques: X-ray and neutron diffraction give time and space averaged ion-water interactions, NMR measurement allows the analysis of the dynamic properties of coordinated water molecules, Raman and IR spectroscopies consider the energies of the interactions between water molecules and ions (*Ohtaki and Radnal 1993*).

Despite the fact that classical theories, such as the Debye-Hückel model or the DLVO theory for colloids, do not take into account ion specificity (*Kunz et al. 2004, Dryzmala and Lyklema 2012*), it is clear that the difference in hydration properties of electrolytes implies that they show different behaviors when interacting in different physical or chemical environments. This led to the concept of ion specificity, that was developed since the works of Franz Hofmeister, whose studies initially concerned meat swelling and effects of electrolytes on protein salting-in and salting-out (*Poulanne 2010*). In the series named after him, cations and anions are classified according to the strength of their interactions with water (*e.g.* ion ability to polarize water): in other words, ions are called "chaotropic" when they are able to break water's structure, by disrupting the Hydrogen bonding network (they can easily lose their hydration sphere), or "kosmotropic" ("anti-chaotropic") when they show the different effects.

During the years, the series has been explored with different measurements, including studies of entropy changes upon hydration (*Kay 1968*), water activity coefficients (*Robinson et al. 1981*), thermal conductivity (*Eigen 1952*), and so on. Density function theory (DFT) based studies on monoatomic and polyatomic anions led to a correlation between ions' solvation structure and their position on the Hofmeister scale (*Baer and Mundy 2013*).

Therefore, the properties of a salt solution itself, such as osmotic pressure, electrical conductivity, viscosity are influenced not only by ionic concentration and valence (*Jones and Dole 1929*), but also by specific ionic interactions, including ion pairing and charge transfer. Variations of these properties are more evident in the case of anions, as they are richer in electrons, rather than with cations (*Collins et al. 2007*).

A first explanation for the specific effects was formulated by Collins (law of matching affinity), who observed that for single valence ions, similarly sized ions are more strongly attracted in water than dissimilar ones. In other words, the strength of the interaction between ions and water is correlated to the strength of the ion's interactions with other ions (*Collins 2004*). Another

important observation, brought to the definition of antagonistic salts by Onuki (*Onuki et al. 2011*), is that at the oil/water interface, a hydrophilic cation and a hydrophobic anion (*e.g.* derived from dissociation of $NaBPh_4$) interact differently with water-rich and oil-rich parts at the interface, and this results in a microphase separation, on the scale of the Debye screening length.

As a matter of fact, specific ion effects occur both at interfaces and in the bulk (air/water, oil/water, ... *Lo Nostro and Ninham 2012*). The analysis of the presence of electrolytes at the air-water interface shows at first, as a non-ion-specific effect, that all salts increase the surface tension, as reported in **Fig 1.2.2** (*Onsanger and Samaras 1934*).

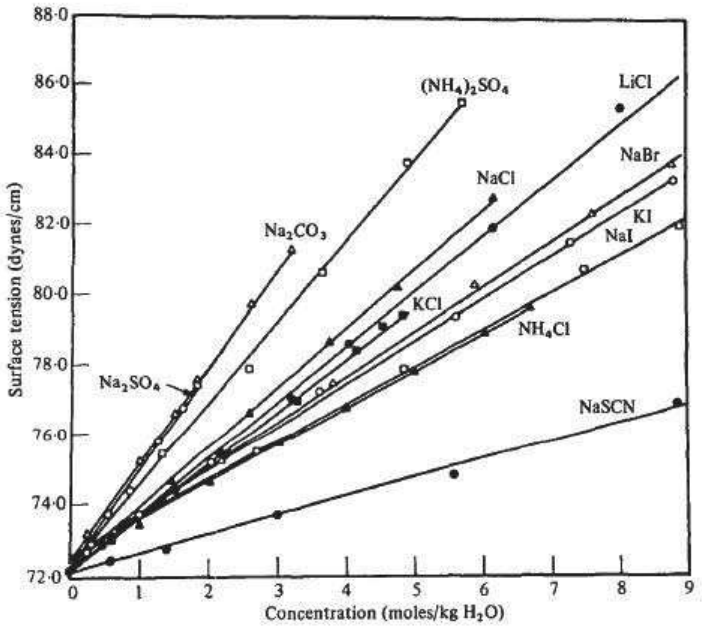

Fig 1.2.2: *Surface tension as a function of the solution concentration for aqueous solutions of inorganic electrolytes (Collins and Washabaugh 1985).*

Conversely, the specific ion effects, which usually emerge at a concentration higher than 100 mM (*Lo Nostro and Ninham 2012*), and depend not only on their chaotropic (water structure-breaking) or kosmotropic (water structure-making) behavior at the air-water interface (*Marcus 2009*), but also on their concentration (*Mancinelli et al. 2007*), are evident when surface potential differences with respect to pure water of several salt solutions are investigated (**Fig 1.2.3**).

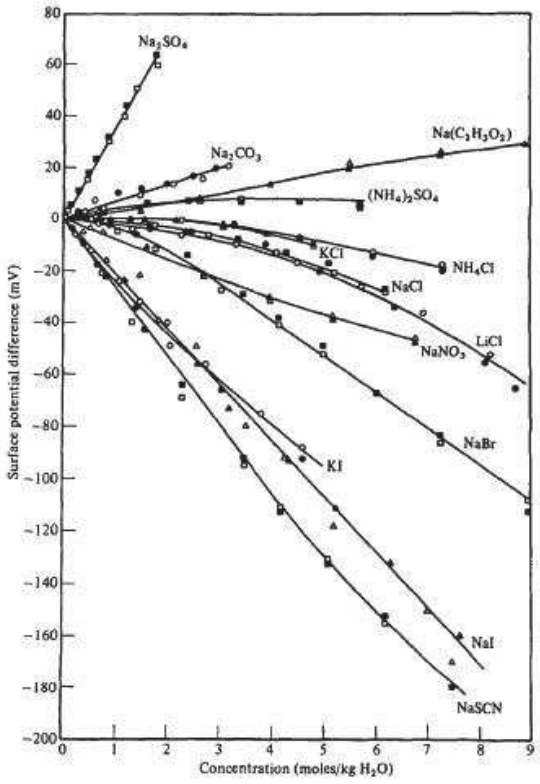

Fig 1.2.3: *Surface potential difference as a function of the solution concentration for aqueous solutions of inorganic electrolytes (Collins et al. 1985).*

Water molecules in the first hydration shell surrounding chaotropes are loosely held, or, in other words, chaotropic electrolytes interact with the first hydration shell less strongly than bulk water, resulting in a surface potential difference decrease. On the other hand, polar kosmotropic electrolytes interact with it more strongly, and increase the surface potential difference (*Collins et al. 1985*).

1.2.1 Ion/interface matching

It is important to stress that Hofmeister scale and the distinction between chaotropic and kosmotropic species give only qualitative considerations, or better to say semi-quantitative information, about ionic effects. The definition given by Collins of matching affinity, mentioned above, found its applicability for the simplest interactions between small ions, and has been then extended by the work of Jungwirth and Tobias (*Jungwirth and Tobias 2002*), who studied the dynamics of several alkali halides at the air/salt solution interface, pointing out the specific propensity of polarizable anions for the interface, which means that ionic size and polarizability

affect in a specific way the ion-water interactions, leading to an additional stabilization due to asymmetric solvation which is not taken into account by classical models.

As of colloidal and biological interest, the theory could be extended with the goal of classifying, and subsequently predicting, the interactions between different types of ions and surfactants' or lipids' headgroups (*e.g.* phosphates, sulfates). Computational studies on the effect of different cations on salt-induced transitions from micelles to vesicles were performed by the groups of Jungwirth and Kunz for the cases of sulfates and carboxylates, leading to a Hofmeister-like ordering of surfactants and lipid head groups (*Vlachy et al. 2009*). In this context, the key point for association is not considered to be the transfer from bulk to the air/water interface as in the original chaotropes/kosmotropes view, but two competing processes on the hard/soft scale favor association. All salts show the increase of the hydrated headgroup area per molecule at the interface, as they compete for water with the head groups, so that these are less hydrated with increasing ionic strength. However, chaotropic ions are more efficient in the case of alkyl sulfate and sulfonate groups, that have higher charge density (*i.e.* they are chaotropes), whereas kosmotropes have higher effects on alkyl carbonates, that have higher charge density (*i.e.* they are kosmotropes), consistent with the matching affinity's principle (**Fig 1.2.4**).

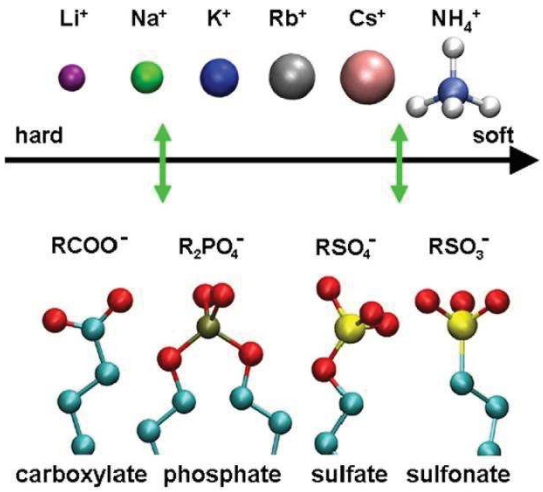

Fig 1.2.4: *Ordering of anionic surfactant head groups and the respective counterions regarding their capabilities to form close pairs, according to the simulations performed for R=CH_3. Green arrows indicate strong interactions, i.e. strong ion pairs (Vlachy et al. 2009).*

Confirmations and further steps into quantification came from the work of the group of Kunz, who performed NMR studies of Na/Li concentration-dependent binding competition on lamellar phases obtained from ionic surfactants (*Dengler et al. 2013*).

Clearly, the association between lipids and ions not only introduces charges at the interfaces, but also leads to significant structural perturbations. Studies of ion binding on Langmuir phospholipid monolayers and bilayers suggested that ion/lipid interactions could not be due only to local chemical binding reactions, but ions rather partition in the lipid interfaces with three types of specific interactions: they can locally bind on available sites, or partition into the interfacial zone, or distribute inhomogeneously because of local fields (*Leontidis et al. 2009*). Calculated binding and partitioning constants confirming this hypothesis depend on the used salt, and the effects of the anions follow the Hofmeister series (*Aroti et al. 2007*). These electrostatic interactions favor elongated lipid domains, and counteract the rounding effects of line tension (*i.e.* mismatches in the height of a lipid membrane that minimize energetically unfavourable exposure of the hydrophobic tail to water, in presence of thicker domains of raft membranes, *Garcia-Saez and Schwille 2010*) in a specific way: while cations mostly interact with the lipid by binding, chaotropic anions are expelled from the surfaces of the lipids and can penetrate between them (**Fig 1.2.5**, *Leontidis et al. 2009 II*).

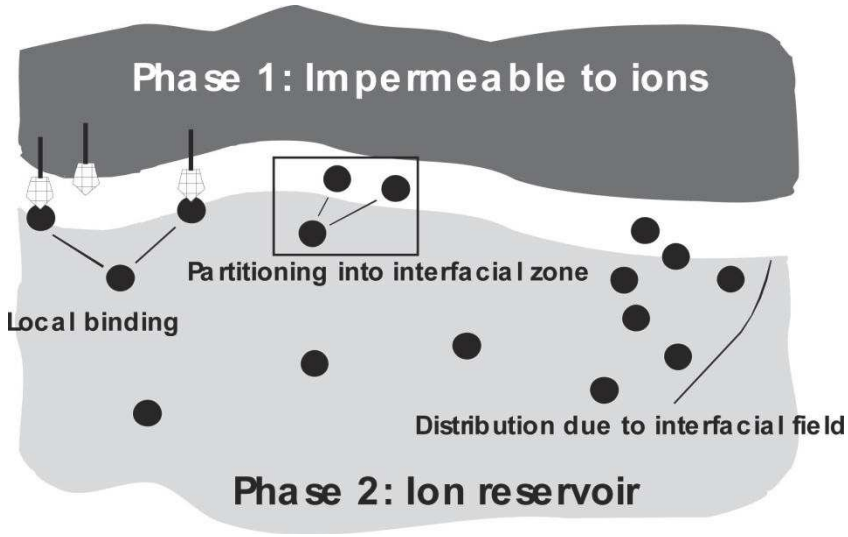

Fig 1.2.5: *Specific ion interactions at a boundary between two phases: local binding at available interacting sites, partitioning into the interfacial zone, inhomogeneous ion distribution due to interfacial field effects (Leontidis et al. 2009).*

At this level no partial inversions observed experimentally could be explained by the theory. Matching affinity could explain standard only observed single inversions. The only way to introduce partial inversion was to postulate partitioning. Therefore, the theory was furthermore extended from easier cases of more homogeneous surfaces to the one of pH-dependent heterogeneous interfaces, both hydrophobic and hydrophilic, by Horinek and Netz, who studied ion specificity on hydrophilic and hydrophobic patchy surfaces, under varying conditions of charge and polarity. Single-ion surface interaction potentials for halide and alkali ions at hydrophobic and hydrophilic interfaces were obtained in order to calculate ion density and electrostatic potential distributions at mixed surfaces of different surface charge (*Schwierz et al. 2013*). The direct anionic Hofmeister series was obtained for negatively charged hydrophobic (*i.e.* non-polar) and for positively charged hydrophilic (*i.e.* polar) surfaces, while a reverse ordering in the series is observed in the cases of negative polar and positive non polar surfaces: large chaotropic anions (*e.g.* I^-) with a high affinity for hydrophobic surfaces, and therefore increase the charge magnitude on negatively charged non-polar surfaces; large chaotropic cations (*e.g.* Cs^+) have similar affinity and compensate the negative charge, giving an effective positive charge. Large anions adsorb on hydrophobic surface and therefore give them an effective negative charge which leads to surface-surface repulsion and therefore stabilization of neutral solutes. The series reversal as the surface charge changes from negative to positive is then also easily explained: for negative surfaces, the adsorption of large anions will certainly be reduced due to electrostatic repulsion, but the trend will be the same; small anions will be more repelled from the surface than large anions, still giving negative surfaces a more negative surface potential in a NaI solution than in a NaF solution, and therefore, the direct series is retained. On a cationic surface, the trend is reversed, since now the magnitude of the surface potential is reduced strongly adsorbing I^- ions more than by the weakly adsorbing F^- ions. For cations, the situation is similar in that large cations such as Cs^+ tend to adsorb on hydrophobic surfaces and thus give them an effective positive surface charge. For neutral and cationic surfaces, larger ions thus tend to be more stabilizing than small ions, which is the indirect series. For surfaces of sufficient negative charge, the cationic series will be reversed and the direct cationic series is obtained (**Fig 1.2.6**).

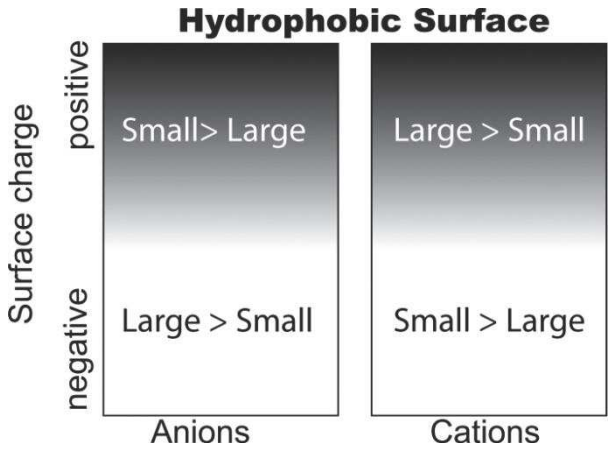

Fig 1.2.6: *Hofmeister ordering for negatively and positively charged hydrophobic surfaces (Schwierz et al. 2013).*

On hydrophilic surfaces, the size-dependence of the ion surface affinity is reverse, explaining the hofmeister series reversl when comparing hydrphobic with hydrophilic surfaces. Partial reversion occurs in intermediate hydrophilicity degrees, as result of competition of charge and solvation effects (**Fig 1.2.7**, *Schwierz et al. 2010*).

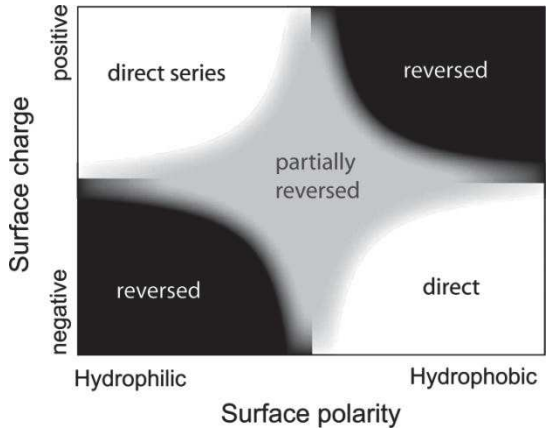

Fig 1.2.7: *Hofmeister phase diagram as a function of surface polarity and charge, derived from modeling results (Schwierz et al. 2010).*

Finally, the pH-dependence was studied by investigations of specific ion binding to protonated neutral and deprotonated charged carboxylic groups at the surface of self-assembled monolayers. Simulations showed a reversed cationic series of the affinity for charged and uncharged groups, as

a result of the surface charge reversal and of reversed affinities for the protonated and deprotonated carboxylates (**Fig 1.2.8**, *Schwierz et al. 2015*).

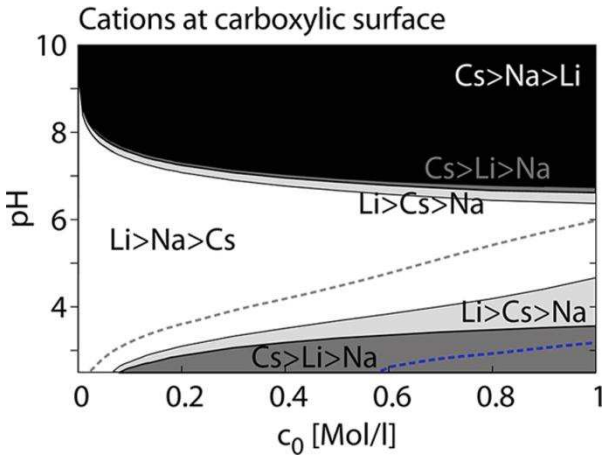

Fig 1.2.8: *Hofmeister pH-dependent state diagram as a function of bulk salt concentration, at surfaces containing carboxylic groups, for different cations (Schwierz et al. 2015).*

In this context, interesting experimental results have been obtained by Peydecastaing and coworkers (*Peydecastaing et al. 2011*), who studied the formation of acetyl and fatty acyl ester functions grafted on solid cellulose. Through esterification, the enthalpy of adsorption of water was reduced, which permits to avoid the usage of toxic formulations, such as coal tar, to reduce wood swelling and deformation. Moreover, thermoplastic properties of these compounds can be tuned by modulating the type and the number of side ester chains, *e.g.* long chain cellulose esters with a low degree of substitution show interesting properties such as water repellency (*Peydecastaing et al. 2011 II*).

Within this framework, aiming to study the effects of the presence of electrolytes in solution taken up by wood cell walls, one should consider that charged particles create a net electrical field, implying that the van der Waals screening force must be considered. Specific dispersion forces (*Kunz et al. 2004 II*) are present from low concentrations (10^{-1} M), but do not play a dominant role.

In our case of wood cell wall impregnated with moles of salt in the external reservoir, the order of the three length scales to be considered is always: Debye screening length < Gouy-Chapman length < distance between charges at the crystalline cellulose surface. In these conditions, the ion-specific attractive potential present or not present for chaotropic and kosmotropic ions (or

matching and non-matching affinity with cellulose), we can represent this effect by an apparent binding constant corresponding to all non electrostatic effects of the ion with the interface.

In order to use this in an EOS of state approach, we have to convert local binding constants to effective potentials between the surfaces of cellulose crystals. For the conversion, we use charge regulation as introduced by Parsegian and Ninham (*Ninham and Parsegian 1971*) and used successfully in hundreds of interacting colloidal systems.

Using this correspondence between chemical binding constants and the EOS, we can simplify the description of the equilibrium between ions, introduced by equilibration of wood with a salt solution used as osmotic reservoir, and adsorbing sites by considering specific constants K, whose values depend on the nature of the binding ions, and assuming that the non-adsorbing ion has a negligible binding constant. In this way, swelling depends only on the free energy of binding of the "dominant" ion, ΔG_s (**Eq. 1.2**):

$$K = \Sigma \delta e^{-\Delta G_s / RT} \qquad \textbf{Eq 1.2}$$

where Σ is the site surface area (the area per cellulose group is known to be 1 nm^2), δ the thickness of the layer for which non-electrostatic attraction plays a role. In “simple” cases such as adsorption of a hard flat wall of silica or other oxydes, the best value to be taken for conversion is the radius of the hydrated ion. However, here the ions adsorbed are located at the surface of flexible hydrophilic molecules, in order to avoid to introduce an extra parameter, we set this “width” of the sterical wall of potential to 0.5 nm, independent from ionic sizes. Very delicate calorimetric studies would allow to determine the width, since this would give an independent measure of the enthalpy of adsorption, therefore allowing to deduce a width for a known binding constant and free energy.

First experimental determination of binding constants for antagonistic salts containing one chaotropic ion is one of the objectives of the experimental part of this work, since it allows one step more than current models of wood cell wall in order to go from parametric EOS/adsorption isotherms towards quantitative modeling based on measurable molecular quantities.

1.3 Equation of State of wood in contact with solutions

The first Equation of state has been formulated in 1873 by van der Waals, who meant to predict ideal vapor-liquid coexistence. Afterward, this has been modified for real gases. Since then, researchers realized that the idea could be extended to the case of more and more complex systems: by measuring functions of state such as temperature, pressure, volume, internal energy, and taking into account their atomic structure and chemical bonds it is possible to predict their behavior and stability under a given set of physical conditions.

In this sense, a first step in colloid science was made by Jean Perrin (Nobel Prize in 1926, *Perrin 1913*). In order to develop Equations of State of colloids, he considered them, as a type of suspension, to physically behave like a liquid, *i.e.* to have less compressibility than gases, which will result in less drastic volume changes, or larger pressure changes, with temperature. Equations of state of colloids give important information concerning the intensity and the decay length of colloidal interactions (*Bonnet-Gonnet et al. 1994*): in stable colloidal dispersions the osmotic pressure increases with the volume fraction occupied by the particles. Experimental osmotic pressure of colloidal dispersions (in the easiest case of spherical particles) and theoretical calculations via Monte Carlo simulations, show to be in good agreement for several different silica and polystyrene dispersions. Monovalent counter-ions are treated according to the Poisson-Boltzmann equation (*Jönsson et al. 2011*)

At first, this approach can find a large number of applications, as in the case of uncharged lipids (*Petrache et al. 1998*): the force balance formulation allows to predict the smectic lattice spacing of a bilayer as a function of the osmotic pressure, summing up the contributions of the repulsive hydration force, van der Waals attraction, and Helfrich elastic repulsive fluctuations.

As the thermodynamic description of charged colloidal suspensions is complicated in the presence of size and charge asymmetries (*Hansen and Löwen 2000*), in the so-called primitive models the solvent is treated as a dielectric continuum (*Colla et al. 2012*). Moreover, theoretical models taking into account the presence of electrolytes consider the colloidal composition (colloidal particles, co-ions, counter-ions) as fixed, while the salt concentration is controlled via an externally regulated chemical potential, *e.g.* experimentally: a selectively permeable membrane (*Deserno and von Grünberg 2002*).

Within this framework, the relation between water adsorption by wood and its dimensional changes can also be represented with a general Equation of State, that provides the relation between observed swelling and state variables, *i.e.* osmotic pressure (*Carrière et al. 2007*). All the molecular and macroscopic forces playing an active role during water uptake are evaluated, and then summed in the form of a sorption isotherm, where the total moisture content is expressed as a function of the relative humidity or, in other words, of the water chemical potential (*Bertinetti et al. 2016*). Two equivalent representations of the Equation of State are often given: in physical-chemistry it is customary to report the osmotic pressure as a function of some typical distance (between cellulose crystals in the case of wood), while materials scientists usually talk about moisture content, *i.e.* mass of water per mass of dry sample, versus relative humidity. The conversion from one language to the other is very simple provided that the molar volume of the solvent and the densities of the solvent and of the material are known.

Starting from a model that reproduces wood composition and its cell wall spatial organization at the nanometric scale, it is possible to develop a force balance, in which derivatives of microscopic chemical, mesoscopic colloidal and macroscopic mechanical contributions are considered in the form of a Master Equation (*Bertinetti et al. 2013*), in the similar representation used in biophysics, in the case of DNA (*LeNeveu et al. 1977, Podgornik et al.* 1998). See **Eq 1.3**:

$$dG = dG_{chemical} + dG_{colloidal} + dG_{mechanical} \qquad \textbf{Eq 1.3}$$

Material's structure is decomposed into a Voronoi tessellation, so that the derivative of the free energies with cell volume (*i.e.* molecular forces) can be calculated and expressed in terms of surface pressure vs. chemical potential. The multi-scale analysis takes into account a microscopic enthalpic term due to the chemical binding difference between cellulose crystals and hemicelluloses, which is the main term opposing to swelling and dissolution: when water uptake causes wood fibrils swelling, the number of contact points per unit length of hemicelluloses decreases. Normally the presence of each contact point gives an attractive contribution of the order of magnitude of 5-50 K_BT, due to an energetic difference in the hydrogen-bonds of the hemicelluloses with the crystalline cellulose with respect to the ones created with the matrix. Mesoscopic terms consist in the configurational entropy of the matrix, and in the hydration force, a repulsive, short-ranged force acting between nano-fibers of cellulose through the hemicelluloses/lignin matrix (*Marčelja 1996*). In the present study, we will consider that the hydration force at the interface is not changing when salt is impregnating, and the electrostatic

force is due to weak adsorption of the chaotropic component of the salt. A macroscopic elastic term due to anisotropy is derived from mechanical modeling only (see **1.1**).

The addition of the entropic term is of primary importance, as shown by Medronho, Lindman and co-workers (*Medronho et al. 2012*), who stated that entropy is the key in cellulose dissolution, despite the fact that the most approved thesis considers that other interactions besides the intramolecular and intermolecular hydrogen bond network plays a negligible role (*Zhang et al. 2002*). As a matter of fact, cellulose is known to be insoluble in water, as well as in many organic solvents (*Medronho and Lindman 2014*). A good solvent to dissolve cellulose must be able to overcome the low entropy gain in the free energy of mixing balance with favorable interactions with the polymers, as in the most cases cellulose is not dissolved up to the molecular level, but rather tends to form colloidal dispersions. In this framework, it is possible to explain the observation of NaOH treatment to be more efficient at low temperatures. This is in opposition with the usual solubility processes in which the entropic driving force increases with temperature, by assuming conformational changes in the cellulose chain, which make the polymer less polar at higher temperatures, so that the attraction with the polar solvent is reduced.

Fig 1.3.1 shows how the calculated energies and their changes with environmental condition (*e.g.* moisture content) for a compression wood tissue (MFA=50°), and sums up the elastic term obtained from mechanical experiments (in green) and the chemical one resulting from water and wood component interactions). This way, changes in the chemical potential of water in the wood cell wall materials can be quantitatively described, and extended to general cases of deformation of nano-composites.

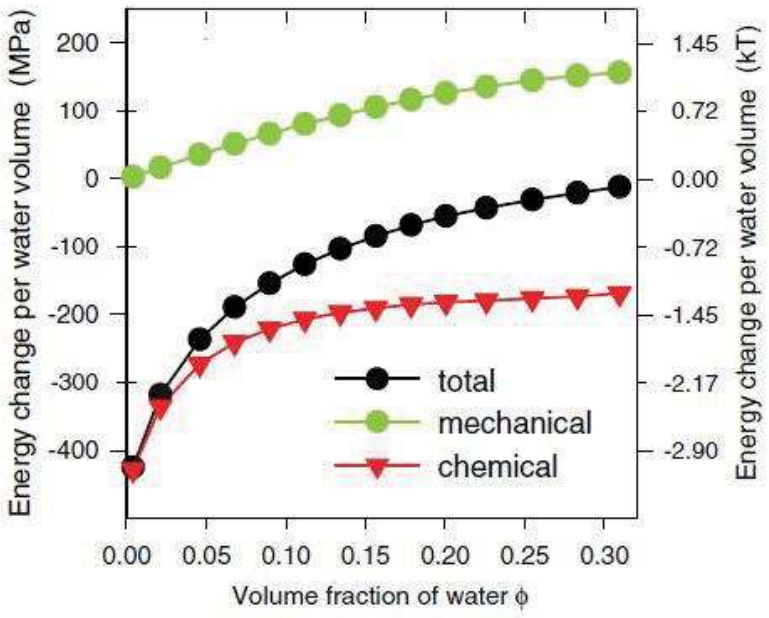

Fig 1.3.1: *Balance of energy density changes for a compression wood tissue with MFA=50° (Bertinetti et al. 2013).*

In this way, thermodynamics and mechanical modeling of the material that takes into account material's geometries and composition, together with molecular and macroscopic forces in play, has been combined and can be compared with experimental data, exploring structures, dimensions, mechanical behavior and energies, and test the predictions of the theoretical framework.

1.3.1 The terms in the force balance

1.3.1.1 Hydration force

Hydration force is a repulsive mechanism acting between polar surfaces separated by a thin layer of water, associated with water ordering at an interface, which has exponetianl decay constants in the size of water molecules. Primary hydration is relate to the binding of water at the interfaces, and to the entropy increase away from the interface, while seconday hydration is linked to the competition between water adsorbed around solutes and at the interface (in presence of salts). In the current model, secondary adsorption is not calculated. The energy per unit length h related to the hydration force between two hexagonal prisms of apothem D_0 is expressed as follows (*Bertinetti et al. 2016*):

$$\frac{\Delta G^{HF}}{h} = \overline{\Delta G_0}\frac{\sqrt{3}}{3} D_0 \lambda e^{\frac{D-D_0}{\lambda}} \qquad \textbf{Eq 1.4}$$

where D is the cellulose nanocrystal separation, ΔG_0 is the contact free energy density related to the energy per mole spent to remove the last water layer between two surfaces, and λ is the typical decay length for the hydration force, taken as 0.19 nm. The pressure term is derived by derivation with respect to D.

1.3.1.2 Crosslinking

The binding of matrix polymers to cellulose crystal is the main term opposing to swelling and dissolution of wood. When water takes apart cellulose crystals, the number of contact point between cellulose per unith length of matrix polymer decreases. In the anaylitical derivation of the term, only lignin is considered to bind on cellulose crystals, because of its aromatic moieties that interact with carbohydrate rings in hydrated environments, with an enthalpy per contact point for sugar/aromatic ring of about 2.5 kT in water. The derivation of the term (*Bertinetti et al. 2016*) starts from the evaluation of Λ, which is the portion of the chain in contact with a cellulose surface with respect to the total chain length:

$$\Lambda = \frac{2\sqrt{3}R}{3\sqrt{(D-2R)^2+\frac{4R^2}{3}}} \qquad \textbf{Eq 1.5}$$

where R is the apothem of the hexagonal prism. The number of monomers per unit length is:

$$\frac{N_{mp}}{h} = \frac{1}{h}\frac{V_0^{mat}}{V_m} \qquad \textbf{Eq 1.6}$$

where V_0^{mat} is the volume between cellulose crystals of the unit cell in dry conditions, and V_m is the volume of the matricx polymers monomer. For this calculations, the molecular weight of a monomer is taken as 170 g mol^{-1} and its density 1.4 g cm^{-3}. Under this approximation the monomers per unit cell in dry conditions are ca. 15. The number of contact points per unit length within the unit cell is:

$$\frac{N_{cp}}{h} = N_{mp}\phi_l\,\Lambda \qquad \textbf{Eq 1.7}$$

where ϕ_l, the volume fraction of lignin in the matrix, is taken as 0.5. The energy per unit length is derivede by combination of these equations:

$$\frac{\Delta G^{cp}}{h} = \frac{N_{cp}}{h}\Delta G_0^{cp} = \frac{2R^3\phi_l\phi_c}{(1-\phi_c)V_m\sqrt{(D-2R)^2\frac{4R^3}{3}}}\Delta G_0^{cp} \quad \textbf{Eq 1.8}$$

The pressure term is then derived by differentiation.

1.3.1.3 Van der Waals forces

Attractive contributes arising from Van der Waals forces acting between cellulose crystals across the hydrated matrix result to be negligibe by two order of magnitude (*Bertinetti et al. 2016*). For small separation, the energy per unit length for the case of two cylinders of radius R is defined as follows:

$$\frac{\Delta G^{VdW}}{h} = -A\frac{\sqrt{R}}{24(D-23)^{3/2}} \quad \textbf{Eq 1.9}$$

where A is the Hamaker constant 0.6 kT.

1.3.1.4 Configurational entropy

The partial free energy of mixeing is derived from the classical expression of Flory for the partial entropy of mixing, under the assumption that the polymers chains have infinite length (*Bertinetti et al. 2016*):

$$\frac{d\Delta G^S/h}{dD} = \frac{d\Delta G^S/h}{dN}\frac{dN}{dV}\frac{dV}{dD} = \sqrt{3D}\frac{RT}{\bar{v}}(\ln\phi_w^m + 1 - \phi_w^m + \chi_0(1-\phi_w^m)^2) \quad \textbf{Eq 1.10}$$

where ϕ_w^m is the water volume fraction within the matrix, and χ_0 is the Flory interaction parameter at low polymer volume fractions, which was taken as 0.5, a value reported in literature for many polysaccharides at water volume fractions >0.2 at room temperature. At low water contents, the entropic force is the dominant term, being higher than hydration, while it is lower at intermediate values of water content. For large hydrations, the two terms are comparable

1.3.1.5 Mechanics

The mechanic term accounts for anisotropic swelling: the material swells mostly in the perpendicular direction with respect to the orientation of the fibres. As a matter of facts, the matrix would swell isotropically, but the constraints given by the presence of cellulose crystals induce anisotropy, as the fibres act like stiff springs and counteract swelling. Thus, the associated elastic energy depends on the winding angle (*i.e.* the MFA) and the relative amount of cellulose.

The total elastic energy per unir heigth stored in the unit cell of the composite during swelling is expressed as follows (*Bertinetti et al. 2016*):

$$\frac{\Delta G^{El}}{h} = \frac{1}{2}\frac{\sqrt{3}}{2} D^2 \frac{1}{9} k E \phi_w^2 \qquad \textbf{Eq 1.11}$$

where k is a constant depending on the microfibrillar angle, and E is the moisture dependent Young's modulus of the matrix.

1.4 Aim of the work

The goal of this study was to start from a model of wood secondary cell walls to attempt a force balance, that allows us to understand and predict swelling of wood with salt solutions, and extend the Equation of State that describes the sorption process of water in wood, by adding an electrostatic term due to the presence of electrolytes

Studies on neutral-lipid membrane interactions remarked the specific effects of adsorption and screening due to the presence of salts on the Equation of State (**Fig. 1.4.1**, *Kunz et al. 2004 II*).

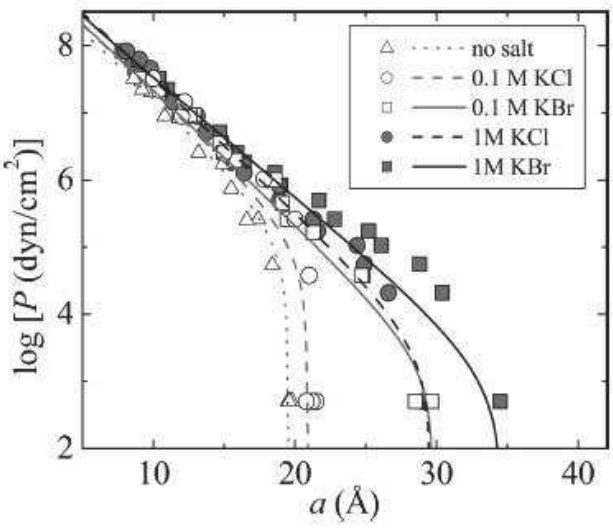

Fig 1.4.1: *DLPC multi-layer equation of state, reported as osmotic pressure vs inter-lamellar spacing as a function of salt nature and concentration (Petrache et al. 2006).*

In the case of wood, a model approximation considers two adjacent cellulose fibers as two planes separated by a matrix layer of a certain thickness, in osmotic equilibrium with a salt solution reservoir. Hofmeister specific effects leading to charge separation processes at the crystal/matrix interface are evaluated via specific binding free energy (for the calculations: a specific binding constant associated to bringing one ion from the reservoir to the interfacial surface), as well as non-specific effects such as divalent cation complexation by hydroxyl groups of the sugars.

A further step consists in the analysis of the calculated sorption isotherms of models of hydrophobic coir fibers and lignin-poor mistletoe fibers, compared with experimentally obtained ones. Both these materials' cellulose content is approximately 50% in weight. In the case of coir fibers the remaining is mainly constituted by lignin, while in mistletoe it is constituted by hemicelluloses. In this way, the individual contributions of the single components of the swelling matrix in the process of water uptake by wood can be rationalized and evaluated.

1.5 Integrating the electrostatic term

The model used for this case of charge regulation, in which charge separation is driven by specific ion adsorption, considere infinite planes separated by a thin matrix layer in equilibrium with a solution reservoir, in the case of weak overlap approximation, *i.e.* the water layer between the crystals is larger than the Debye length (which indicates the thickness of the diffuse electric double layer), so that the interaction can be considered as simply due to electrostatic properties next to an isolated plane. In order to take into account ion specificity, **Eq 2.1** was introduced ($K = \Sigma\delta e^{-\Delta G_S/RT}$), describing the equilibrium between ions in solution and adsorbed ions. In this equation specific binding constants accounting for the different affinity of each ion pair to the matrix surface are related via an exponetianal correlation to the free energy of adsorption. The formulation of the constant (for the derivation see paragraph **2.5.3**) explicits its dependance from two parameters, the occupation rate and the electrostatic potential, whose expressions depende from each others. Thus, the system of obtained equations can not be solved analitically, and requires iterated calculations: given a certain ion concentration, and a defined constant which is

the derived from comparison with experimental results, the values of occupation rate and of electrostatic satisfying the equation are obtained and used in the Poisson-Boltzmann equation to obtain the value of eccess osmotic pressure due to specific electrostatics (see **Fig 1.5.1**).

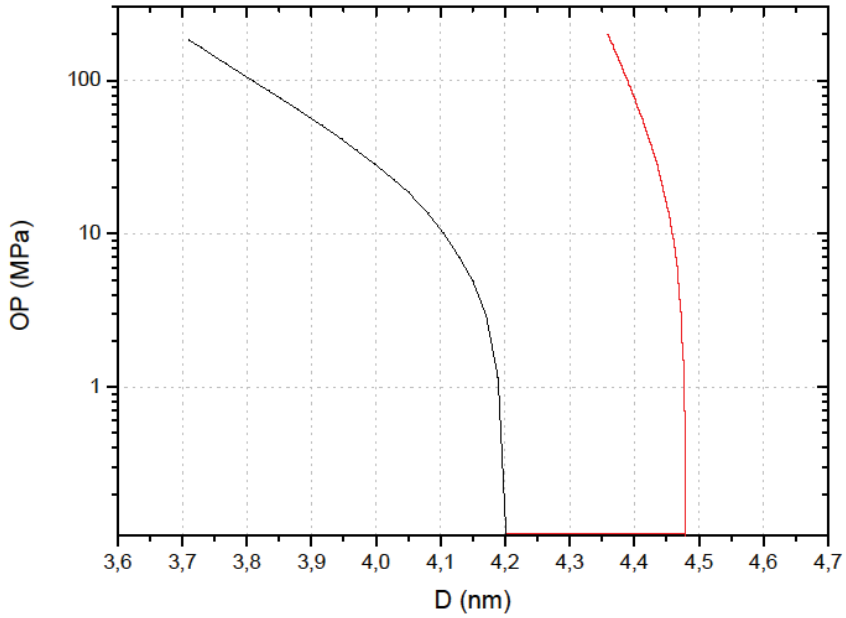

Fig 1.5.1: *Calculated Equation of State with (red curve) and without (black curve) taking into account the electrostatic term. The horizontal red line account for the maximum extra swelling, i.e the swelling difference due to the presence of adsorbed ions, considered in fully hydrated conditions.*

For this calculation, a "standard" values of ΔG_s= 6kT was used, as it is typical for the case of binding of chaotropic ions to a charged lipid interface (*Aroti et al. 2007*, *Leontidis et al. 2009*). The area of a surface site, Σ, was set to 1 nm^2, and the ion diameterδ to 0.5 nm. The overwhelming contribute of the electrostatic term in the force balance shift the EOS curve to higher values of swelling, with a sensitive increase of the swelling, in the order of few ångstroms. Moreover, each of the parameters introduced in the model can be tuned, as shown in **Fig. 1.5.2**:

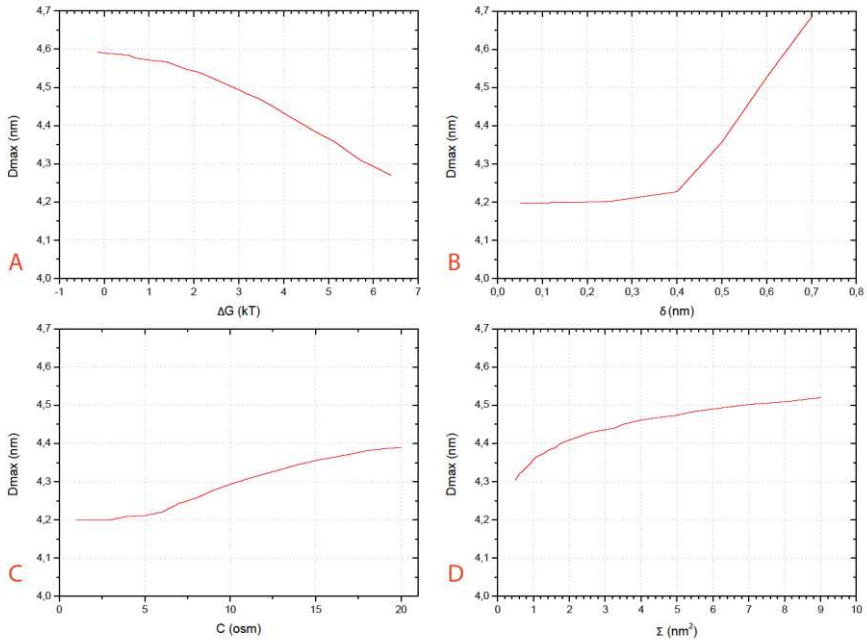

Fig 1.5.2: *Calculated maximum swelling in the presence of electrolytes, reported as a function of the free energy of adsorption (A), the diameter of the adsorbing ion (B), the salt concentration (C) and the surface of the adsorbing site (D), while all the other parameters are kept as constant.*

Fig 1.5.2a shows the dependance of the maximum swelling D_{max} as a function of the free energy of adsorption (*i.e.* as a function of the bidning constant): results show an increase of D_{max} at small values of binding constanty, with variation in the order of 3 Å, until charge saturation, leading to a constant value. **Fig 1.5.2.b** reports the variations of D_{max} with the ionic size, which apperar to be the most effecting parameter, showing neglectable variations until a "critical value" of 0.4 nm diameter, after which the maximum swelling increase linearly with ionic size. Smaller increases in the value of D_{max} are also registered with variations of ionic concentration (**Fig 1.5.2.c**) and the area of the adsorbing sites (**Fig 1.5.2.d**). The discussion of the effects of these parameters is proposed in paragraph **4.3.1**.

References

(*Andelman 1995*) D. Andelman *Electrostatic properties of membranes: the Poisson-Boltzmann theory*, in *Handbook of Biological Physics*, 1995 Elsevier Science B.V.

(*Araujo et al. 1992*) C.D. Araujo, A.L. MacKay, J.R.T. Hailey, K.P. Whittall, H. Le *Proton magnetic resonance techniques for characterization of water in wood: application to white spruce*, 1992 Wood Sci. Technol. 26, 101

(*Aroti et al. 2007*) A. Aroti, E. Leontidis, M. Dubois, T. Zemb, G. Brezesinski *Monolayers, bilayers and micelles of zwitterionic lipids as model systems for the study of specific anion effects*, 2007 Colloid Sufaces A 303, 144

(*Baer and Mundy 2013*) M.D. Baer, C.J. Mundy *An ab initio approach to understanding the specific ion effect*, 2013 Farad. Discuss. 160, 89

(*Berry and Roderick 2005*) S.L. Berry, M.L. Roderick *Plant-water relations and the fibre saturation point*, 2005 New Phytol. 168, 25

(*Bertinetti et al. 2013*) L. Bertinetti, F.D. Fischer, P. Fratzl *Physicochemical basis for water-actuated movement and stress generation in nonliving plant tissues*, 2013 PRL 111, 238001

(*Bertinetti et al. 2015*) L. Bertinetti, U.D. Hangen, M. Eder, P. Leibner, P. Fratzl, I. Zlotnikov *Characterizing moisture dependent mechanical properties of organic materials humidity controlled static and dynamic nanoindentation of wood cell walls* 2015 Phil. Mag. 95, 1992

(*Bertinetti et al. 2016*) L. Bertinetti, T. Zemb, P. Fratzl *Chemical, colloidal and mechanical contributions to the state of water in wood cell walls*, 2016 New. J. Phys. 18, 083048

(*Bonnet-Gonnet et al. 1994*) C. Bonnet-Gonnet, L. Belloni, B. Cabane *Osmotic pressure of latex dispersions*, 1994 Langmuir, 10, 4012

(*Boquet et al. 1980*) R. Boquet, J. Chirife, H.A. Iglesias *Technical note: on the equivalence of isotherm equations*, 1980 J. Fd Technol. 15, 345

(*Brunauer et al. 1938*) S. Brunauer, P.H. Emmett, E. Teller *Adsorption of gases in multimolecular layers* 1938 J. Am. Chem. Soc. 60, 2, 309

(*Burgert and Fratzl 2009*) I. Burgert, P. Fratzl *Actuation systems in plants as prototypes for bioinspired devices*, 2009 Phil. Trans. R. Soc. A 367, 1541

(*Burgert and Fratzl 2009 II*) I. Burgert, P. Fratzl *Plants control the properties and actuation of their organs through the orientation of cellulose fibrils in their cell walls* 2009, Integr. Comp. Biol. 49, 1, 69

(*Carrière et al. 2007*) D. Carrière, M. Page, M. Dubois, T. Zemb, H. Cölfen, A. Meister, L. Belloni, M. Schönhoff, H. Möhwald *Osmotic pressure in colloid science: clay dispersions, catanionics, polyelectrolyte complexes and polyelectrolyte multilayers*, 2007 Colloids Surf. A 303, 137

(*Colla et al. 2012*) T.E. Colla, A.P. dos Santos, Y. Levin *Equation of state of charged colloidal suspensions and its dependence on the thermodynamic route*, 2012 J. Chem. Phys. 136, 194103

(*Collins 2004*) K.D. Collins *Ions from the Hofmeister series and osmolytes : effects on proteins in solution and in the crystallization process*, 2004 Methods 34, 300

(*Collins et al. 2007*) K.D. Collins, G.W. Neilson, J.E. Enderby *Ions in water characterizing the forces that control chemical processes and biological structure*, 2007 Biophys. Chem. 128, 95

(*Collins and Washabaugh 1985*) K.D. Collins, M.W. Washabaugh *The Hofmeister effect and the behaviour of water at interfaces*, 1985 Q. Rev. Biophys. 18, 4, 323

(*Cosgrove 2005*) D.J. Cosgrove *Growth of the plant cell wall*, 2005 Nat. Rev. Mol. Cell Biol. 6, 853

(*de Boer 1955*) J.H. de Boer *The dynamical character of adsorption* 1955, Ber. Bunsen-Ges. Phys. Chem. 59, 3, 227

(*Dengler et al. 2013*) S. Dengler, A. Klaus, G.J.T. Tiddy, W. Kunz *How specific are ion specificities? A pilot NMR study*, 2013 Farad. Discuss. 160, 121

(*Dent 1980*) R. W. Dent *A sorption theory for gas mixtures* 1980, Polym. Eng. Sci. 20, 4, 286

(*Derome et al. 2011*) D. Derome, M. Griffa, M. Koebel, J. Carmeliet *Hysteretic swelling of wood at cellular scale probed by phase-contrast x-ray tomography*, 2011 J. Struct. Biol. 173, 180

(***Deserno and von Grünberg 2002***) M. Deserno, H.H. von Grünberg *Osmotic pressure of charged colloidal suspension: a unified approach to linearized Poisson-Boltzmann theory*, 2002, Phys. Rev. E 66, 011401

(***Downes and MacKay 1958***) J.G. Downes, B.H. MacKay *Sorption kinetics of water vapor in wool fibers*, 1958 J. Polym. Sci. 28, 45

(***Dryzmala and Lyklema 2012***) J. Dryzmala, J. Lyklema *Surface tension of aqueous electrolyte solutions. Thermodynamics*, 2012 J. Phys. Chem. A 116, 6465

(***Eigen 1952***) M. Eigen, *Zur Theorie der Wärmeleitfiihigkeit des Wassers*, 1952 Ber. Bunsen-Ges. Phys. Chem. 56, 3, 176

(***Elbaum et al. 2008***) R. Elbaum, S. Gorb, P. Fratzl *Structures in the cell wall that enable hygroscopic movement of wheat awns*, 2008 J. Struct. Biol. 164, 101

(***Engelund et al. 2013***) E.T. Engelund, L.G. Thygesen, S. Svensson, C.A.S. Hill *A critical discussion of the physics of wood–water interactions*, 2013 Wood Sci. Technol. 47, 141

(***Eronen et al. 2011***) P. Eronen, M. Österberg, S. Heikkinen, M. Tenkanen, J. Laine *Interactions of structurally different hemicelluloses with nanofibrillar cellulose*, 2011 Carbohyd. Polym. 86, 1281

(***Fernandes et al. 2011***) A.N. Fernandes, L.H. Thomas, C.M. Altaner, P. Callow, V.T. Firsyth, D.C. Apperley, C.J. Kennedy, M.C. Jarvis *Nanostructure of cellulose microfibrils in spruce wood*, 2011 PNAS 108, 47, E1195

(***Fratzl and Barth 2009***) P. Fratzl, F.G. Barth *Biomaterial systems for mechanosensing and actuation*, 2009 Nature 462, 442

(***Fratzl and Weinkamer 2007***) P. Fratzl, R. Weinkamer *Nature's hierarchical materials*, 2007 Prog. Mater. Sci. 52, 1263

(***Fratzl et al. 2008***) P. Fratzl, R. Elbaum, I. Burgert *Cellulose fibrils direct plant organ movements*, 2008 Farad. Discuss. 139, 275

(***Garcia-Saez and Schwille 2010***) A.J. Garcia-Saez, P. Schwille *Stability of lipid domains*, 2010 FEBBS Lett. 584, 1653

(*Gerber et al. 1999*) P.J. Gerber, J.A. Heitmann, T.W. Joyce, J. Buchert, M. Siika-aho *Adsorption of hemicellulases onto bleached kraft fibers*, 1999 J. Biotechnol. 67, 67

(*Goswami et al. 2008*) L. Goswami, J.W.C. Dunlop, K. Jungnikl, M. Eder, N. Gierlinger, C. Coutand, G. Jeronimidis, P. Fratzl, I. Burgert *Stress generation in the tension wood of poplar is based on the lateral swelling power of the G-layer*, 2008 Plant J. 56, 531

(*Hansen and Löwen 2000*) J.P. Hansen, H. Löwen *Effective interactions between electric double layers*, 2000 Annu. Rev. Phys. Chem. 51, 209

(*Harrington et al. 2010*) M.J. Harrington, K. Razghandi, F. Ditsch, L. Guiducci, M. Rueggeberg, J.W.C. Dunlop, P. Fratzl, C. Neinhuis, I. Burgert *Origami-like unfolding of hydro-actuated ice plant seed capsules*, 2010 Nat. Commun. 2, 337

(*Ibrîm et al. 1997*) Q. Ibrîm, R.P. Evershed, P.E. van Bergen, T.M. Peakman, E.C. Leigh-Firbank, M.C. Horton, D. Edwards, M. Biddle, B. Kjølbye-Biddle, P.A. Rowley-Conwy *How pine cones open*, 1997 Nature 390, 668

(*Ihli et al. 2014*) J. Ihli, W. Ching Wong, E.H. Noel, Y.Y. Kim, A.N. Kulak, H.K. Chrisenson, M.J. Duer, F.C. Meldrum *Dehydration and crystallization of amorphous calcium carbonate in solution and in air*, 2014 Nat. Commun. 5, 3169

(*Jarvis 2011*) M.C. Jarvis *Plant cell walls: supramolecular assemblies*, 2011 Food Hydrocoll. 25, 257

(*Jones et al. 1929*) G. Jones, M. Dole *The viscosity of aqueous solutions of strong electrolytes with special reference to Barium chloride*, 1929 J. Am. Chem. Soc. 51, 10, 2950

(*Jönsson et al. 2011*) B. Jönsson, J. Persello, J. Li, B. Cabane *Equation of state of colloidal dispersions*, 2011 Langmuir 27, 6606

(*Jungwirth and Tobias 2002*) P. Jungwirth, D.J. Tobias *Ions at the air/water interface*, 2002 J. Phys. Chem. B 106, 6361

(*Kay 1968*) R.L. Kay *The effect of water structure on the transport properties of electrolytes*, in *Trace Inorganics in Water*, 1968 American Chemical Society

(*Keckes et al. 2003*) J. Keckes, I. Burgert, K. Frühmann, M. Müller, K. Kölln, M. Hamilton, M. Burghammer, S.V. Roth, S. Stanzl-Tschegg, P. Fratzl *Cell-wall recovery after irreversible deformation of wood*, 2003 Nat. Mater. 2, 810

(*Knobler and Gerlbart 2009*) C.M. Knobler, W.M.Gerlbart *Physical chemistry of DNA viruses*, 2009 Annu. Rev. Phys. Chem. 60, 367

(*Kunz et al. 2004*) W. Kunz, P. Lo Nostro, B.W. Ninham *The present state of affairs with Hofmeister effects*, 2004 COCIS 9, 1

(*Kunz et al. 2004 II*) W. Kunz, L. Belloni, O. Bernard, B.W. Ninham *Osmotic coefficients and surface tensions of aqueous electrolyte solutions: role of dispersion forces*, 2004 J. Phys. Chem. B 108, 2398

(*LeNeveu et al. 1977*) D.M. LeNeveu, R.P. Rand, V.A. Parsegian, D. Gingell *Measurement and modification of forces between lecithin bilayers*, 1977 *Bioph. J. 18, 209*

(*Leontidis and Aroti 2009*) E. Leontidis, A. Aroti *Liquid expanded monolayers of lipids as model systems to understand the anionic Hofmeister series: 2. Ion partitioning is mostly a matter of size*, 2009 J. Phys. Chem. B 113, 1460

(*Leontidis et al. 2009*) E. Leontidis, A. Aroti, L. Belloni *Liquid expanded monolayers of lipids as model systems to understand the anionic Hofmeister series: 1. A tale of models*, 2009 J. Phys. Chem. B 113, 1447

(*Limousin et al. 2007*) G. Limousin, J.P. Gaudet, L. Charlet, S. Szenknect, V. Barthès, M. Krimissa *Sorption isotherms: a review on physical bases, modeling and measurement*, 2007 Appl. Geochem. 22, 249

(*Lo Nostro and Ninham 2012*) P. Lo Nostro, B.W. Ninham *Hofmeister phenomena: an update on ion specificity in biology*, 2012 Chem. Rev. 112, 2286

(*Marčelja 1996*) S. Marčelja *Hydration in electrical double layers*, 1996 Nature 385, 689

(*Marcus 2009*) Y. Marcus *Effect of ions on the structure of water: structure making and breaking*, 2009 Chem. Rev. 109, 1346

(*Masic et al. 2015*) A. Masic, L. Bertinetti, R. Schuetz, S.W. Chang, T.H. Metzger, M.J. Buehler, P. Fratzl *Osmotic pressure induced tensile forces in tendon collagen* 2015 Nat. Commun. 6, 5942

(*Mancinelli et al. 2007*) R. Mancinelli, A. Botti, F. Bruni, M.A. Ricci *Hydration of Sodium, Potassium, and Chloride ions in solution an the concept of structure maker/breaker*, 2007 J. Phys. Chem. B 111, 13570

(*McNeil et al. 1984*) M. McNeil, A.G. Darvill, S.C. Fry, P. Albersheim *Structure and function of the primary cell walls of plants*, 1984 Ann. Rev. Biochem. 53, 625

(*Medronho and Lindman 2014*) B. Medronho, B. Lindman *Competing forces during cellulose dissolution: from solvents to mechanisms*, 2014 COCIS 19, 1, 32

(*Medronho et al. 2012*) B. Medronho, A. Romano, M. Graça Miguel, L. Stigsson, B. Lindman *Rationalizing cellulose (in)solubility: reviewing basic physicochemical aspects and role of hydrophilic interactions*, 2012 Cellulose, 19, 581

(*Mouritsen 2004*) O.G. Mouritsen *Life - As a matter of fat*, 2004 Springer Science & Business Media

(*Nakamura et al. 1981*) K. Nakamura, T. Hatakeyama, H. Hatakeyama *Studies on bound water of cellulose by differential scanning calorimetry*, 1981 Text. Res. J. 51, 9, 607

(*Netz 2004*) R.R. Netz *Water and ions at interfaces*, 2004 COCIS 9, 192

(*Ninham and Parsegian 1971*) B.W. Ninham, V.A. Parsegian *Electrostatic potential between surfaces bearing ionizable groups in ionic equilibrium with physiologic saline solution*, 1971 J. Theor. Biol. 31, 405

(*Nishiyama 2009*) Y. Nishiyama *Structure and properties of the cellulose microfibril*, 2009 J. Wood Sci. 55, 241

(*Okoh and Skaar 1980*) K.I.A. Okoh, C. Skaar *Moisture sorption isotherm of the wood and inner bark of ten southern U.S. hardwoods*, 1980 Wood Fiber Sci. 12, 2, 98

(*Ohtaki and Radnal 1993*) H. Ohtaki, T. Radnal *Structure and dynamics of hydrated ions*, 1993 Chem. Rev. 93, 1157

(*Onsager and Samaras 1934*) L. Onsager, N.N.T. Samaras *The surface tension of Debye-Hückel electrolytes*, 1934 J. Chem. Phys. 2, 528

(*Onuki et al. 2011*) A. Onuki, R. Okamoto, T. Araki *Phase transitions in soft matter induced by selective solvation*, 2011 Bull. Chem. Soc. Jpn. 84, 6, 569

(*Parsegian and Zemb 2011*) V.A. Parsegian, T. Zemb *Hydration forces: Observations, explanations, expectations, questions*, 2011 COCIS 16, 618

(*Patera et al. 2013*) A. Patera, D. Derome, M. Griffa, J. Carmeliet *Hysteresis in swelling and in sorption of wood tissue*, 2013 J. Struct. Biol. 182, 226

(*Perrin 1913*) J. Perrin *Les atomes*, 1913 Flammarions, re-edited 1991

(*Perrin 1926*) J. Perrin *Discontinuous structure of matter*, 1926 Nobel Lecture

(*Petrache et al. 1998*) H.I. Petrache, S. Tristram-Nagle, J.F. Nagle *Fluid phase structure of EPC and DMPC bilayers*, 1998 Chem. Phys. Lipids 95, 83

(*Petrache et al. 2006*) H.I. Petrache, T. Zemb, L. Belloni, V.A. Parsegian *Salt screening and specific ion adsorption determine neutral-lipid membrane interactions*, 2006 PNAS 103, 21, 7982

(*Peydecastaing et al. 2011*) J. Peydecastaing, C. Vaca-Garcia, E. Borredon Bi-acylation of cellulose: determining the relative reactivities of the acetyl and fatty-acyl moieties, 2011 Cellulose 18, 1015

(*Peydecastaing et al. 2011 II*) J. Peydecastaing, C. Vaca-Garcia, E. Borredon *Interactions with water of mixed acetic-fatty cellulose esters*, 2011 Cellulose 18, 1023

(*Podgornik et al. 1998*) R. Podgornik, H.H. Strey, V.A. Parsegian *Colloidal DNA*, 1998 COCIS 3, 534

(Poulanne amd Halonen 2010) E. Poulanne, M. Halonen *Theoretical aspects of water holding in meat*, 2010 Meat Sci. 86, 1, 151

(*Poppet et al. 2009*) R. Poppet, P. Niemz, S. Croptier *Adsorption and desorption measurements on selected exotic wood species analysis with the Hailwood-Horrobin model to describe the sorption hysteresis*, 2009 Wood Res. 54, 4, 43

(*Razghandi et al. 2014*) K. Razghandi, L. Bertinetti, L. Guiducci, J.W.C. Dunlop, P. Fratzl, C. Neinhuis, I. Burgert *Hydro-actuation of ice plant seed capsules powered by water uptake*, 2014 BBN 3, 1

(*Robinson et al. 1981*) J.B. Robinson, J.M. Strottmann, E. Stellwagen *Prediction of neutral salt elution profiles for affinity chromatography*, 1981 PNAS 78, 4, 2287

(*Salmén 2004*) L. Salmén *Micromechanical understanding of the cell-wall structure*, 2004 C. Biologies 327, 873

(*Schwierz et al. 2010*) N. Schwierz, D. Horinek, R.R. Netz *Reversed anionic Hofmeister series: the interplay of surface charge and surface polarity*, 2010 Langmuir 26, 10, 7370

(*Schwierz et al. 2013*) N. Schwierz, D. Horinek, R.R. Netz *Anionic and cationic Hofmeister effects on hydrophobic and hydrophilic surfaces*, 2013 Langmuir 29, 2602

(*Schwierz et al. 2015*) N. Schwierz, D. Horinek, R.R. Netz *Specific ion binding to carboxylic surface groups and the pH dependence of the Hofmeister series*, 2015 Langmuir 31, 215

(*Sidorenko et al. 2007*) A. Sidorenko, T. Krupenkin, A. Taylor, P. Fratzl, J. Aizenberg *Reversible switching of hydrogel-actuated nanostructures into complex micropatterns*, 2007 Science 315, 487

(*Simpson 1973*) W.T. Simpson *Predicting equilibrium moisture content of wood by mathematical models*, 1973 Wood Fiber Sci. 5, 1, 41

(*Simpson 1980*) W.T. Simpson *Sorption theories applied to wood*, 1980 Wood Fiber Sci. 12, 3, 183

(*Skaar 1988*) C. Skaar *Moisture sorption thermodynamics*, in *Wood-water relations* 1988 Springer-Verlag

(*Spinu et al. 2011*) M. Spinu, N. Dos Santos, N. Le Moigne, P. Navard *How does the never-dried state influence the swelling and dissolution of cellulose fibres in aqueous solvent*, 2011 Cellulose 18, 247

(*Sumi et al. 1963*) Y. Sumi, R.D. Hale, B.G. Ranby *The accessibility of native cellulose microfibrils*, 1963 Tappi 46, 2, 126

(*Trefalt et al. 206*) G. Trefalt, S.H. Behrens, M. Borkovec *Charge regulation in the electrical double layer: ion adsorption and surface interactions*, 2016 Langmuir 32, 380

(*van der Berg and Bruin 1981*) C. van der Berg, S. Bruin *Water activity and its estimation in food systems: theoretical aspects*, in *Water activity: influences on food quality*, 1981 Academic Press

(*Van der Waals 1910*) J.D. Van der Waals *The equation of state for gases and liquids*, 1910 Nobel Lecture

(*Vlachy et al. 2009*) N. Vlachy, B. Jagoda-Cwiklik, R. Vácha, D. Touraud, P.J. Jungwirth, W. Kunz *Hofmeister series and specific interactions of charged headgroups with aqueous ions*, 2009 Adv. Colloid Interface Sci. 146, 42

(*Volkova et al. 2012*) N. Volkova, V. Ibrahim, R. Hatti-Kaul, L. Wadsö *Water sorption isotherms of Kraft lignin and its composites*, 2012 Carbohyd. Polym. 87, 1817

(*Wang et al. 2014*) J. Wang, P. Mukjopadhyaya, P. I. Morris *Sorption and capillary condensation in wood and the moisture content of red pine*, 2014 J. Bldg. Phys. 37, 4, 327

(*Weinkamer and Fratzl 2011*) R. Weinkamer, P. Fratzl *Mechanical adaptation of biological materials - the examples of bone and wood*, 2011 Mat. Sci. Eng. 31, 1164

(*Xiao and Song 2011*) T. Xiao, X. Song *A molecular Debye-Hückel theory and its application to electrolyte solutions*, 2011 J. Chem. Phys. 135, 104104

(*Zavitsas 2001*) A.A. Zavitsas *Properties of water solutions of electrolytes and nonelectrolytes*, 2001 J. Phys. Chem. B 105, 7805

(*Zhang et al. 2002*) L.N. Zhang, D. Ruan S.J. Gao *Dissolution and regeneration of cellulose in NaOH/thiourea aqueous solution*, 2002 J. Polym. Sc. Polym. Phys. 40, 1521

2. Impregnation and swelling of wood with salts: ion specific kinetics and thermodynamics effects

A. Barbetta, P.Fratzl, T. Zemb, L. Bertinetti, 2016 Adv. Mater. Interfaces

DOI: 10.1002/admi.201600437

The effects of salt impregnation are studied within wood cell walls, occurring upon soaking from concentrated salt solutions. Osmotic de-swelling is in some cases followed by ion specific swelling linked to Hofmeister effects. Taking into account microstructure, this study models the free energy changes associated with the ions and water uptake at molecular, colloidal, and macroscopic mechanical scales, to show that slow swelling until osmotic equilibrium originates from charge separation of the salt diffused into wood cell wall material. Kinetic effects as well as mechanical effects linked to transfer of species and swelling of the interstitial matrix between cellulose crystals are discussed. Predictions by minimal models taking into account non-electrostatic ion complexation allow to estimate the order of magnitude of the non-electrostatic binding free energy of adsorbed chaotropic anions and complexed divalent cations to be 8 and 10 kJ mol^{-1}, respectively.

2.1 Introduction

Swelling of a colloidal solution or gel by uptake of water is an important phenomenon to be understood and mastered in chemical and materials engineering. Salt-induced swelling of meat was discovered and studied by Hofmeister (*Poulanne and Halonen 2010*) in the late 19th century while investigating alternative ways of sterilization (*Kunz et al. 2004*). Water-holding in meat causes swelling of the myofibril and is controlled by electrostatic and osmotic forces. Different anions and cations have different capacities of inducing swelling, according to the Hofmeister series, which was elaborated in the 1880s with the idea of classifying ions according to the strength of their interaction with water, beyond electrostatic effects. The concept of chaotropes and kosmotropes, as well as the hard–soft classification of ions elaborated in the seventies, allows only qualitative and semi-quantitative considerations about ion properties, since no intrinsic quantitative scaling could be introduced (*Kunz and TIddy 2009*). The matching affinity concept introduced by Collins (*Collins 1997, Collins 2004*), and then thoroughly described by Jungwirth and Kunz, can be considered the first attempt to quantify these effects, as it correlates the tendency of oppositely charged ions to form ion pairs in water to the absolute free energies of hydration. The predictive theories were extended to the case of surfaces covered with charged groups by the concept of matching affinity (*Vlachy et al. 2009*), and finally to partially hydrophobic patchy surfaces by Schwierz et al. (*Schwierz et al. 2010*). These two extensions of initial theories taking quantitatively into account dispersion forces, volume effects as well as entropic effects, allow to explain the frequently observed and unexplained inversions of Hofmeister classification (*Schwierz et al. 2013*). In this context, a useful distinction between polarization and size effects has been introduced by Leontidis and co-workers in their studies of lipid interfaces with different curvatures (*Aroti et al. 2007*). The theory and understanding of swelling of colloidal gels or hybrid materials has been recently extended by introducing the idea of a heterogeneous interface limiting the bulk water, considered as an interface constituted by a hydrophobic phase surface that deforms upon depletion of kosmotropic ions, and a charged hydrophilic phase surface, where ion-pair matching matters (*Schwierz et al. 2013, Schwierz et al. 2015*). This situation is similar to the case of emulsification via antagonistic salts studied by Onuki: if a combination of hydrophilic cation and hydrophobic anion (or the reverse) are located at the interface of two partially miscible mixed fluids, charge separation occurs and the low surface tension leads to spontaneous emulsification.

In this case, the surface has homogeneous properties (*Onuki et al. 2011*). This has been generalized, if the surface is patchy, in the work by Schwierz et al. mentioned before.

In the interaction between partially dehydrated ions adsorbed in the wood cell wall material, *i.e.* in our case monovalent chaotropic anions, a dispersion term is present, but does not have a dominant role (*Lima et al. 2008*). This term must be taken into account together with Van der Waals screening, due to the presence of a generated electric double layer, and with a (modified) hydration force term to explain the temperature-dependent swelling of liposomes by salts (*Petrache et al. 2006*).

In this paper, we aim to qualitatively and quantitatively discuss these effects as observed in the swelling of wood upon soaking in electrolyte solutions. We consider the "primitive level" of model, *i.e.* we regard water as a homogeneous medium. Then, the swelling can be treated as an "Equation of State". Osmotic pressure (OP) is counted with analogy to the gases studied by Boltzmann, as the pressure term is combined to the molar volume of the dissolved colloid. The Nobel prize work by Jean Perrin considered osmotic pressure of a dispersion of micron-sized solidified emulsions to determine the Boltzmann constant and hence the Avogadro number by establishing the Equation of State, including gravity as an external field (*Perrin 1913*). A large number of partial or global swelling behaviors, analyzed in the form of equations of state, have been established since the revival of this approach by Jean Perrin, considering multi-lamellar liposome swelling (*LeNeveu et al. 1976, Le Neveu et. al 1977*). In this work, the link between the chemical engineering approach, based on establishing water uptake versus relative humidity, and the colloidal approach (*Chan et al. 2015*)— now more often designed as "nano-science"— determining the osmotic pressure versus volume differences at known chemical potential of solutes such as salts or osmolytes, is determined experimentally for different salts during impregnation of compression wood by concentrated salt solutions. At equilibrium, in the absence of any semi-permeable membrane at the macroscopic wood surface, and if there is no charge separation of the impregnated salt, swelling, and de-swelling are not observed. Conversely, swelling in the presence of buffers and other solutes is qualitatively understood in terms of a molecular force balance (*Zemb and Leontidis 2013, Zemb and Leontidis 2014*). Studies of kinetics and equilibrium behavior versus salt activity directly demonstrate that charge separation occurs (*Petrache et al. 2006*), where charge separation refers to the adsorption of one of the ionic species at the surfaces while the counter ions remain in the bulk water at the mid-plane between surfaces.

We stress that osmolarity and not the molarity has to be considered (*Wolfe and Bryant 1992*) in order to model the effects of salt swelling in terms of electrostatic swelling due to selective non-electrostatic adsorption of one of the two ions to the interface, which is represented by an excess free energy of adsorption of one of the ions of the salt on a given interface inside the colloidal system (*Leontidis et al. 2009*). Similar Equations of State in the presence of salts have been established previously. In the case of latex in the presence of monovalent and multivalent co-ions, the extraordinary influence of electrolytes, in a concentration in the order of nanomoles per liter, has been determined and explained (*Reus et al. 1999*). Moreover, the long range effects of the presence of an elusive "corona" of polyelectrolyte multilayers at the surface of colloidal particles have been investigated by the osmotic stress technique (*Dubois et al. 2006*). Wood cell walls as well as condensed DNA phases locally show hexagonal symmetry, and theoretical expressions of osmotic and hydration forces are available in this case (*Strey et al. 1997, Podgornik et al. 1998*), as well as in the one of liposomes of charged and uncharged lipids (*Dubois et al. 1998, Demé and Zemb 2011*).

Interestingly, wood cell walls, as solids, have a characteristic property: due to long range interactions, the mechanical energy has to be considered and added to the classical chemical and colloidal terms in the master equation governing the conservation of the free energy (*Bertinetti et al. 2013*).

Wood is a cellular, heterogeneous, anisotropic, hygroscopic material of colloidal size ultrastructure. Wood material is characterized by inert, stiff crystalline cellulose nano-fibers (35%–50%) parallel to each other and of diameter of about 2.5 nm, embedded in a softer, less anisotropic polymeric matrix of hemicelluloses (20%–35%) and lignin (10%–25%), and water (*Fengel and Wegener 2003*). The distribution of the matrix polymers between the cellulose crystals is not precisely known, although several hypotheses have been formulated in recent studies(*Fratzl et al. 2008, Burgert and Dunlop 2011*). For this reason, we do not distinguish between the matrix polymers and we consider the cellulose crystals to be embedded in a homogeneous matrix (**Fig 2.1.1a**). In dry conditions, the intercrystalline space is filled only by matrix polymers, while as the hydration raises the distance between the cellulose crystals increases as well and the complex fluid in the intercrystalline gap becomes a concentrated aqueous solution of hemicelluloses and lignin. Here, we will simplify this fluid assuming that cellulose crystals remain "coated" by a layer

of matrix polymers and a water layer is formed at the interface between these cellulose/matrix polymers bundles (**Fig 2.1.1b**).

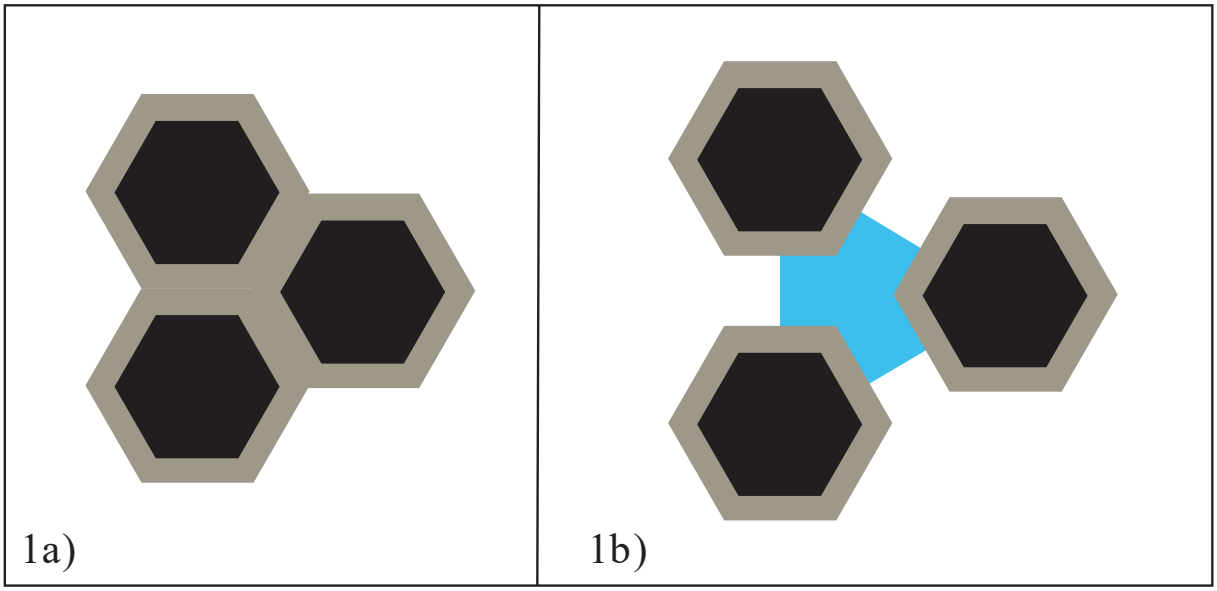

***Fig 2.1.1**: Model of the cross-sectional view of wood material: crystalline cellulose nano-fibers, in black, are embedded in a matrix (grey) of hemicelluloses and lignin. a) dry b) as the hydration increases, the distance between cellulose fibers increases as well and a water layer is formed between cellulose crystals/matrix polymers bundles.*

Using this simple model of the structure at nanometric scale we can decompose the molecular forces, as the sum of chemical, colloidal, and mechanical partial free energies and balance them with the water chemical potential (*Bertinetti et al. 2013*).

In the current work, experimental data of swelling of wood samples immersed in salts solutions of fixed osmotic pressure are collected with a tensile device. Absorption of different salts within the wood cell walls is described. We distinguish between transient and equilibrium states, and examine the consequences for wood swelling. A coarse-grained predictive model including electrostatic terms at the colloidal scale is discussed.

2.2 Results and discussion

Fig 2.2.1 shows typical strain changes upon soaking wood samples in different electrolytic solutions. In the first case (Fig **2.2.1a**) a sample immersed in a solution with monovalent cation, NaI, immediately undergoes positive swelling. After about 2 h, the sample was washed with water. This resulted in a fast partial shrinkage. Interestingly, in the case of divalent ions ($CaCl_2$, **Fig 2.2.1b**), the swelling due to the presence of the salt is preceded by a fast significant shrinkage of the material, of about 0.2%, which occurs within the first 2 min after immersion. The difference in swelling dynamics underlies a difference in ions/cell walls constituents interactions. The observed dynamics, in fact, is due to the combination of two phenomena: osmotic compression due to the initial osmotic pressure of the surrounding electrolytic solution, that induces water to flow out of the material, and salts diffusion within the cell walls, that, as experimentally observed, induces a volume increase. In the case of monovalent ions, these two processes occur at the same time. On the other hand, the fact that they are distinguishable in presence of divalent ions indicates that these diffuse more slowly than electrolytes with monovalent cations.

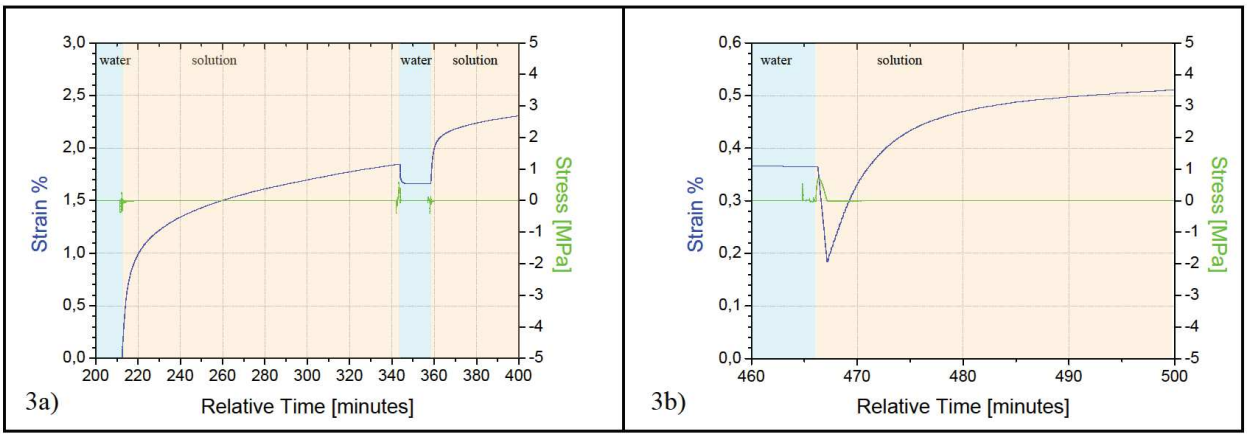

***Fig 2.2.1**: a) Detail of the swelling profile for a sample immersed in a solution with monovalent ions (NaI) b) Detail of the swelling profile for a sample immersed in a solution with a divalent ion ($CaCl_2$).*

The mathematical description of water and solute diffusion into the wood tissues is rather complex, as the material is organized into several hierarchical levels, that have different geometries, and it is out of the scope of this paper. However, in literature, water diffusion in wood

has been described using Fick's laws and analyzed with exponential decay models (*Time 1998*). For this reason, by fitting the strain curves of different salts after the first immersion in solutions with an exponential decay model, we can evaluate characteristic time constants for each solution and compare the diffusion behavior of the different ionic couples.

In **Fig 2.2.2** we present, for a series of salts, their diffusion coefficient in aqueous medium versus the characteristic time constant t1 obtained by fitting the strain changes, which gives semi-quantitative indications about the diffusion of each salt in wood.

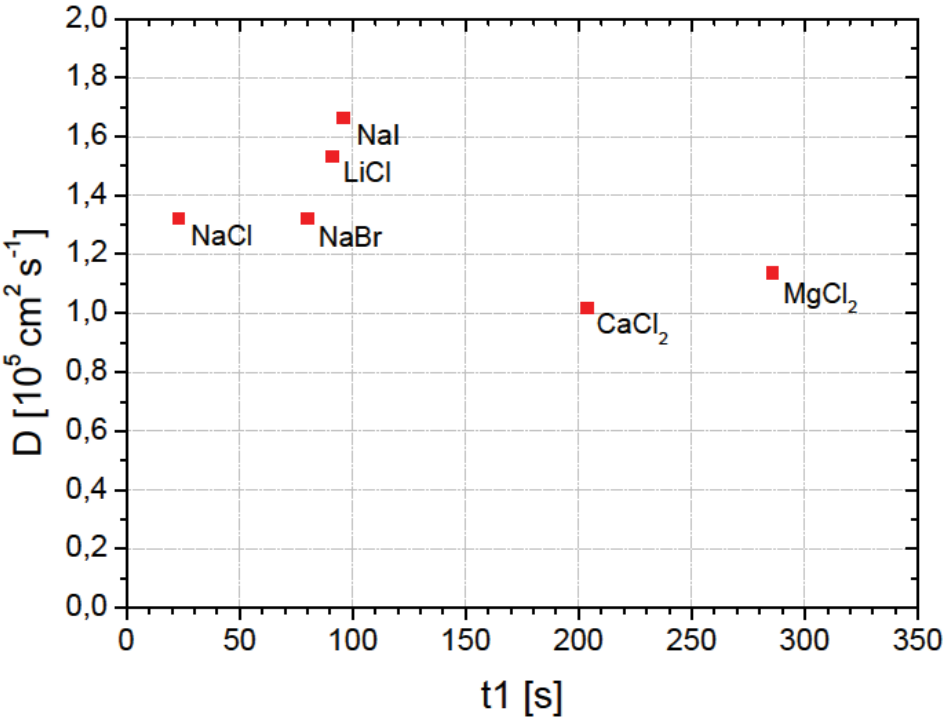

***Fig 2.2.2**: Diffusion coefficients in water and time constants for diffusion in the material are plotted for different salts.*

It can be observed that monovalent and divalent ions behave differently. Similarly to the case of salts in resin columns, where in the gels the travel velocity of electrolytes and their sorption time are influenced by ionic valence, we notice slower diffusion for divalent ions. This means that, for the solutions considered in this work, the divalent cation is the one with the higher influence on the diffusion kinetics. This can be understood considering that they have a bigger hydration sphere, which is not withdrawn during diffusion, and that double positive charged ions interact

more strongly with the hydroxyl groups of the polysaccharides, therefore diffusing slower than monovalent ones.

Apart from the kinetic aspects of the impregnation, the partial irreversibility observed after washing with water, *e.g.* up to 0.3% strain for samples treated with the NaI solution, indicates that (1) ions don't act simply as osmotic agents from outside the wood material, otherwise a complete cycle would not induce swelling, but rather they are able to diffuse inside the tissues and (2) they are irreversibly adsorbed at the interface between the wood constituents.

The maximum swellings near equilibrium reached after several cycles of 2 h immersion in solution are reported in **Fig 2.2.3**. It is worth noticing that comparable results are obtained with one single, much longer, immersion of 72 h. The immersion of samples in ion solutions determines a positive strain, *i.e.* promotes swelling of wood tissues, in the case of all the electrolytic solutions considered in this work. The largest strain values are observed in the case of NaI and $CaBr_2$, and reach respectively 3% and 2.5%, and the trends seem to follow the Hofmeister series.

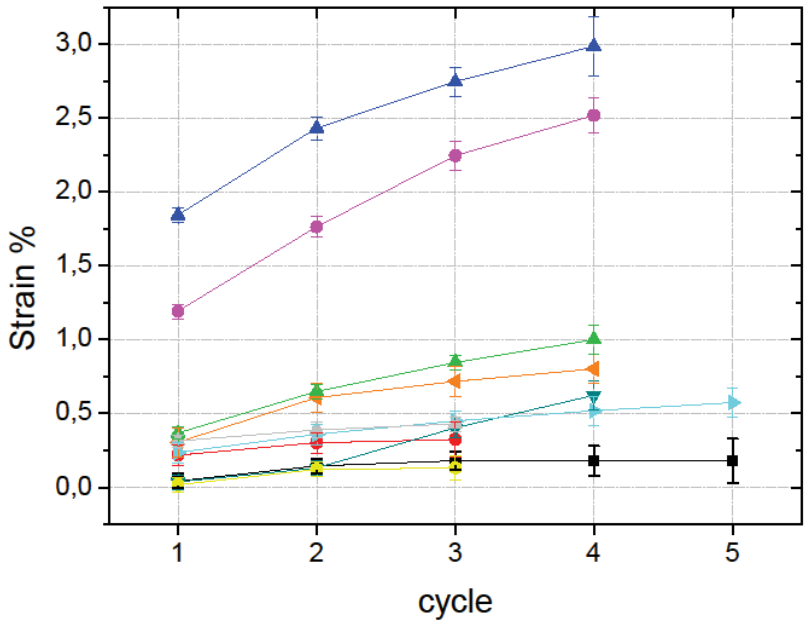

***Fig 2.2.3**: Mean axial strain after serial salted solution immersions of compression wood foils, reported as a function of the number of cycles of washing. A cycle consists of immersing the sample in salted solution and washing it with water after equilibration. NaI (blue), $CaBr_2$ (magenta), $MgBr_2$ (green), CsCl (orange), LiCl (dark cyan), $CaCl_2$ (cyan), CsBr (grey), NaBr (red), NaCl (black), $MgCl_2$ (yellow).*

The original Hofmeister series aimed to empirically rank electrolytes according to their salting-in or salting-out ability in different systems, such as proteins, colloids, collagen. During the years, the series proved to be valid in a wide range of physical and chemical adsorption processes at surfaces (*Zhang 2010*), despite the controversial lack of a predictive quantification at a molecular level (*Schwierz et al. 2015*), as ion behaviors are hard to be described with one single parameter. As a general statement, in the Hofmeister classification salts are defined depending on their capacity to interact with water more weakly than water with itself (chaotropic ions) or to have the opposite behavior (kosmotropic ions). From the analysis of the results, we find that swelling is more pronounced if the salts are made by one chaotropic and one kosmotropic ion, as in the case of NaI or $CaBr_2$, where the maximum strain values reached after four cycles of washing are respectively 3.0 ± 0.2% and 2.5 ± 0.1%. One way to understand the ensemble of the swelling results is to consider that molecular interactions between ions and water molecules as well as between ions and wood constituents lead to selective adsorption: for monovalent electrolyte solutions, during the adsorption process the chaotropic ion (*e.g.* I^-) can easily lose its hydration sphere and is ejected from bulk water, while the kosmotropic one (e.g., Na^+), preferentially remains hydrated in bulk water. At the hard solid surface–water interface, which in this case can be partially hydrophobic either because of cellulose crystals or because of the lignin, chaotropic ions adsorb, while the one with the opposite charge stays in the more hydrated space between the crystals. This causes charge separation, that in turn produces a net electrical field at the interface, that generates a repulsive force between cellulose crystals. As a result, the mean distance between the crystals increases and so does the hydration of the material. For the sake of simplicity, we will consider the ions to adsorb on the matrix layer around cellulose crystals (**Fig 2.2.4**).

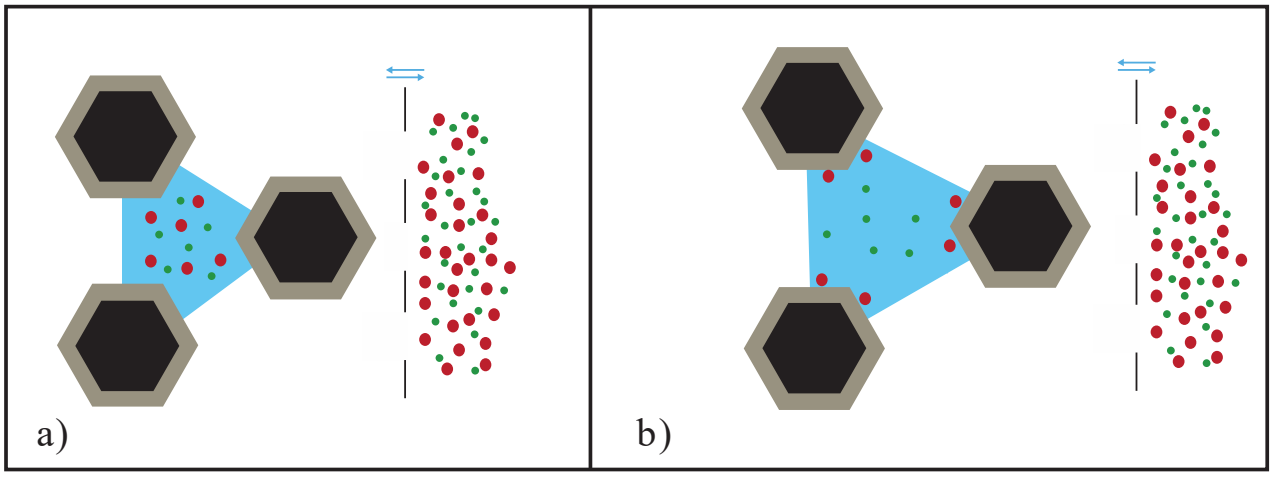

***Fig 2.2.4**: Ions are introduced by equilibration with a solution used as osmotic reservoir. I- chaotropic ion (in red) are ejected from bulk water and adsorb on the matrix layer (grey) around the cellulose crystals (black), while Na^+ kosmotropic ion (in green) preferentially stay in bulk water. Therefore, salts constituted by one chaotropic and one kosmotropic ion (NaI, $CaBr_2$) induce charge separation and cause the maximum swelling (b). Swelling is limited in case of salts made of ions with similar characteristics in the Hofmeister series, when no specific adsorption occurs (a).*

The situation is different when divalent cations are involved, as already discussed, because divalent cations (Ca^{2+} and Mg^{2+}) are able to chemically bind the surface of the cellulose crystals via bidentate complexation (*Schneck et al. 2011*). This produces a net positive charge, and from there the principle of matching affinity plays a role. The anions matching with calcium and magnesium will reduce the charge and the swelling, while those ions that match less to the bound calcium will produce a larger swelling, and therefore the charge separation is stronger. Within this framework, the axial strain will not depend only on the valency of the ions, but mostly on the difference between the non-electrostatic surface adsorption properties of the two ions of the salt investigated: swelling is limited when ionic hydration properties are similar and no specific adsorption occurs in presence of salts made of two kosmotropic ions (e.g., 0.2 ± 0.1% strain for samples immersed in a NaCl solution, 0.3 ± 0.1% in a NaBr solution, 0.5 ± 0.1% in a $CaCl_2$ solution) as well as in presence of salts made of two chaotropic ions. Specimens treated with CsBr, which is constituted by two adsorbable chaotropic ions, undergo a low 0.4 ± 0.1% strain, since these two ions are both adsorbed at the surface and there is no induced swelling. This illustrates the general principle of antagonistic salts, according to which the maximum effect is given by the combination

of a chaotrope and a kosmotrope, rather than by the specific characteristic of the single ion in solution (*Collins 1997, Collins 2004, Onuki et al. 2011 II, Onuki and Araki 2012*).

It is well known that wood materials undergo drastic reactions in alkaline medium, which include dissolution of undegraded polysaccharides, alkaline hydrolysis of glycosidic bonds, degradation, and decomposition of dissolved polysaccharides, etc. The first step in this process always involves the deprotonation of hydroxyl groups by OH− ions, which induces large swelling (*Fengel 2003*). The fact that some of the solutions used have higher pH than others could have been the main reason of the higher strains measured. To test this hypothesis tensile experiments with a sample immersed in a pH=12 medium, produced by 10×10^{-3} m NaOH solution, has been performed in order to evaluate the effect of a strong base on the swelling of cellulosic material. The results show the specimen to undergo a 0.9% strain after a period of 30 h of equilibration (**Fig 2.5.1**, Supporting information). Although strong bases charge the surface of the cellulose crystals, they produce a smaller swelling than some of the antagonistic monovalent salts investigated in this study: impregnation by NaOH produces only one third of the macroscopic swelling with respect to sodium iodide, while pH is four units higher for NaOH than for NaI. This allows to rule out a significant effect of pH on the swelling induced by salts solutions.

2.2.1 Equation of state

Observed results gave important qualitative indications concerning the mechanisms of electrolytes sorption in wood materials and led to the development of the discussed model, based on charge separation. In order to perform quantitative analysis, one has to take into account all the molecular forces in play.

Water uptake in wood and relation between anisotropic swelling and osmotic pressure variations can be represented by a general Equation of State, that links OP to the distance between the cellulose crystals in wood cell wall materials (*Bertinetti et al. 2016*). Starting from the cell wall micro-structural model described in **Fig 2.1.1**, structure and composition of the material are taken into account to develop a model with chemical and mechanical contributions to predict the effects of ions adsorption and resulting charge separation. The force balance leads to the development of the EOS, in which molecular and macroscopic forces between wood building blocks, that are responsible for the solvent uptake, are independently considered and then summed. This multi-scale approach includes a microscopic chemical contribution due to the chemical binding

difference between the hemicelluloses and the crystalline fibers. At a colloidal scale, hydration force between cellulose crystals through the inter-crystalline matrix and configurational entropy of hemicelluloses are evaluated. A macroscopic mechanical term must be also taken into account, considering that the matrix swells anisotropically because of the presence of the stiff cellulose fibers. Results of the calculations are in reasonable agreement with experimental results of sorption and desorption, apart from a little hysteresis and in the limit of the experimental error.

As salts can diffuse inside cell walls, water chemical potential in the reservoir and in the matrix equilibrate. Moreover, at the equilibrium, the water activity in the reservoir and the colloidal sample are by definition equal, while the concentrations are not. For this reason, observed swelling is only caused by charge separation effects, due to specific excess adsorption of the anion over the cation (or the reverse).

This electrostatic term, due to the presence of electrolytes, is added supposing that dominant charge separation occurs at the surface of the structure described in **Fig 2.2.4**, made of cellulose and a matrix layer. Divalent cations are known to be complexed by hydroxyls and produce an excess of positive charge at the cellulose surface. This effect is independent from ion specific Hofmeister effects. The calculation approximates adjacent cellulose crystals as two infinite parallels planes, separated by a matrix layer of a known thickness, in osmotic equilibrium with a salt solution reservoir. Equations used for this case of charge regulation (*Parsegian and Ninham 1973, Belloni 1986, Belloni 2000*), where charge separation is driven by a specific ion adsorption effect and is represented by a binding free energy ΔG, are explicated in Supporting information for planes in low charge approximation. The equilibrium between ions and adsorbing sites follows the law of mass action (**Eq 2.9** in the Supporting information) and is characterized by specific binding constants K.

The first step in terms of free energy for the ions adsorption quantification is made by the following evaluation (*Bertinetti et al. 2016*), with and without the electrostatic term due to charge separation. One of the ions is bound via a binding constant K to a site. All sites at the surface are counted equivalent and with an area Σ of 1 nm^2. The thickness of the layer δ for which non-electrostatic attraction comes in play is set to 0.5 nm, independently of ionic sizes. To avoid introducing other parameters, the nonbinding ion is assumed to have a binding constant of 1/1000 of the dominant binding one. This ensures that the whole swelling depends only on one physical quantity, the free energy of binding of the dominant ion (*Petrache et al. 2006*). The equilibrium for

the remaining ions follows Poisson–Boltzmann distribution. In this case, the link between the binding constant of the dominant ion and the gain in free energy associated to bringing one ion from bulk water to the surface is given by **Eq 2.1**

$$K = \Sigma\delta e^{-\Delta G_s/RT} \qquad \textbf{Eq 2.1}$$

where ΔG_S is the binding energy in J mol^{-1}.

Introducing explicit binding constants, the explicit extra swelling δ^* (*i.e.* $D - D_w$, intended as the difference between cellulose crystals distance after treatments with electrolytes and the distance after first wetting) is calculated for the different strengths of ion binding to the initial neutral surface and the results are reported in **Fig 2.2.5**. The free energy of apparent binding of chaotropic ions to a charged lipid interface has been quantified by Aroti and co-workers and was found to reach about –6 kT (*Aroti et al. 2007, Leontidis et al. 2009*). Obtained values for ΔG_0 are in our case positive, thus the binding of ions at the interface with neutral sugars or aromatic moieties results to be much weaker. Nevertheless, as the concentrations used in this work are much higher (15 osm), the site occupation can reach 10% (Fig **2.5.2** in the Supporting information).

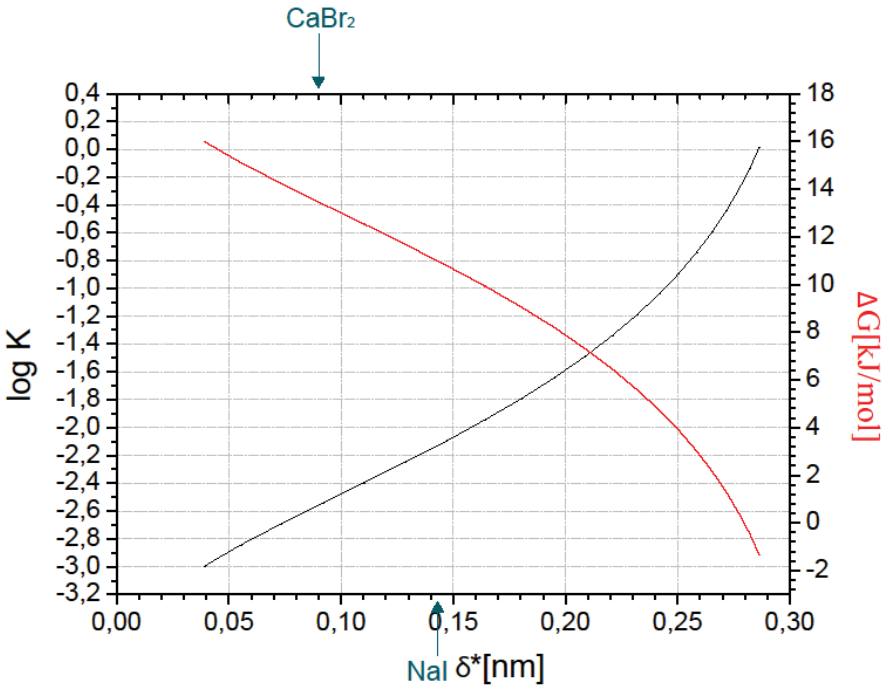

Fig 2.2.5: *Equilibrium constant K [M]$^{-1}$ for the ions adsorption at the interface (black) and free energy of binding (red) are reported as a function of the crystals extra swelling for a 15.2 osm solution.*

The model allows also to calculate the values of δ^* for different K at several ions concentrations. This can be then compared to swelling experiments performed on samples soaked in solutions of increasing concentration of salts, thereby exploring the electrolytes influence from the millimolar range to the reference concentration. In **Fig 2.2.6a**, a typical swelling isotherm for NaI is reported in terms of axial strain (black squares). On the same graph, in green, the intercrystalline strain ε_D *(i.e.* δ^*/D_w) for cellulose crystals as measured by SAXS (small angle X-ray scattering in the Supporting information) for the sample in equilibrium with [NaI] = 15 osm is also reported. As expected, ε_D is larger than the macroscopic axial strain of the wood slice, ε_x. The extra swelling predicted from the model for the same concentration range is reported in **Fig 2.2.6b** for different values of K. There, we report also (black squares) the rescaled values of ε_x (where we consider that an ε_x of 3% corresponds to a ε_D of about 5.3% for the most concentrated solutions) so that we can directly compare the results of the calculations of the extra swelling induced by the salts with the experimental ones.

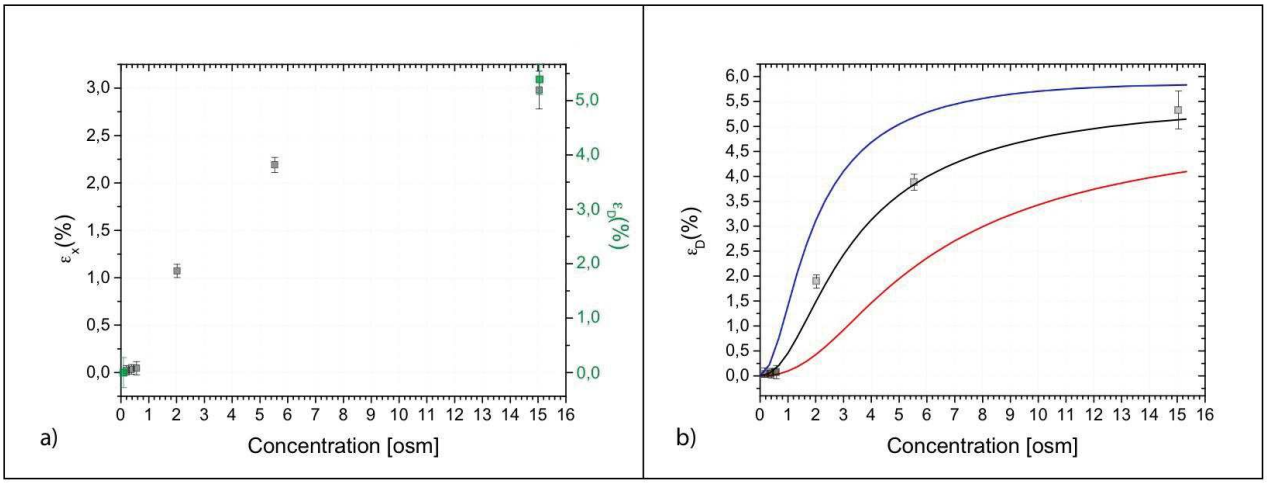

Fig 2.2.6*: a) Mean axial strain (ε_x) of wood foils after immersion in solutions of NaI (black squares) as a function of salt concentration. Green squares refer to the center-to-center strain for cellulose crystals as measured by SAXS for the samples equilibrated in water and in the most concentrated salt solution b) Calculated inter-crystalline strain$\varepsilon_D = (\delta^* - D_w)/D_w$ as a function of increasing NaI concentration for different equilibrium constants (blue, black and red respectively for K equal to 0.1, 0.035 and 0.015 M^{-1}). The experimental axial strains are converted in inter-crystalline strain (black squares) as described in the text and compared with the predictions of the model.*

The charge regulation model used here captures the observed swelling isotherm quite satisfactorily for K = 0.035 M^{-1} (**Fig 2.2.6**). This suggests that this model can be successfully applied for wood cell wall hybrid materials and can be used to get a good estimate for the standard free energy of adsorption of the ion pairs extracted from the reservoir, i.e., the lumen, to the wood cell wall, associated to the charge regulation process. In the case of NaI this is about 8 kJ mol^{-1}.

2.3 Conclusion

We measured the effects of solution uptake by wood cell walls with different electrolytes. In all cases, the presence of monovalent or divalent ions produces a positive strain, which can be monitored and quantified with a tensile stage that measures the axial strain of the sample in response to its immersion in water and in solutions. Salts have specific effects on swelling, depending on their composition, concentration, pH. Interestingly, the maximum swelling is induced when the salt is made by one chaotropic and one kosmotropic ion. The main driving force of the sorption process is the charge separation of the electrolytes due to specific adsorption of divalent cations or chaotropic anions on the crystalline cellulose nanofibers.

The use of **Eq 2.1** assimilating the surface concentration and bulk concentration to a Boltzmann factor requires to define a thickness of the interface for which an ion is subject to non-electrostatic effects. This distance, as the thickness of the interface, must be defined self-consistently (*Ninham and Parsegian 1971*) in charge regulated interfaces. In this work, we define the distance to the interface as the average hydrated ion radius and set this to 0.5 nm. Within this framework, the free energies of charge separation and adsorption from the bulk are estimated to be of the order of ≈ 3.2 kT (8 kJ mol^{-1}) for the most antagonistic salt investigated here (NaI). In the case of salts containing divalent cations, calcium or magnesium, the induced swelling is due to weak cations bindings to the hydroxyl groups located at the surface of cellulose crystals.

No interface sites are occupied in the case of NaCl, a “neutral” salt in the Hofmeister series, while the sites occupation ratio can reach 10%–20% in the case of NaI. The latter corresponds well to the order of magnitude observed on dispersed microcrystalline cellulose (*Chiang et al. 1994*).

To our knowledge, this is the first quantitative evaluation of the effects of impregnation of wood cell wall by electrolytes: only one physical quantity is needed, *i.e.* the effective free energy of binding of the dominant ion that adds an electrostatic term coming from nonelectrostatic interaction (*Levin 2002*). This extra electrostatic term due to charge separation allows to understand the initial transient kinetics as well as the equilibrium excess swelling induced by salts solutions.

2.4 Experimental section

Spruce (*Picea abies*) compression wood slices 150 µm thick were cut along the longitudinal direction of the tree with a Leica-rm2255 microtome, and immediately stored in a freezer (–20 °C temperature) to keep the material in its natural conditions. Specimens were unfrozen at 4 °C before the beginning of experiments.

The length changes of the slices at constant force using a tensile device were measured as sketched in **Fig 2.4.1**. The sample was fixed in between two aluminum clamps, and fitted in a Plexiglas cuvette of a 20 mL volume, allowing the samples to be completely immersed in solution continuously for the whole experiment. On one side a 5 N load cell (Honeywell 31E) measured the axial tensile force, while on the other side a stainless-steel arm could be driven along the same axis via a PI M-126.DG1 linear motor stage, which controlled the strain. A custom written software allowed the system to drive the motor either to control the strain or to keep the force constant.

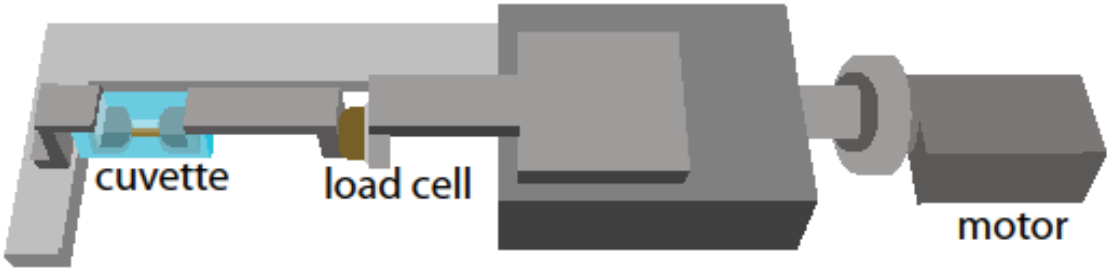

Fig 2.4.1: *Tensile stage for in-situ measurements of osmotically driven wood swelling in fully hydrated conditions. The load cell (brown) allows the user to control and measure the axial tensile forces, while the linear motor (right part of the stage) controls and measures the strain.*

This setup allowed measuring the axial length changes the sample underwent, which were related to tissue volume changes (*i.e.* swelling). Tests were performed under force control: a wet sample of a typical length of 30 mm approximately and width of 3 mm was clamped and immersed in MilliQ water. In a typical experiment a de-frozen wood sample was equilibrated under 0 N force overnight. During that time significant swelling occurred, up to 3% of its length. The length of the macroscopic sample was considered at equilibrium after first immersion to be the reference to compute the sample strain. Samples were then immersed cyclically in water and then in salt solutions for periods of 2 h, and their strain were plotted as a function of the number of cycles.

Solutions were prepared with salts (Alfa Aesar) just before the experiments. Swelling of tissues was heavily influenced by the OP of the surrounding solution, and solutions of different salts exerted a significant OP depending on the nature of the ions, their stoichiometry, and their concentration. Therefore, this study worked with solutions of constant osmotic pressure, even with different concentrations, in order to be able to quantitatively compare results for different salts. This was possible by choosing the osmotic pressure generated by a saturated NaCl solution (6.10 M) as reference, where the water activity is 0.76, corresponding to a 37.7 MPa OP (15.2 osm). For the other salts, the different values of the osmotic coefficients at different concentrations were taken from literature and then fitted to calculate the concentrations at which these solutions produced the same OP than the NaCl one, within the limits of the experimental error (±0.04 in water activity). pH of the solutions was measured with a Mettler Toledo FE20 FiveEasy pH meter. Calculations and relevant characteristics of the solutions are reported in **Table**

2.1 in the Supporting information. Diffusion coefficients at given concentrations were obtained by fitting values available in literature.

Small angle X-ray diffraction experiments were performed at μ-spot beamline of the BESSY II synchrotron radiation facility in Berlin. In the setup, the primary beam coming from a 7T wavelength-shifter (λ = 0.689 Å, E = 18 keV) was hitting the sample and the scattered signal was collected on a 2D MarMosaic 225 detector. Beam size was controlled by a 50 μm pinhole. Sample-detector distance was 840 mm, calibrated using a silver behenate standard. Compression wood samples, pretreated overnight with different salts solutions, were measured in hydrated state thanks to a custom built metallic frame equipped with plastic windows on the sides, which allowed them to stay immersed in a thin water layer (0.2 mm) during the whole experiment. Several measures of the same samples, in different points, were taken. Typical measuring time was 120 s for each point.

2.5 Supporting information

2.5.1 Salt solutions properties

SALT	Concentration [M]	Relative Humidity [%]	Osmotic Pressure [MPa]	pH	Diffusion Coefficient in water [10^5 cm^2s^{-1}]
NaCl	6.10	76	37.7	6.15	1.32
NaBr	5.01	78	34.2	6.50	1.32
NaI	4.70	78	34.2	8.43	1.66
LiCl	4.40	77	35.9	6.09	1.53
CsCl	6.56	75	39.6	6.99	2.31
CsBr	6.23	79	32.4	6.36	2.09
$CaCl_2$	2.65	80	30.7	4.89	1.02
$MgCl_2$	2.51	79	32.4	5.08	1.14
$CaBr_2$	2.47	80	30.7	7.56	1.01
$MgBr_2$	2.32	78	34.2	6.53	1.11

***Table 2.1**: Relevant characteristics of the salts used for experiments.*

2.5.2 pH effect

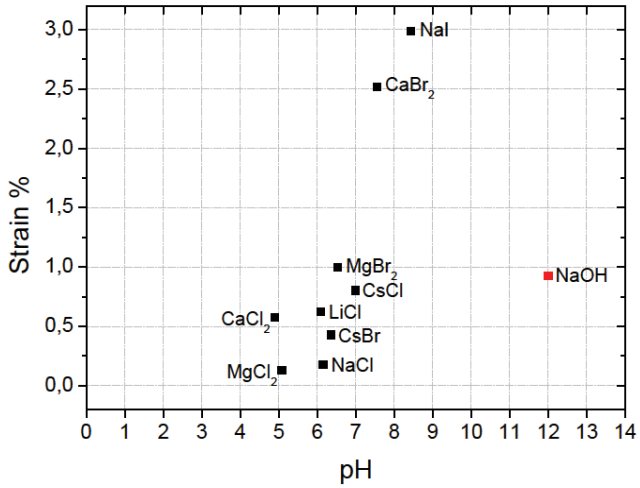

***Fig 2.5.1**: Tensile strains of different salt solutions at their established concentration reported as a function of pH.*

2.5.3 Electrostatic term added to the Equation of State describing swelling induced by charge separation

Evaluation is performed starting from the Poisson-Boltzmann equation in the weak overlap approximation (the water layer $D - D_0$ is larger than the Debye length, where D_0 is the crystal distance in dry conditions). In this case, the interaction is simply due to electrostatic properties next to an isolated plane. The result is:

$$\Pi = 64kTc_s'\gamma^2 e^{-\kappa(D-D_0)} \quad \textbf{Eq 2.2}$$

$$E = 64kTc_s'\gamma^2 e^{-\kappa(D-D_0)}/\kappa \quad \textbf{Eq 2.3}$$

where $c_s^{'}$ is the total concentration of salt (supposing that ions are monovalent),

$$\kappa = \sqrt{8\pi L_B}c_s' \quad \textbf{Eq 2.4}$$

is the screening length (L_B= Bjerrum length),

$$\gamma = \tanh({}^{\varphi_s}/_4) \quad \textbf{Eq 2.5}$$

is a coefficient related to the electrostatic potential φ_s at the surface plane

$$\varphi_s = {}^{e\psi_s}/_{kT} \quad \textbf{Eq 2.6}$$

where ψ_s is the surface potential, which is related to the surface charge density Σ_s via the Graham equation:

$$\sinh({}^{\psi_s}/_2) = {}^{2\pi L_B \Sigma_s}/_{\kappa} \quad \textbf{Eq 2.7}$$

Ion adsorption on surface sites follows the Law of mass action. Let us call $\Sigma_0$the surface site density (so that ${}^1/_{\Sigma_0}$ is the surface occupied by one single site) and Z_0 the initial charge of every site, in units *e*. We imagine that every ion *i* is potentially capable to adsorb on a site via the reaction:

site + ions $\rightleftarrows$ *site-ion* **Eq 2.8**

regulated by the Law of mass action:

$$K_i = {(site - ion)}\Big/{(site)(c_i(surf))} \quad \textbf{Eq 2.9}$$

where K_i, the equilibrium constant, is given. The ion concentration at the plane of contact is

$$c_i^{'} e^{(-Z_i \varphi_s)} \quad \textbf{Eq 2.10}$$

where $c_i^{'}$ is the concentration of ion *i* in the reservoir and Z_i its valence (supposed to be ±1). We define α_i as the occupation rate of sites by the ion *i*, so that

$$K_i = {\alpha_i}\Big/{(1 - \sum_j \alpha_j) c_i^{'} e^{(-Z_i \varphi_s)}} \quad \textbf{Eq 2.11}$$

The surface charge density can be obtained by summing all the contributions *i*:

$$\Sigma_s = \Sigma_0 (Z_0 + \sum_j \alpha_j Z_j) \quad \textbf{Eq 2.12}$$

The solution of the three coupled Equations **Eq 2.6**, **Eq 2.11** and **Eq 2.12** permits to obtain the values of all the quantities, including γ, needed to calculate the excess of pressure Π and this has to be added to the chemical, colloidal and macroscopic terms in the Equation of State to describe the case of wood in equilibrium with an outside reservoir of electrolytes.

2.5.4 Site occupation

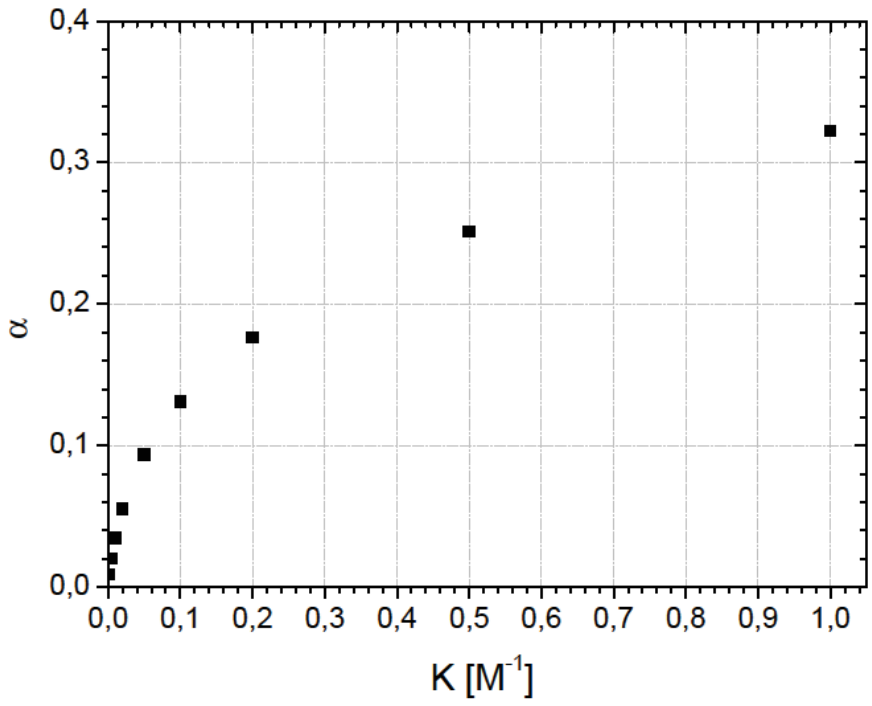

***Fig 2.5.2**: Site occupation rate is reported as a function of binding constant for a 15 osm solution.*

2.5.5 Measurement of the extra swelling by SAXS

The extra swelling δ^* (D-D_w) and the related inter-crystalline strain ε_D, δ^*/D_w, has been obtained by measuring D and D_w from small angle x-ray scattering as follows (adapted from *Chiang et al. 1994*): first, the 2D scattering pattern measured for a wood slices in liquid (in water and soaked in salt solution respectively for D_w and D) has been transmission and background corrected. The obtained 2D scattering pattern has been spherically averaged and a typical 1D scattering function $q\,I(q)$ is shown in **Fig 2.5.3a**. This is dominated by the scattering of pores and other cavities at small q (see red curve in **Fig 2.5.3a**), but this contribution becomes negligible for q larger than 0.5 nm^{-1} and was disregarded here. For q larger than 2.5 nm^{-1} $q\,I(q)$ is constant q (see green curve in **Fig 2.5.3a**). The $q\,I(q)$ was then subtracted by this constant at large q and divided by $B = (2J_1(R/q)/(R/q))^2$ where J_1 is the Bessel function of the first kind and R is the radius of the cellulose crystals (1.25 nm). Finally, the resulting curve (**Fig 2.5.3b**) was fitted with a Gaussian close

to its maximum (red in **Fig 2.5.3b**) and the position of the maximum was taken to calculate the distance D (or D_w) between the crystals. For each state (wet or soaked in salts), 25 scattering patterns were measured from two different wood slices over an area of about 0.25 mm^2 and the averages values and the associated standard errors are reported in **Fig 2.2.6**.

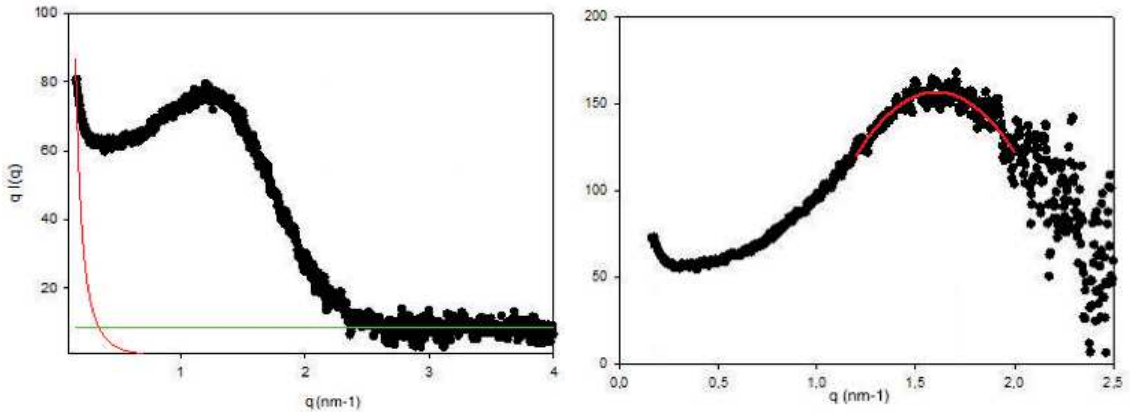

***Fig 2.5.3**: Left: typical 1D scattering intensity, $q\ I(q)$, plotted vs the scattering length, as obtained by spherical averaging 2D SAXS patterns from a tangential section of compression wood of spruce. At low q, scattering is dominated by pores and cavities (red curve), while at higher q it becomes constant (green line). Right: scattering function $q\ I(q)/B$ obtained as described in the text. The curve is fitted around its maximum with a Gaussian function (red) to find the q corresponding to the distance between cellulose crystals.*

References

(*Aroti et al. 2007*) A. Aroti, E. Leontidis, M. Dubois, T. Zemb, G. Brezesinski *Monolayers, bilayers and micelles of zwitterionic lipids as model systems for the study of specific anion effects*, 2007 Colloid Sufaces A 303, 144

(*Belloni 1986*) L. Belloni *Electrostatic interactions in colloidal solutions: comparison between primitive and one-component models*, 1986 J. Chem. Phys. 85, 519

(*Belloni 2000*) L. Belloni *Colloidal interactions*, 2000 J. Phys. Condens. Matter 12, R549

(*Bertinetti et al. 2013*) L. Bertinetti, F.D. Fischer, P. Fratzl *Physicochemical basis for water-actuated movement and stress generation in nonliving plant tissues*, 2013 PRL 111, 238001

(*Bertinetti et al. 2016*) L. Bertinetti, T. Zemb, P. Fratzl *Chemical, colloidal and mechanical contributions to the state of water in wood cell walls*, 2016 New. J. Phys. 18, 083048

(*Burgert and Dunlop 2011*) I. Burgert, J.W.C. Dunlop *Mechanical integration of plant cells and plants*, 2011 Signaling and comunication in Plants, Springer

(*Chan et al. 2015*) W.W. Chan, S. Glotzer, M.C. Hersam, Y. Gogotsi, A. Javey, C.R. Kagan, A. Khademhosseini, N.A. Kotov, S. Lee, H. Möhwald, P.A. Mulvaney, A E. Nel, P.J. Nordlander, W.J. Parak, R.M. Penner, A.L. Rogach, R.E. Schaak, M.M. Stevens, A.T.S. Wee, C.G. Willson, H.L. Tierney, P.S. Weiss *Grand plans for Nano*, 2015 ACS Nano 9, 11503.

(*Chiang et al. 1994*) W.D. Chiang, R.L. Thomas, M.E. Kunkel *Calcium binding by cellulose and lignin*, 1994 Food Chem. 50, 191

(*Collins 1997*) K.D. Collins *Charge density-dependent strength of hydration and biological structure*, 1997 Biophys. 72, 65

(*Collins 2004*) K.D. Collins *Ions from the Hofmeister series and osmolytes : effects on proteins in solution and in the crystallization process*, 2004 Methods 34, 300

(*Demé and Zemb 2011*) B. Demé, T. Zemb *Hydration forces between bilayers in the presence of dissolved or surface-linked sugars*, 2011 COCIS 11, 584

(*Dubois et al. 1998*) M. Dubois, T. Zemb, N. Fuller, R.P. Rand, V.A. Parsegian *Equation of state of a charged bilayer system: measure of the entropy of the lamellar–lamellar transition in DDABr*, 1998 J. Chem. Phys. 108, 7855

(*Dubois et al. 2006*) M. Dubois, M. Schönhoff, A. Meister, L. Belloni, T. Zemb, H. Möhwald *Equation of state of colloids coated by polyelectrolyte multilayers*, 2006 Phys. Rev. E 74, 051402

(*Fengel and Wegener 2003*) F. Fengel, G. Wegener *Wood - chemistry, ultrastructure, reactions*, 2003 Verlag Kessel

(*Fratzl et al. 2008*) P. Fratzl, R. Elbaum, I. Burgert *Cellulose fibrils direct plant organ movements*, 2008 Farad. Discuss. 139, 275

(*Kunz and Tiddy 2009*) W. Kunz, G.J. Tiddy *Specific ion effects*, 2009 World Scientific

(*Kunz et al. 2004*) W. Kunz, J. Henle. B.W. Ninham *'Zur Lehre von der Wirkung der Salze' (about the science of the effect of salts): Franz Hofmeister's historical papers*, 2004 COCIS 9,19

(*LeNeveu et al. 1976*) D.M. LeNeveu, R.P. Rand, D. Gingell, V.A. Parsegian *Apparent modification of forces between lecithin bilayers*, 1976 Science 30, 399

(*LeNeveu et al. 1977*) D.M. LeNeveu, R.P. Rand, V.A. Parsegian, D. Gingell *Measurement and modification of forces between lecithin bilayers*, 1977 *Bioph. J. 18, 209*

(*Leontidis et al. 2009*) E. Leontidis, A. Aroti, L. Belloni *Liquid expanded monolayers of lipids as model systems to understand the anionic Hofmeister series: 1. A tale of models*, 2009 J. Phys. Chem. B 113, 1447

(*Levin 2002*) Y. Levin *Electrostatic correlations: from plasma to biology*, 2002 Rep. Prog. Phys. 65, 1577

(*Lima et al. 2008*) E.R.A. Lima, D. Horniek, R.R. Netz, E.C. Biscaia, F.W. Tavares, W. Kunz, M. Boström *Specific ion adsorption and surface forces in colloid science*, 2008 J. Phys. Chem. B 112, 1580

(*Ninham and Parsegian 1971*) B.W. Ninham, V.A. Parsegian *Electrostatic potential between surfaces bearing ionizable groups in ionic equilibrium with physiologic saline solution*, 1971 J. Theor. Biol. 31, 405

(*Onuki et al. 2011*) A. Onuki, R. Okamoto, T. Araki *Phase transitions in soft matter induced by selective solvation*, 2011 Bull. Chem. Soc. Jpn. 84, 6, 569

(*Onuki et al. 2011 II*) A.Onuki, T. Araki, R. Okamoto *Solvation effects in phase transitions in soft matter*, 2011 J. Phys. Condens. Matter 23, 284113

(*Onuki and Araki 2012*) A. Onuki, T. Araki *Selective solvation in aqueous mixtures: interface deformations and instability*, 2012 J. Phys. Soc. Jpn 81, SA004

(*Parsegian and Ninham 1973*) V.A. Parsegian, B.W. Ninham *Van der Waals forces in many-layered structures: generalizations of the Lifshitz result for two semi-infinite media*, 1973 J. Theory Biol. 38, 101

(*Perrin 1913*) J. Perrin *Les atomes*, 1913 Flammarions, re-edited 1991

(*Petrache et al. 2006*) H.I. Petrache, T. Zemb, L. Belloni, V.A. Parsegian *Salt screening and specific ion adsorption determine neutral-lipid membrane interactions*, 2006 PNAS 103, 21, 7982

(*Podgornik et al. 1998*) R. Podgornik, H.H. Strey, V.A. Parsegian *Colloidal DNA*, 1998 COCIS 3, 534

(*Poulanne and Halonen 2010*) E. Puolanne, M. Halonen *Theoretical aspects of water-holding in meat*, 2010 Meat Sci. 86, 151

(*Reus et al. 1999*) V. Reus, L. Belloni, T. Zemb, N. Lutterbach, H. Versmold *Fusion of colloidal crystals induced by monovalent and asymmetric salt: an osmotic pressure and ultra-small-angle X-ray scattering study*, 1999 Colloids Surf. A 151, 449

(*Schneck et al. 2011*) E. Schneck, B. Demé, C. Gege, M. Tanaka *Membrane adhesion via homophilic saccharide-saccharide interactions investigated by neutron scattering*, 2011 Biophys. 100, 2151

(*Schwierz et al. 2010*) N. Schwierz, D. Horinek, R.R. Netz *Reversed anionic Hofmeister series: the interplay of surface charge and surface polarity*, 2010 Langmuir 26, 10, 7370

(*Schwierz et al. 2013*) N. Schwierz, D. Horinek, R.R. Netz *Anionic and cationic Hofmeister effects on hydrophobic and hydrophilic surfaces*, 2013 Langmuir 29, 2602

(*Schwierz et al. 2015*) N. Schwierz, D. Horinek, R.R. Netz *Specific ion binding to carboxylic surface groups and the pH dependence of the Hofmeister series*, 2015 Langmuir 31, 215

(*Strey et al. 1997*) H.H. Strey, V.A. Parsegian, R. Podgornik *Equation of State for DNA liquid crystals: fluctuation enhanced electrostatic double layer repulsion*, 1997 Phys. Rev. Lett. 78, 895

(*Time 1998*) B. Time *PhD thesis*, 2011 Norwegian University of Science and Technology

(*Vlachy et al. 2009*) N. Vlachy, B. Jagoda-Cwiklik, R. Vácha, D. Touraud, P.J. Jungwirth, W. Kunz *Hofmeister series and specific interactions of charged headgroups with aqueous ions*, 2009 Adv. Colloid Interface Sci. 146, 42

(*Wolfe and Bryant 1992*) J. Wolfe, G. Bryant *Mechanics of swelling*, 1992 NATO ASI Subseries

(*Zemb and Leontidis 2013*) T. Zemb, E. Leontidis *Equilibrium in soft-matter systems under the influence of competing forces*, 2013 COCIS 18, 493

(*Zemb and Leontidis 2014*) T. Zemb, E. Leontidis *Equilibrium in soft-matter systems under the influence of competing forces: part II*, 2014 COCIS 19, 1

(*Zhang and Cremer 2010*) Y. Zhang, P.S. Cremer *Chemistry of Hofmeister anions and osmolytes*, 2010 Ann. Rev. Phys. Chem. 61, 63

Acknowledgements

The authors thank Luc Belloni, Laboratoire Interdisciplinaire sur l'Organisation Nanometrique et Supramoleculaire CEA, for his precious help in the mathematical treating of the electrostatic term of the Equation of State, Klaus Bienert and Marco Bott, Max Planck Institute of Colloids and Interfaces, for technical support and development of the in situ mechanical testing devices, Stefan Siegel and Chenghao Li for their support during the X-ray measurements at the µ-spot beamline (BESSY II, Helmholtz–Zentrum fur Materialien und Energie, Berlin, Germany). The excellence laboratory LABEX-Chemisyst ANR is acknowledged for the French-German PhD Stipendium. T.Z. acknowledges European Research Council project "Rare earth recycling with low harmful emissions" (REE-CYCLE) No. 320915 and the Humboldt fundation for support through the Humboldt-Gay Lussac prize. The financial support by DFG through Leibniz Award to P.F. is also aknowledged. This work was fully undertaken within the scope of the French–German agreement L.I.A. RECYCLING between CNRS/INC and MPG/MPIKG. The authors thank Helmuth Mohwald and Ingo Burgert for numerous helpful discussions.

3. Nano-, Meso- and Macro-swelling characterization of impregnated compression wood cell walls

A. Barbetta, L. Bertinetti, J. Lautru, R. Podor, T. Zemb 2017 Wood Sci. Tech. accepted

Wood cell walls when contacted with humid atmosphere or an aqueous solution containing electrolytes or polymers undergo the phenomenon of swelling. In this work, experimental data were produced to quantify the effects of the adsorption water and solutes, which were introduced in the material by equilibration with a solution used as osmotic reservoir. For this reason, different environmental setups have been developed, allowing the control of temperature, water chemical potential, and ionic strength during the sorption process.

The aim of this paper is to describe three experimental setups, focused at different levels: at the nanometric scale, small angle scattering at controlled humidity; at the mesoscopic scale, environmental scanning electron microscopy; at the macroscopic scale, tensile stage involving immersion of samples in solutions. Applicability and efficiency of the three setups are described.

Moreover, it was shown how the combination of the results obtained via the three methodologies can be compared to expectations from a general Equation of State (EOS approach), where wood swelling with water and salt solutions is presented as the dependence of the distance between adjacent cellulose fibrils on the osmotic pressure. The total pressure calculated takes into account chemical, colloidal and mechanical terms in the force balance of the wood cell wall.

3.1 Introduction

Wood is a heterogeneous and anisotropic nano-composite (*Fratzl and Weinkamer 2007*). At nanometric scale, it is organized into stiff crystalline cellulose fibrils (50%) of a typical thickness of 2.5 nm, and parallel to each other, with a typical spacing distance between 1 and 4 nm. Fibrils are embedded in a softer and more isotropic matrix (*Altaner et al. 2006*), mostly comprised of hemicelluloses (20-35%), lignin (15-30%) and water (*Fengel and Wegener 2003*). The nano-structure of cellulose and the distribution of the polymers of the matrix in the cellulose structure are not yet known in all cases, but are readily characterized by small-angle X-ray microtomography using compression wood (*Fernandes et al. 2011*). The gel between cellulose crystals is hygroscopic and swells while absorbing water (*Elbaum et al. 2008*). From a macroscopic point of view, wood cell walls can be described as mechanical model, based on the assumption that the matrix, if it was ideally free of any constraints, would tend to swell isotropically, but the presence of the stiff fibrils that act as rigid anisotropic elements, induces significant elastic strain. This strain is strongly dependent on the winding angle of the cellulose micro-fibrils (*Salmén 2004*) that regulates tensile and compressive stress generation (*Fratzl et al. 2009*).

Understanding and rationalizing the process of water uptake by wood is a point of primary importance, as it implies remarkable dimensional and structural changes, and variations of material's mechanical properties. As a matter of fact, biological organisms optimize their interactions with water to obtain composition and structure dependent properties on which they rely to accomplish certain vital function (e.g. seed dispersal, spatial re-orientation, organ locomotion (*Fratzl and Barth 2009*). These interactions include volume changes, mechanical properties changes, conformational changes, and can induce passive hydro-actuated swelling or shrinkage, which the organism translates into movements or into stress generation thanks to their sensors and actuators (*Elbaum et al. 2008*). Considering forces in play during material deformation, the observed swelling can be understood as the balance resulting from different contributions, attractive and repulsive, acting simultaneously. Chemical and elastic mechanical terms have always been taken into account in wood chemistry, but the importance of the entropic and colloidal terms has been considered only recently by the work of Medronho et al. (*Medronho et al. 2012*), who showed that a good solvent to dissolve cellulose should overcome the low

entropy gain in the balance of the free energy of mixing with the polymers (*Medronho and Lindman 2014*). This provides better chances to compare theoretical calculations with experimental observations, including the meso-scale (i.e. the colloidal scale) (*Singh et al. 2015*, *Alves et al. 2016*). All the terms are summed in the form of a constitutive master equation (*Bertinetti et al. 2013*, **Eq 3.1**):

$$dG = dG_{chemical} + dG_{colloidal} + dG_{mechanical} \qquad \textbf{Eq 3.1}$$

This formulation takes into account microscopic chemical (i.e. the integral of all chemical interactions via bonds with the nearest neighbor), mesoscopic colloidal (i.e. electrostatics, van der Waals, solvation and entropic terms) as well as macroscopic mechanical contributions (*Bertinetti et al. 2016*). In the case of wood cell walls, van der Waals forces between crystals are negligible by two orders of magnitude. Repulsive hydration forces between cellulose crystals separated by a layer of water adsorbed of the crystals with restricted conformation, giving rise to an exponentially decaying hydration force between crystals, are taken into account (*Parsegian and Zemb 2011*). Configurational entropy of the matrix (*Chang et al. 2012*, *Bertinetti et al. 2016*), and chemical cross-linking between the cellulose fibrils and the matrix components (*Whitney et al. 1998*) are combined with the elastic energy generated by the material's anisotropy (*Fratzl et al. 2009*). This approach is consistent with the multi-scale organization of natural materials into building blocks, whose components are assembled at different hierarchical levels to form composites able to obtain specific structural and mechanical properties (*Weinkamer and Fratzl 2011*). Moreover, it leads to the formulation of a general Equation of State (*i.e.* the relation between osmotic pressure and distance between adjacent cellulose crystals) with only a minimal number of parameters, all measurable independently, as already known for other tissues (see the case of multi-lamellar vesicles (*LeNeveu et al. 1977)*, DNA (*Podgornik et al. 1977*) as well as generic "meat" (*Poulanne and Halonen 2010*)). With respect to the general sorption models (BET, GAB, Dent, Pierce, etc.) (*Volkova et al. 2012*), based on experimental parametric sorption isotherms, an Equation of State has the peculiarity of taking into account structural and compositional specific information of the material to predict water sorption.

At the industrial scale, wood is mostly used without any impregnation (*Rowell 2014*). Nevertheless, the development of wood processing technologies, in which wood material is treated with several kinds of chemicals to induce changes in the chemical nature that increase its properties, led to significant results in increasing wood properties, in terms of dimensional

stability, chemical and biological resistance (preservatives), durability (fire retardants) etc. These processes involve treatments with specific reactants (*Kazi et al. 1998*). Wood modification implies the formation of covalent bonds between the polymeric constituents of the wood cell walls and reactants, including epoxides, isocyanates, anydrides, diols (*Mathias et al. 1991*). The most common processes involve either reactions of furfurylation or acetylation (*Mantanis 2017*), whose primary effect is a considerable increase in dimensional stability, with a sensitive decrease of the degrading effects of weathering with respect to the untreated wood, due to the substitution of the hydrophilic hydroxyl groups with hydrophobic side groups (*Beckers et al. 1998*).

Historically, swelling of cellulose induced by various salts has been studied for a long time, and salts swelling power was for the first time related to the degree of hydration of their cations by Von Weirman in 1912 (*Rahim and Huque 1966*). Later studies that started to classify salts effect according to the lyotropic series were performed on cellulose (*Heymann and McKillop 1939*), and its derivatives, such as methylcellulose (*Heymann et al. 1937*). Within this framework, the theoretical knowledge regarding wood swelling with water has been later extended to the case of swelling after impregnation of wood with solutions containing electrolytes. By means of TEM micrographs, $AgNO_3$ has been proved to impregnate wood at the microfibrillar level and increase the swelling by softening the cell walls (*Wallström and Lindberg 2000*).

Several salts have recently been experimentally investigated (*Barbetta et al. 2017b*), exploring the Hofmeister series, which defines ions as structure-making or structure-breaking, according to the strength of their interactions with water (*Baer and Mundy 2013*). A particular custom-built tensile stage allowed the measurement of dimensional changes, in terms of axial strain, occurring in the wood material fully immersed in water and in different salt solutions, while kept in iso-stress and isoosmolar conditions. Results showed that all salts induce a positive swelling, and that the maximum swelling can be obtained by using a salt composed of a chaotropic ion combined with a kosmotropic one (*e.g.* NaI, $CaBr_2$). In contact initially with water then later with concentrated salt solutions, wood materials undergo two different processes: first water flows out because of the difference in osmotic pressure between the external solution, but later ions diffuse and adsorb within the wood cell walls, inducing an important re-swelling. In the case of so-called "antagonistic" salts, i.e. chaotropic anion associated with kosmotropic cation, according to the definition given by Onuki (*Onuki et al. 2011*), the chaotropic species easily loses the first hydration shell. As a consequence, they appear as "ejected" from bulk water and adsorb on the

hemicelluloses structure. This creates a net electrical field that drives fully hydrated kosmotropes within the matrix+fibrils structure, and causes swelling. In terms of the Equation of State, a colloidal electrostatic term due to the presence of salts can be added to the force balance.

The aim of the present work is to combine complementary multi-scale techniques to compare swelling observed at different scales for compression wood and to compare those to the generic Equation of State for impregnated and non-impregnated spruce compression wood, in which swelling is presented in the form of variation of the distance between adjacent crystalline cellulose fibrils as a function of the osmotic pressure. For this purpose, environmental setups allowing the control of several parameters, such as temperature, water chemical potential (experimentally: relative humidity RH), and ionic strength of the solution used were developed and tested in order to be able to follow the changes occurring in the material at different scales, taking advantage of three different techniques, whose applicability, experimental protocols, advantages and disadvantages of these techniques are described in the present work:

- at the nanometric scale, small-angle X-ray scattering (SAXS) allows the evaluation of absolute distance (nm) between adjacent cellulose fibrils of samples pretreated with different salt solutions, and in conditions of maximum swelling (*i.e.* they are fully immersed in solution);

- at the microscopic level, environmental electron scanning microscopy (ESEM) is used to measure longitudinal and transversal elongation of pretreated samples, during dehydration and rehydration cycles at different temperatures;

- at the macroscopically observable scale, via a mechanical tensile stage (TS) it is possible to monitor in-situ relative dimensional changes, in terms of axial strain, during impregnation of the material with different salt solutions.

A schematic representation of the three techniques used at different scale, including a highlight on the sample dimensional changes analyzed during each experiment, and a sketch of the typical output graphs, is shown in **Fig 3.1.1**.

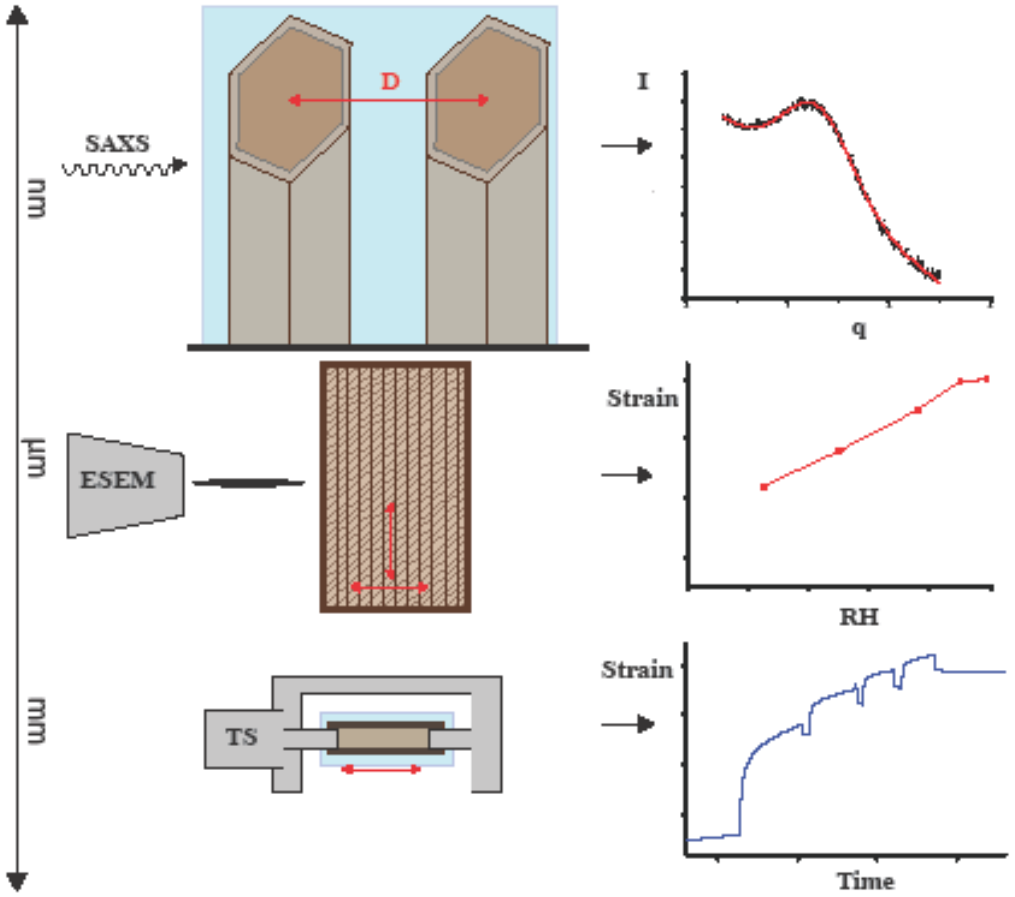

***Fig 3.1.1**: Schematic representation of the three different techniques used, at the different scales: at the nm scale, SAXS (on top) quantifies the absolute center-to-center distance between adjacent cellulose crystals; in the µm range, ESEM (in the middle) quantifies materials' reactions to humidity and temperature changes; at micrometer level, TS (bottom) follows in-situ dimensional relative changes of samples during solution uptake.*

ESEM studies on spruce wood fibers were performed by the group of Burgert (*Eder et al. 2008*) with the aim of following in-situ micro-tensile tests of fracture strength and behavior of various tissue types, in their hydrated state. Actually, one of the most relevant concerns of wood industry is the knowledge and optimization of the drying process, in terms of improved drying time, cost and quality (*Elustondo et al. 2010*). In this sense, the differential shrinkage due to material anisotropy and specific properties of its components (*i.e.* propensity to collapse and the propensity to induce drying stress) is studied. Observed differences showed the primary influence of cell geometry, material porosity and cell wall thickness in structural stabilization of the material. Less drastic conditions were analyzed by Bernabei and Salvatici (*Bernabei and Selvatici 2016*), who

studied swelling and shrinkage deformations of the wood material constituent elements (*i.e.*: cell wall, cell lumen, fractures, parenchymatic rays, etc.) during heating, in a wide range of temperature (20-400 °C), where no cracking due to thermal treatment was detected. Moreover, determination of the dependence of porosity and shrinkage on drying, studied by the group of Perré (*Redman et al. 2016*), showed the effects of fibres geometry on the anisotropic swelling to explain collapse and structural degradation occurring during drying.

The investigation of the swelling of wood cell walls in contact with humid atmosphere and aqueous solutions containing electrolytes with the three devices mentioned above, aims to obtain consistent results at the three scales, to be interpreted within the frame of a multi-scale approach. This can give an overall picture of the topic, including the analysis of dimensional changes at the supra-molecular scale, in terms of absolute distances, upon water and solution uptake by wood (SAXS), study of the dynamics and thermodynamics aspects of impregnation (TS), and quantification of the different sensitivity of pretreated material to environmental conditions (ESEM).

Finally, the knowledge of the experimental Equation of State can be further expanded to the case of materials impregnated with swelling agents (*e.g.* NaI).

3.2 Materials and methods

Slices from spruce (*Picea abies*) compression wood, with a thickness of 100 µm, were cut along the longitudinal direction of the tree, using a Leica-rm2255 microtome, and were directly stored in a freezer (-20°C), so that their natural conditions were kept. Samples were unfrozen in a fridge at 4°C the day before the beginning of the measurements. The choice of compression wood was made consistent with the previous works, because of its microfibrillar angle (*i.e.* the spiral angle of the cellulose fibrils winding around the central lumen) can reach ca. 45°, and it is higher than normal wood (*Gorisek and Torelli 1999*). As the tensile stage measurements are related to the strain in the direction parallel to the fibrils orientations (see Paragraph **3.2.3**), a higher angle implies a more sensitive response of the registered values to swelling. The measurement of the

microfibrillar angle of the samples was performed via X-ray diffraction experiments, as described in literature (*Bertinetti et al. 2013*, supporting information), with a Nanostar instrument (Bruker AXS). The scattered intensity was obtained from 2D patterns and plotted versus the azimuthal angle and the center of the Gaussian curve representing the MFA distribution was taken as the reference value for the calculations.

Solutions were prepared with salts (supplied by Alfa Aesar) just before the experiments and at room temperature, by adding weighed quantities of salts to defined volumes of milliQ water. 15.2 osm concentration was chosen for all the solutions, consistent with the previous experiments (*Barbetta et al. 2017b*), in which the concentration of a saturated NaCl solution (15.2 osm), that produces 37.7 MPa Osmotic Pressure (OP), was chosen as reference, and the concentrations of the other solutions were chosen to produce the same OP, within the limit of the experimental error. For all the experiments, unfrozen dry samples were immersed in water overnight. In the case of the experiments with salt impregnation, wood samples were immersed in the electrolytic solution for a period of ca. 2 hours, , and then washed with water to avoid crystallization and deposition of the salt on the sample. In the case of the measurements carried out with TS, the immersion and washing steps were performed in-situ while measuring the strain. This allowed us to evaluate the rate of irreversibility of the process.

3.2.1 SAXS

Small Angle X-ray Scattering experiments were performed at the µ-spot beamline at BESSY II synchroton radiation facilities (Berlin). The setup is constituted of a 7T wavelength-shifter as source for the primary beam, a toroidal mirror to focus the beam horizontally and vertically, a double crystal monochromator equipped with three pairs of crystals, zone plates and mirrors as second and third focusing options, slits, filters and pinholes at different positions, the experimental hutch with goniometer, sample scanner, and a 2D MarMosaic 225 detector to collect the scattered signal. The wavelength used was 0.689 Å (E=18 keV). Beam size was controlled by a 50 µm pinhole. Sample-detector distance was set to 840 mm, and calibrated with a silver behenate standard. A typical measuring time of 120 seconds for each point was chosen, and several measures of the same sample, but in different spots, were performed. Pre-treated compression wood slices were measured in fully hydrated conditions, by means of a custom built metallic frame (**Fig 3.2.1**), which allows them to be immersed during the measurement in a water layer (0.2 mm), sufficiently thin to avoid any noise in the signal.

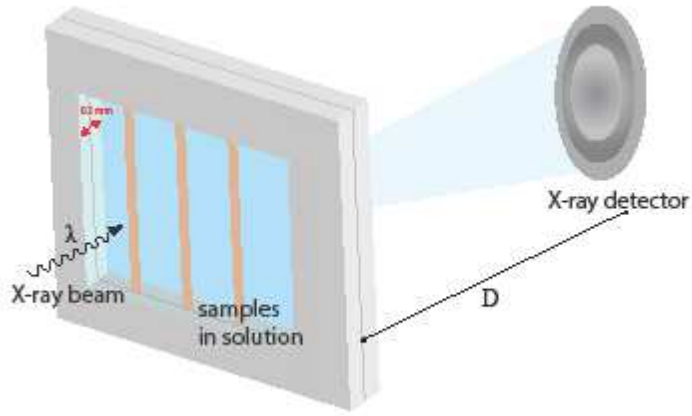

Fig 3.2.1: *Custom-built frame to measure samples in fully hydrated conditions, while immersed in a 0.2 mm water layer. λ= 0.689 Å, D=840 mm.*

Data analysis was performed according to the studies of Jakob et al. (*Jakob et al. 1996*): in their work, they proved that scattering intensities derived from cellulose fibrils of the cell-wall layer have cylindrical symmetry around the longitudinal axis of the stem (**Fig 3.2.2**). Therefore, spherical coordinates (q, φ) should be used to integrate the scattering intensity (**Eq 3.2**).

$$I(\vec{q}) = I(q, 0\Omega) = I(q, \varphi) \qquad \textbf{Eq 3.2}$$

in which the solid angle Ω, decomposed into the two Eulerian angles φ and χ, is independent from χ, the angle measured in the plan perpendicular to the symmetry axis.

The mathematical derivation of the spherical average of the intensity, $\tilde{I}(q)$, as described in literature, is reported in **Eq 3.3**:

$$\tilde{I}(q) = \frac{1}{4\pi}\int_{\Omega} I(q, \Omega)d\Omega = \frac{1}{2}\int_0^{\pi} d\varphi I(q, \varphi)\sin\varphi \qquad \textbf{Eq 3.3}$$

$\tilde{I}(q)$ description can be simplified as follow (**Eq 3.4**):

$$\tilde{I}(q) = bgr + (const)\left(\frac{1}{q}\right)\left(\frac{2J_1(qR)}{qR}\right)^2 \qquad \textbf{Eq 3.4}$$

where bgr indicates the background, R is taken as 1.25 nm for all the specimen, and J_1 is the Bessel function of the first kind.

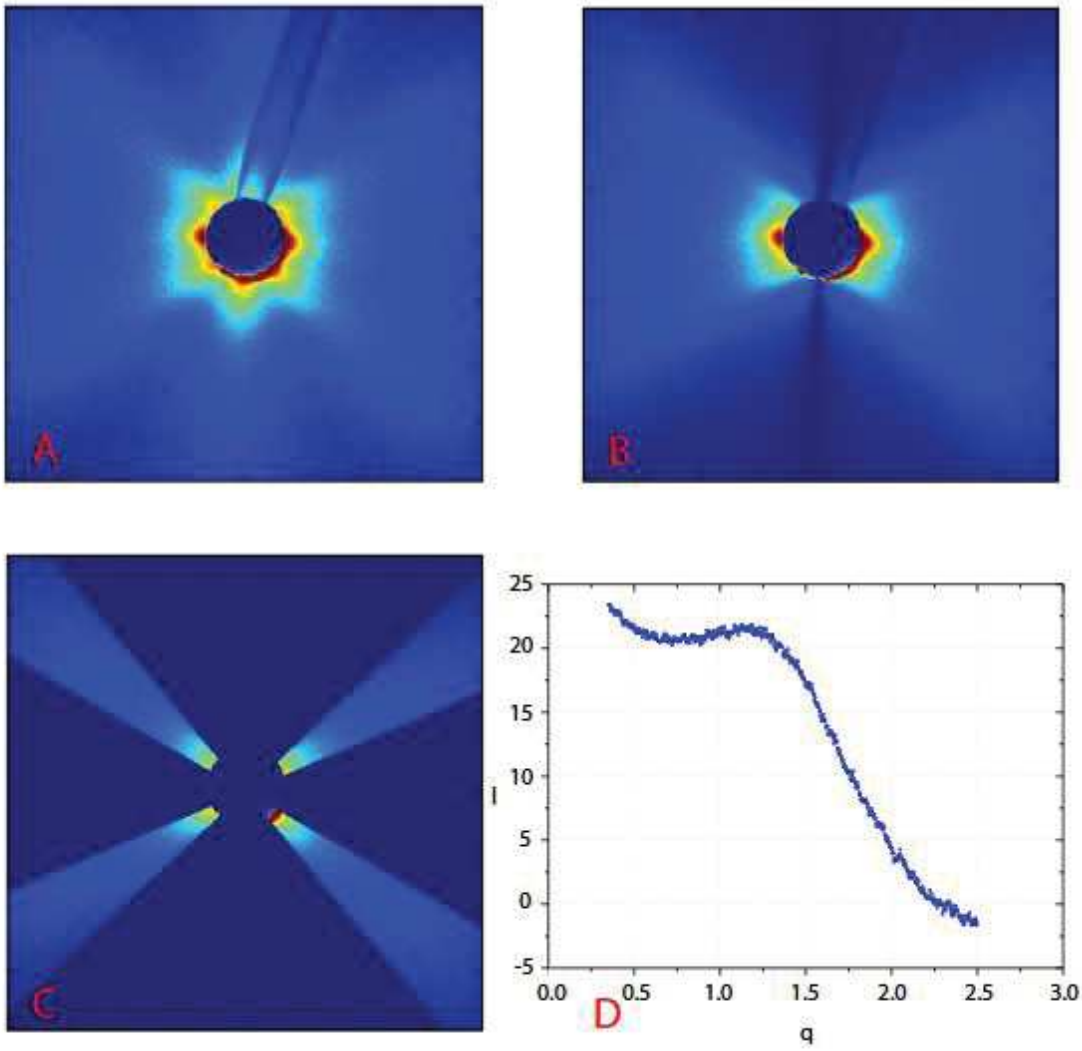

***Fig 3.2.2**: From the collected pattern (A) to the integrated intensity signal fitted with Bessel functions (D): pattern as it appears after application of cylindrical symmetry (B) and after selective masking to isolate sample signal (C).*

3.2.2 ESEM

In-situ wetting and drying experiments were performed using a FEI Quanta 200 Environmental scanning electron microscope (Eindhoven, Netherlands), equipped with a field electron gun (sketched in **Fig 3.2.3**). Specific attention was paid to the sample preparation, the use of a Peltier stage, the choice of the experimental conditions and the image processing.

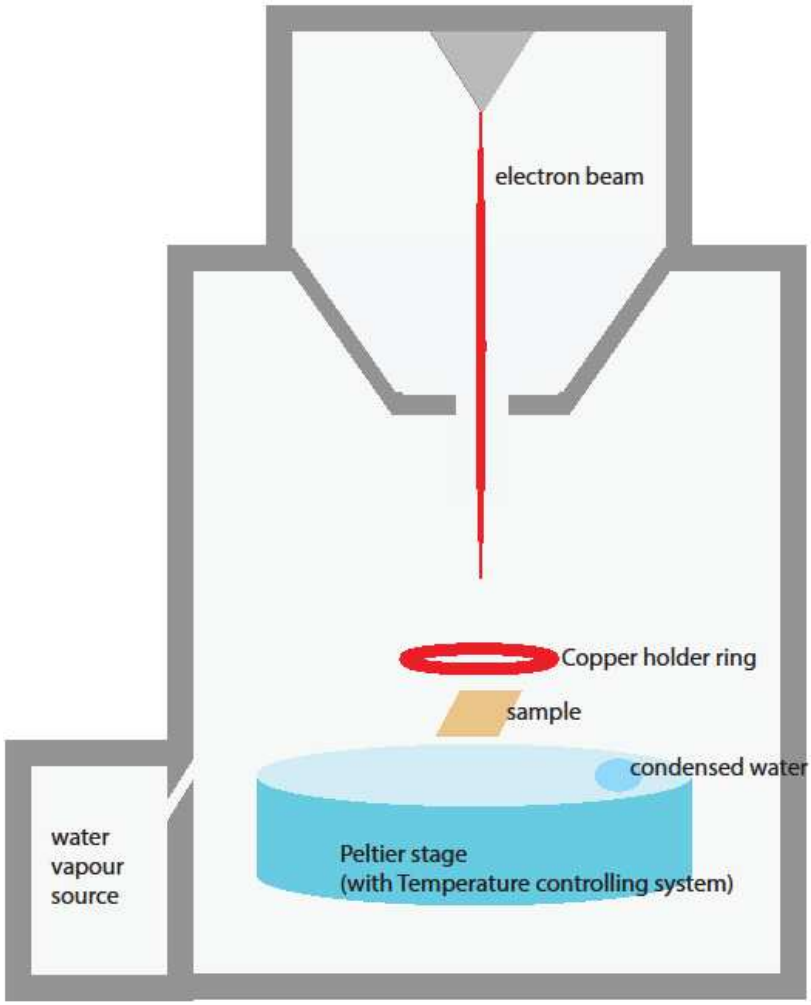

***Fig 3.2.3**: Schematic representation of ESEM chamber: sample is fixed via a copper holding system to a Peltier stage, which allows to control temperature. A tunable water vapour source allows the user to control the humidity in the chamber.*

Several 2-5 mm x 2-5 mm large pieces of wood were cut from the stored slices. Samples were immersed for a period of 2 hours in the salt solutions, then washed for at least 30 minutes in milli-Q water, at 4°C.

Once ready, the sample was inserted in between the aluminum sample holder and a copper flat washer, in order to stick it and to avoid twisting and deformation during the hydration and

dehydration experiments. The sample holder is put on the Peltier stage that allows the user to regulate the sample temperature with an acceptable precision (±0.1°C) in the temperature range from -10°C to +60°C. The maximum water vapor that can be incorporated in the ESEM chamber reaches 2400 Pa. According to the liquid/gas water equilibrium, a 100% relative humidity value can be reached in the temperature range from 0°C to 20°C.

A key-point for the success of the experiments is the control of the initial pumping sequence. A purge cycle was necessary before each analysis, allowing the air initially present in the ESEM chamber to be replaced by water vapor, in order to obtain a pure water vapor atmosphere. Part of the volume of the air in the ESEM chamber was pumped out without dehydrating the sample (RH was kept close to 100%). The gas was then replaced by water vapor. Successive purges led to 99.5% water vapor in the chamber. The number of needed purges depends on the experimental temperature (*e.g.* for experiments performed at 5°C 12 purges between 600 and 1000 Pa were necessary). The pumping sequence was validated by condensing liquid water on the sample holder at 10°C, with a water pressure of 1230 Pa.

As the studied material turned out to be very sensitive to electron beam damages, a particular attention was put in the choice of electron beam conditions. Experiments were performed with various accelerating voltages, between 5 and 30 keV), beam intensities and frame times (generally: 3 seconds), depending on the pressure of the chamber, in order to limit the sample exposure to the electron beam, and to reduce electron beam damages while recording images with a high signal-noise ratio.

Once the sample was introduced into the ESEM chamber under wet conditions (99.5% RH) at T=5°C, the temperature was kept constant. Three different zones of each sample were observed: low magnification images (image size 1024x880 pixels) were recorded every 2 minutes on the first zone, for a total time of 16 minutes (Position 1). One low magnification image was recorded at t=12 minutes on the second zone (1024x880 pixels, Position 2) and another low magnification image was recorded at t=13 minutes on the third zone (4096x3520 pixels, Position 3). Then, water vapor pressure in the chamber was tuned in order to decrease RH to 90%, and the image sequences were recorded again. This protocol was repeated at 76%, 50% and 25% RH. Afterwards, the ramp was repeated in the opposite direction.

After all the images were recorded at T=5°C (Pvap= 873 Pa), the same cycle was performed at 10°C (Pvap=1230 Pa), 15°C (Pvap= 1706 Pa) and 20°C (Pvap=2340 Pa).

Image processing was performed using Fiji software (*Schindelin et al. 2012*): at first, stack alignment was processed, and a semi-automatic tracking of two clear details on the image series was performed using the TrackMate plug-in implemented in the software. From the extracted coordinate dataset, the distances between the two details were calculated for the image series (**Fig 3.2.4**). In the case of the Position 1, sample overexposure led to remarkable beam damaging effects, while problems with analysis of Position 3 concerned an overproducing of tracking points by the plug-in, due to the high resolution. Therefore, most reliable results were obtained with the analysis of Position 2.

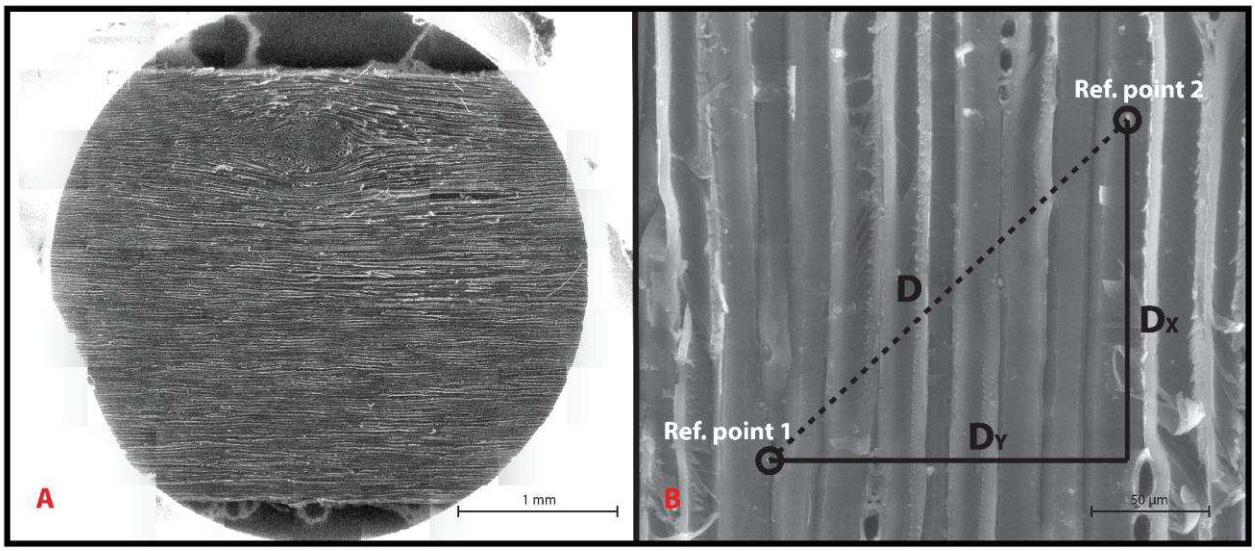

Fig 3.2.4: *Collected images for a wood sample after impregnation cycle with NaI, at two different scales: on the left (A), 33x magnification gives an overall view of the central zone of the sample, from which the three described positions were chosen; on the right (B), 500x magnification, used for sample analysis. Two different points, which could be recognized for the whole duration of the experiment, were chosen as references to calculate sample's dimensional changes during temperature and humidity cycles.*

3.2.3 TS

In-situ length changes of the sample during impregnation with different salt solutions were performed via a custom-built Tensile Stage setup (sketched in **Fig 3.2.5**), which has been already described in literature (*Barbetta et al. 2016*).

***Fig 3.2.5**: In the tensile stage the sample is fixed in between two clamps and fully immersed in solution. Setup's main components are: a load cell (in brown) to control and measure axial tensile forces, and a linear motor (on the right part of a strain) to control and measure the strain.*

The setup is made of three main components: 1) The sample holding system consists of two stainless-steel "L"-shaped arms, with clamps on the sides facing each others. The sample slices (tipically: 100 or 150 µm thick, 2 cm long, 3 mm wide) can be fixed between the clamps by screwing the two plates of each clamp. A metal cuvette of a 25 mL volume can fit in this stage, so that the sample is fully immersed in solution during the entire experiment. 2) A PI M-126.DG1 linear motor stage is connected to one of the two arms, and allows it to be driven along one axis, with a maximum distance between the two clamps of 3.5 cm. 3) a 0.5 N load cell (Honeywell 31E Low) measures and controls the axial force along the same axis. The load cell was screwed on the fixed arm to avoid noise due to the movements.

A custom written software allows the motor to drive the arm either to control the strain (Motor control mode) or to regulate the force (Force control mode). Values of motor position and force are logged by the software as a function of time.

Once clamped, samples were immersed in milli-Q water and stretched by moving the motor until buckling was removed. This can be noticed by a net linear increase of the force registered by the load cell with increasing distances. Force was calibrated in this condition, and samples were then equilibrated overnight under 0 N force. In that time, an axial elongation of 3% of its length was

observed. The length of the sample after this time was considered as the reference distance for the strain calculations. Measurements consisted in cyclical immersions of the sample in water and solutions, for periods of 2 hours and for a maximum number of 5 cycles. Experiments were performed in iso-stress conditions (*i.e.* imposing with the load cell a force of 0 N), by recording the variation of the motor position as a response of the different salt solutions. To quantify the effects produced by each solution, it was necessary to work in iso-osmotic conditions: a 6.1 M NaCl solution, which produces a 37.7 MPa osmotic pressure, was taken as reference, as in the previous work (*Barbetta et al. 2016*), and the NaI and NaBr solutions were prepared with the same osmolarity (15.2 osm). For this, values of osmotic coefficients were taken from literature and fitted to obtain the required concentration. After the experiments were finished, sample strains were plotted as a function of the number of cycles, for each solution used.

Measure at macroscopic scale: The particularly modified tensile stage with humidity control environmental cell was used (*Bertinetti et al. 2015*). This cell allows the measurement of dimensional changes occurring in dry samples: the sealed chamber is kept at constant temperature of 25°C via a Huber cooling bath circulation thermostat, while humidity was controlled with a Setaram Wetsys humidity generator, working with a 200 ml/min flow, and measured with a Sensirion Sht75 digital humidity and temperature sensor, placed in the vicinity of the sample.

3.3 Results and discussion

Fig 3.3.1 resumes the impregnation and dehydration cycle for the case of the two samples, with and without impregnation with electrolytes. In this figure, cellulose crystals are represented as black hexagons, coated by a thin layer of matrix, shown in grey. At this point of our knowledge, we are not yet able to evaluate single contributions of the individual components of the swelling matrix, which are therefore represented as indistinguishable. Chaotropic I^- is sketched in red, while kosmotropc Na^+ in green. Dry samples were immersed in water until equilibration (step A). Sample length at this state was taken as reference. Some of samples were immersed in salt

solution, and then washed (step C1); a positive strain was registered for all samples after this step. The same dehydration process was then performed for both pre-treated (step C2) and non-pre-treated samples (B), and strain was registered.

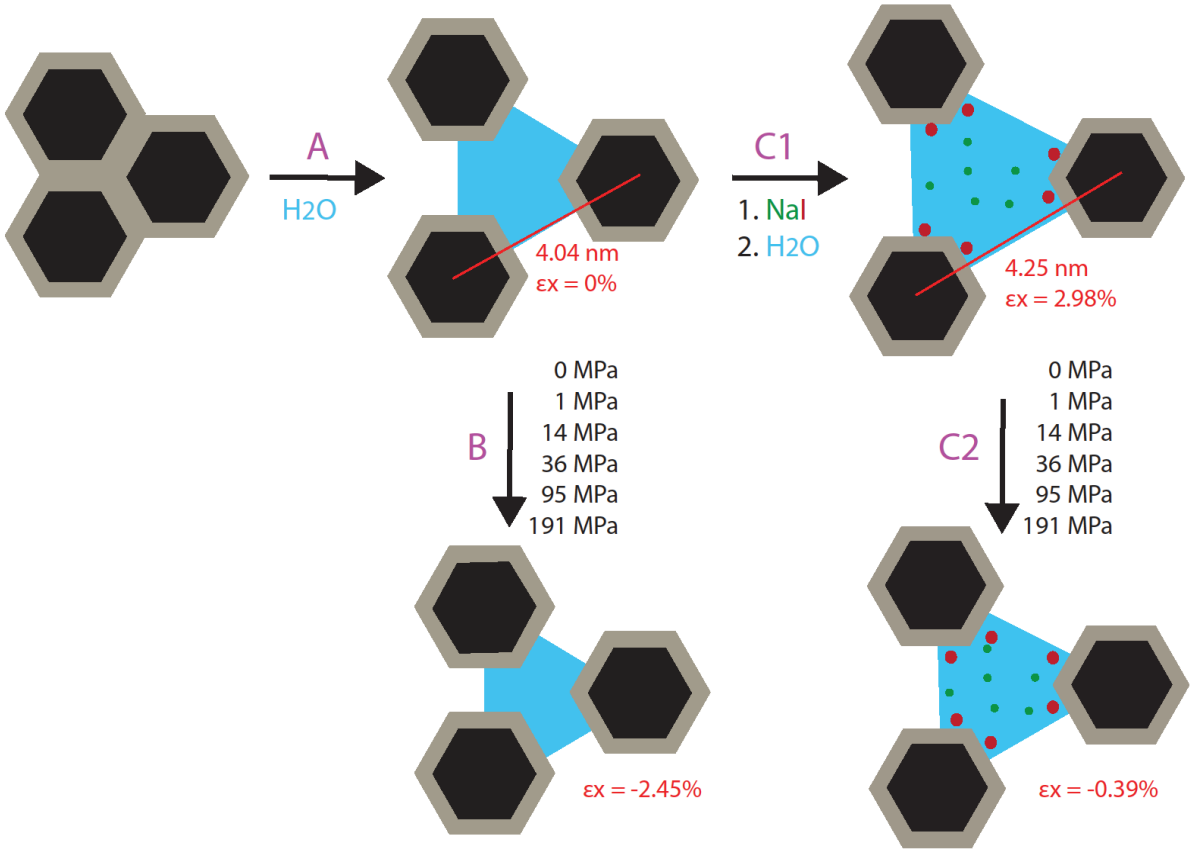

Figure 3.3.1: *Top view of a schematic representation of wood cell wall material: hexagonal and parallel crystalline cellulose fibrils (black) surrounded by a thin layer of a matrix of hemicelluloses and lignin (grey). Dry samples were immersed in water until equilibration (A), and inter-crystalline distance was measured via SAXS technique. The strain measured is this condition was taken as the reference for strain calculation. Then, samples were either dehydrated (B) or further treated (C1) by impregnation with NaI solution (I^- ions in red, Na^+ ions in green) before dehydration (C2).*

At first, preliminary considerations should be done to explain what the strains observed with the tensile stage and the ESEM measurements refer to. As already discussed, the results obtained from experiments performed with the tensile stage are evaluated by considering the swelling in terms of axial strain, ε_x. In order to convert this value into swelling between crystals, one should take into account that the fibrils are winding around the central lumen with a certain angle, the

so-called micro-fibrillar angle (MFA) (*Weinkamer and Fraztl 2011*). In the case of the compression wood specimen used, this is around 45 degrees. The peculiarity of experiments performed with ESEM is that data analysis allowed us to take into account strain in both transversal and in longitudinal directions, as the elongation was intended as distance in between recognizable points, and this could be separated into the two contributions ε_x, in parallel direction with respect to fiber orientation, and ε_y, in the perpendicular tangential direction. At first, the relationship between ε_x and ε_y at different relative humidity values is reported in **Fig 3.3.2**:

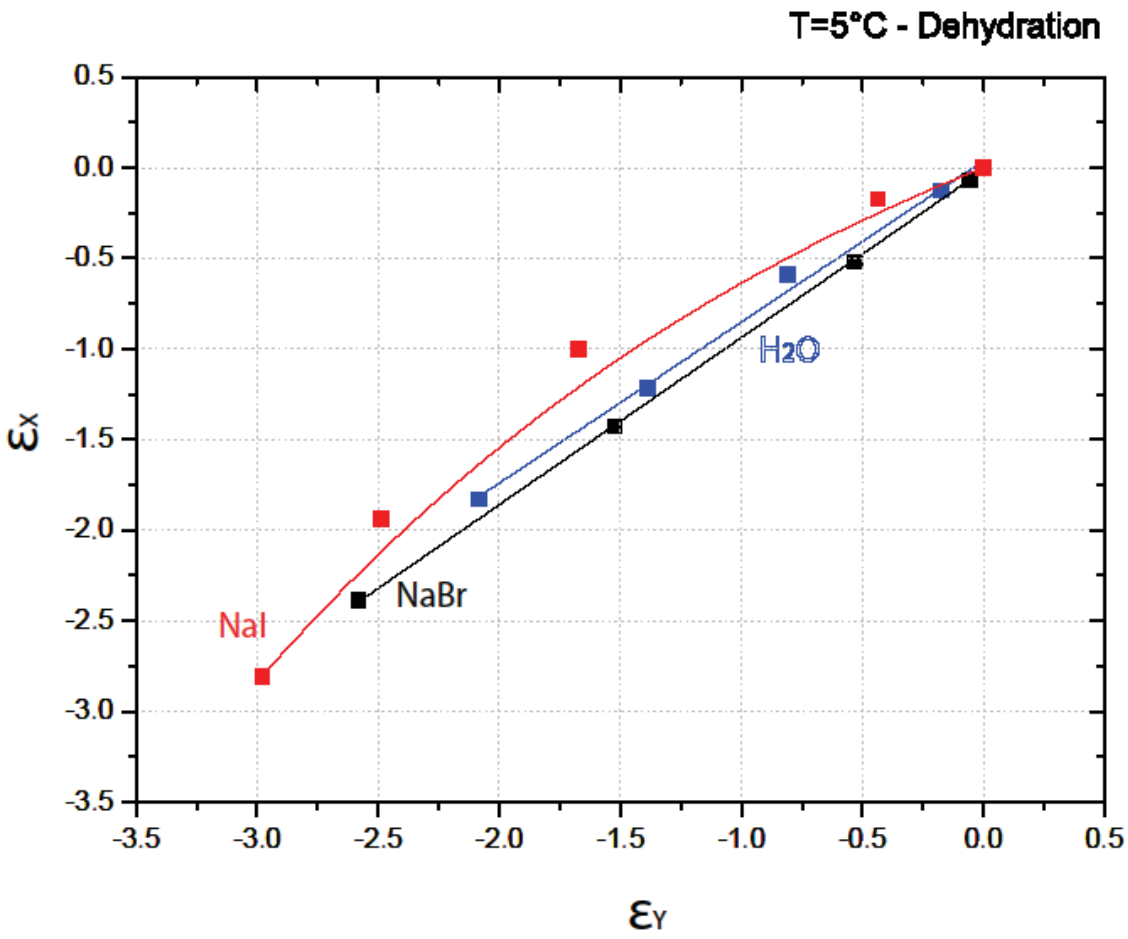

***Fig 3.3.2**: Elongation in the two directions, parallel and perpendicular with respect to fiber orientation, measured at 5°C with ESEM, is reported for the case of sample immersed in water (blue), NaBr solution (black) and NaI solution (red).*

The trends, even at low temperatures, show a linear correspondence in the cases of water and NaBr, a salt which does not induce remarkable swelling on wood (ε_x=0.3% after several cycles of impregnation, as measured with tensile stage). On the other hand, the fitted curve for the case of NaI (ε_x=3% with tensile stage) is based on a non-linear exponential growth curve, and the strain on the transversal direction ε_y leads to values more than 10% higher than the longitudinal ones at low humidity, implying the fact that the microfibrillar angle increases with swelling, as reported in literature. Nonetheless, we also point out that fibers might detach, and eventually twist, during the temperature and relative humidity cycles. This affects the measurement of the ε_y, and might lead to a overestimation of this values. For this reason, and in order to compare the results with the ones obtained via Tensile Stage experiments, we focused on the analysis of ε_x.

In the ESEM experiment strain was calculated by taking the initial point (wet condition) as reference. This means that it was not possible to report the results in a way in which they were comparable for the different salts without the support of other techniques. The problem was solved by taking the maximum swelling measured with TS as starting point for data evaluation (raw data are shown **Fig 3.3.3a**). For all the three samples, a remarkable shrinkage is registered with decreasing relative humidity. Samples pre-treated with, NaI salt, inducing high swelling, undergo slightly higher dimensional changes ($\varepsilon_{x(100\%RH\rightarrow25\%RH)}$= -3.4 ± 0.6%) if compared to the samples that were simply immersed in water ($\varepsilon_{x(100\%RH\rightarrow25\%RH)}$= -2.5 ± 0.5%) and the ones pre-treated with NaBr, whose impregnation induces negligible swelling ($\varepsilon_{x(100\%RH\rightarrow25\%RH)}$= -3.1 ± 0.4%). Results obtained for the untreated sample were compared with the ones obtained via the modified tensile stage, **Fig 3.3.3b**), in which untreated samples, previously immersed in water (step A in **Fig 3.3.1**), were clamped into an isolated chamber, with the possibility of controlling the relative humidity, thanks to a humidity generator. In this case, compression wood foils, of the same thickness as the ones used in the described setups, undergo a strain ε_x of ca. 6.7 ± 0.4% when environmental humidity is driven from dry to water-saturated vapor. Data comparison shows a sensitive difference of ca. 2.5% strain between the results obtained with the ESEM ($\Delta\varepsilon_x$= 2.5% ca.) and TS ($\Delta\varepsilon_x$= 5% ca.) for the step between 100% RH and 25% RH.

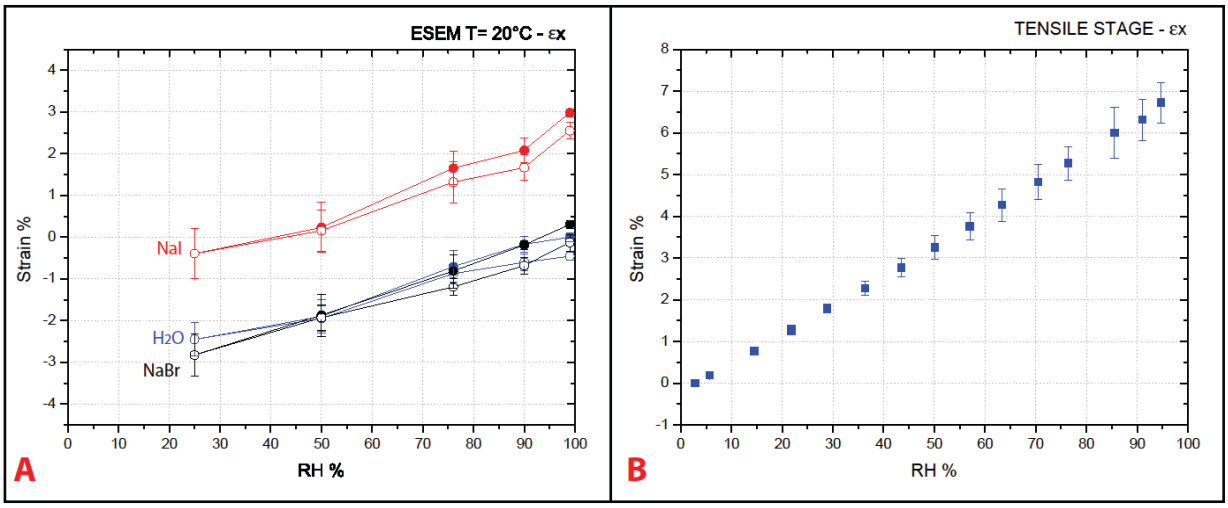

Fig 3.3.3: *Strain results as a function of relative humidity measured at 20°C with ESEM (A) and at 25°C with TS (B). Samples were untreated (blue), or pre-treated with NaBr solution (black) and NaI solution (red).*

This discrepancy may have different origins. At first, image deformation as a function of the acceleration voltage leads to an error of ca. 0.5%. Moreover, it should be considered what can be called an "individual effect": data analysis of tensile stage experiments takes into account the final effects of all the fibers of the sample, and therefore gives an averaged result of their strain, while on the other hand ESEM analysis of ε_x takes into account one single fiber per time. In this sense, fibers behavior could vary from case to case. It is pointed out that, despite this fact, there is no evidence of registered individual values of ε_x(TS) higher than ε_x(ESEM): this ensured that the difference in the result is not due to an incorrect choice of representative samples. A third aspect that should be considered is a temperature difference of ca. 5°C between the operative conditions in the ESEM controlled chamber (20°C) and the environmental temperature of the fume-hood, where the TS experiments were performed (ca. 25°C). **Fig 3.3.4** shows trends for the case of the three samples analyzed via microscopy, as a function of the chamber temperature.

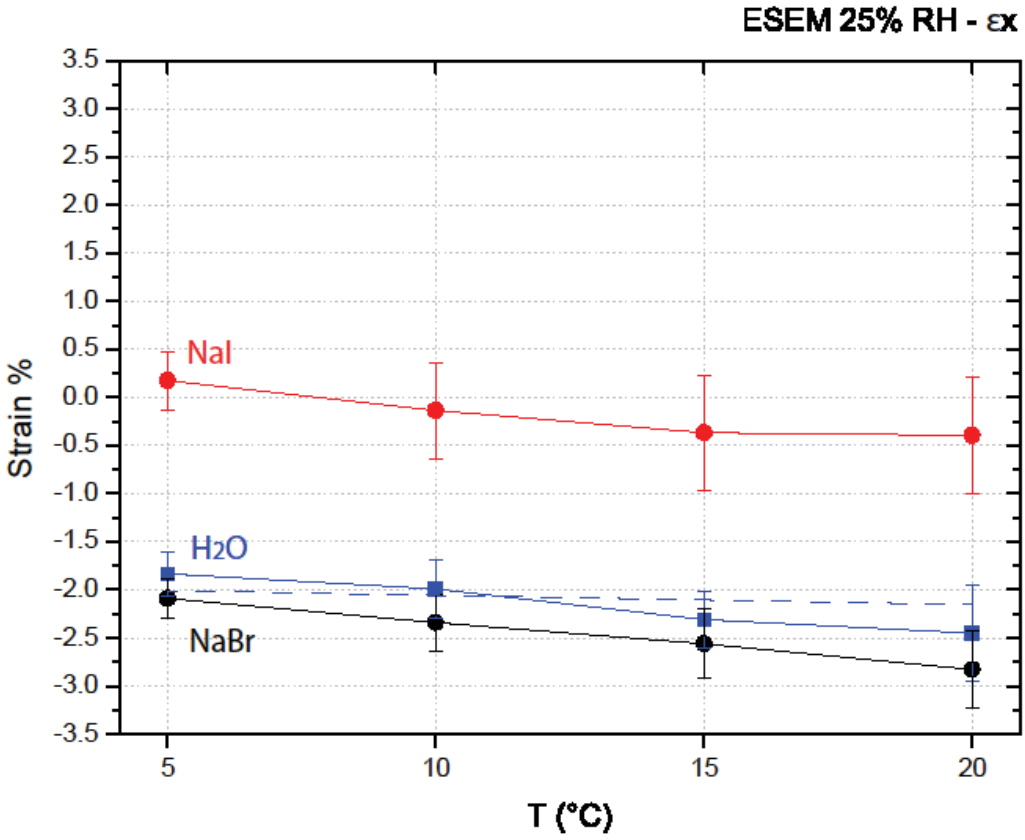

***Fig 3.3.4**: Temperature-dependent sample shrinkage measured with ESEM at constant 25% relative humidity, for samples immersed in water (blue), NaBr solution (black) and NaI solution (red). The blue dashed line represents the curve of water uptake predicted by the theoretical model.*

In all cases, we observe a slight temperature-dependent decrease of the swelling with decreasing relative humidity. For the case of the non-pretreated sample, strain varies by 0.6% over a temperature range of 15°C. This could be attributed to an increase of the configurational entropy of the matrix constituted by water, hemicelluloses and lignin, as confirmed by implementing the theoretical model of Bertinetti et al. (*Bertinetti et al.* 2016) to predict water uptake, obtained by writing the master EOS in the form described by **Eq 3.1** with calculations at different temperatures. Derivation is computed using as input parameter a chemical cross-link enthalpy per contact point of 2.5 K_BT in water. In the model, hydration force and the entropy of mixing of the matrix are the two dominant contributions to swelling. The mixing entropy, which depends on temperature, is evaluated assuming that polymers have infinite chain, according to the Flory

expression for the partial entropy of mixing, and assuming for the interaction parameter χ at low volume fraction a value of 0.5 (*Bertinetti et al. 2016*).

Theoretical and experimental results show a negligible dependence of the strain on temperature. Again, we can assume that the temperature difference between the two different setups contributes to the difference in strain, but neither this aspect itself could explain all the observed difference.

The most delicate step in the ESEM analysis concerns the sample holding system: specimens' displacement and twisting are limited by the presence of the copper ring, but not avoided at all. On the other hand, a too strong holding (*e.g.* sticking) would inhibit sample swelling. Thanks to the automatic alignment plug-in from Fiji software, one can overcome displacement, but eventual partial sample bending and consequent detaching from the stage could not be controlled, and not even evaluated, as the image focus, which could give indications of bending, must be tuned for each step, according to temperature and relative humidity conditions. In this regard, we calculated that a lifting with an angle of 10° would imply a loss of 1.5% on the measurement of ε_x, while an angle of 12.5° gives an error of -2.5%. It is therefore reasonable that this small and undetectable movement of the samples in the Peltier stage could be the main source of error. In this sense, at the current state-of-art, experiments performed with the Tensile Stage in controlled humidity conditions could give more reliable results.

3.3.1 Vapor pressure paradox

The term "vapor pressure paradox" refers to a particularity of water uptake by phospholipids (*Rand and Parsegian 1989*): lipid samples in a 100% humidity water vapor atmosphere do not take up the same amount of water as when they are in direct contact with liquid water, but less (*Jendrasiak and Mendible 1976*). Therefore, the water layer between a bilayer is thicker in the second case (*Tristram-Nagle et al. 1998*). This is a consequence of the fact that hydrating from the vapour creates an interface different from the case of samples immersed in solution (*Podgornik and Parsegian 1997*): this imposes an extra surface tension that inhibits fluctuations responsible for a repulsive entropic force, which increases spacing.

In the case of wood, wetting tests were performed with the tensile stage on dry compression wood samples: de-frozen slices were equilibrated overnight in iso-stress mode, under constant 0 N force condition. During that time, an increase of the axial strain ε_x of 3% ca. was registered. This

value appears significantly lower than the ones measured with increasing and decreasing humidity, showing an opposite behavior with respect to the case of vapor pressure paradox.

3.3.2 Experimental Equation of State

Raw data analyzed in the previous section can be further elaborated and implemented in the form of an experimental Equation of State, which describes the relation occurring between the osmotic pressure OP and the center-to-center distance between adjacent cellulose crystals (d). With this goal, absolute distances at maximum swelling (*i.e.* 100% RH) were calculated with Small Angle X-ray Scattering experiments in fully hydrated conditions, as described in **3.2.1**, for the sample pre-treated with NaI, and for the one simply immersed in water, which was used as a reference. Data analysis gave values of 4.25 nm and 4.04 nm, respectively. In order to relate SAXS and ESEM results, and therefore relate the point in the EOS at 100% humidity to the others, the measured strain ε_x must be at first re-scaled into an inter-crystalline strain, ε_D, considering that fibers are oriented with an angle of 45°, as typical for spruce compression wood (*Barbetta et al. 2016*). From that, values of d at each humidity step can be obtained by calculations from ε_D. Moreover, for the case of the sample pre-treated with a swelling agent, this angle is also slightly depending on swelling (as reported in **Fig 3.3.2**).

Results of data elaboration, reported in **Fig 3.3.5**, qualitatively show the higher sensitivity to humidity changes of the sample treated with the swelling agent, NaI (red points).

For the case of untreated samples (i.e. wood simply immersed in water) experimental results are presented, obtained via desorption ESEM measurement (blue filled points) and with the humidity controlled TS described with respect to Figure 9b (blue empty points). In both red and blue curves, the shaded areas from the points, leading to the continuous lines of the same colors, represent the incertitude due to the ESEM experimental setups problems. In particular, the continuous lines correspond to a 2.5% uncontrollable error.

Results can be compared with the calculated results obtained from modeling (*Bertinetti et al. 2016*, *Barbetta et al. 2017a*). The black line represents the theoretically predicted sorption behavior at its lower limit, which was calculated summing up all the contributions in the force balance, and multiplying all the attractive terms by a factor of 1.5 and dividing all the repulsive ones by 1.5. The limits take into account possible inaccuracies and variability of the literature data used in the model, and the fact that the accuracy of the model itself could be further refined, by

considering the interactions between the matrix components, which is neglected at the current state, as the matrix is considered as an homogeneous medium, and by taking into account the topology of the lignin network. The force balance included the enthalpy of chemical binding between cellulose fibrils and the matrix, the hydration repelling cellulose crystals in the water medium, the configurational entropy of the matrix, van der Waals force between crystals, and the elastic energy generated by anisotropic swelling. Further implementations of the model could include in the calculation an electrostatic term that takes into account the contribute to swelling given by the presence of electrolytes, according to their nature and concentration.

As shown in the figure, a reasonable consistency between the experimental and the calculated curve can be observed for the case of untreated wood.

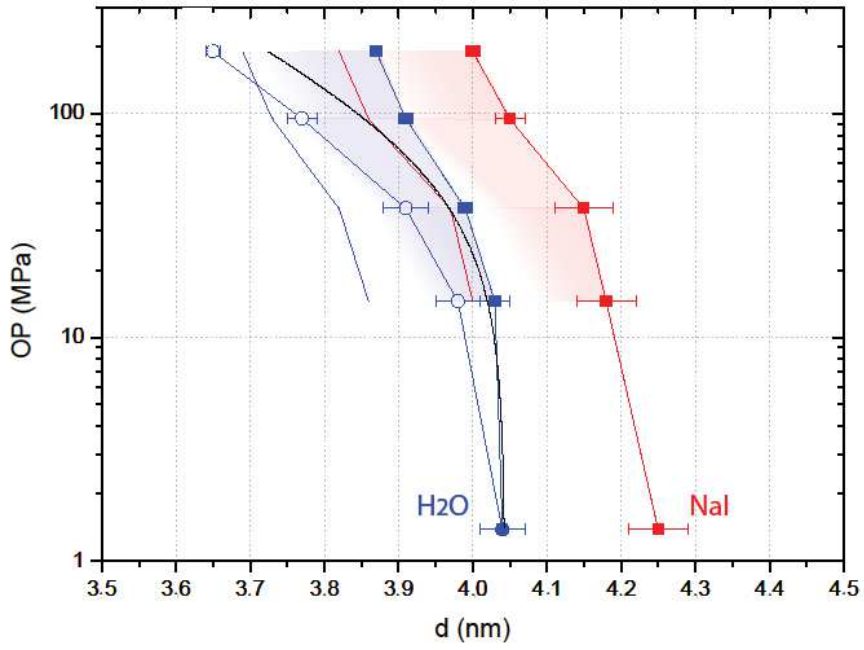

***Fig 3.3.5**: Compression wood Equation of State for samples immersed in water (blue) and impregnated with NaI solution, reported as osmotic pressure as a function of intercrystalline distance. Point of maximum swelling was measured with SAXS experiment in fully hydrated conditions. Empty points refer to humidity controlled TS measurements, the filled ones to ESEM. The shaded areas represent the error committed with ESEM measurement, due to uncontrollable bending of the sample, to a maximum of 2.5%, indicated by the lines. Black line refers to theoretical sorption behavior, in its lower limit where all the contributes opposing to swelling are multiplied by a factor of 1.5 and ones favouring swelling divided by the same factor*

An alternative way to present the same results, more often used in materials' science, is in the form of a sorption isotherm, in which material's moisture content is reported as a function of the relative humidity. The conversion is made considering the geometrical model which is described in **Fig 3.3.1** and the correlation between the intercrystalline distance and the moisture content that are given in Supplementary information. Results reported in the form of MC vs. RH for the case of the untreated sample via TS in controlled humidity conditions (**Fig 3.3.3b**) are shown in the Supplementary information. The results look consistent, within the limits of the experimental errors, with respect to recent literature data concerning spruce sorption analysis (*Hill et al. 2009*, *Murata et al. 2013*).

3.4 Conclusion

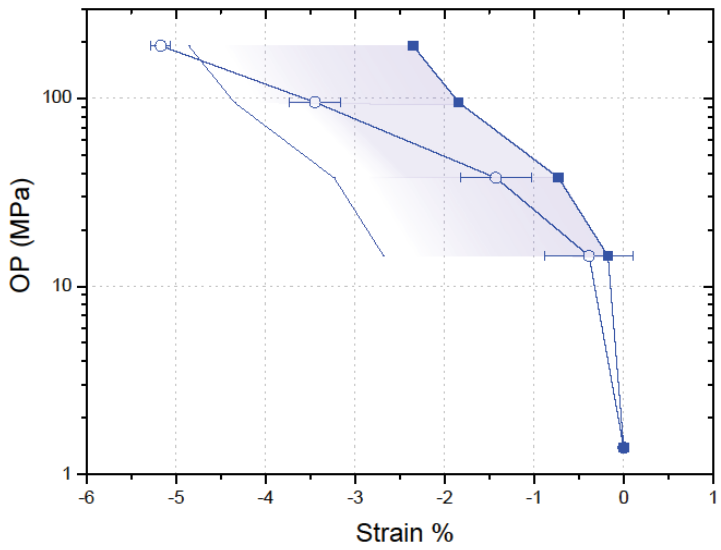

Fig 3.4.1: *Compression wood Equation of State for samples immersed in water, reported as osmotic pressure as a function of axial strain. Empty points refer to humidity controlled TS measurements, the filled ones to ESEM. The shaded areas represent the error committed with ESEM measurement, due to uncontrollable bending of the sample, to a maximum of 2.5%, indicated by the lines.*

Fig 3.4.1 resumes the humidity-dependent axial strain changes registered during a dehydration experiment for spruce compression wood foil, with both a macroscopic tensile stage device, and by means of ESEM, a technique giving information at the microscopic scale. In this work, it was attempted to establish an experimental protocol, consisting of a multi-scale combination of different techniques, to define the response of wood to environmental condition changes, in terms of an experimental Equation of State. In particular, the goal of testing different experimental procedures was to extend the knowledge concerning wood impregnation with water or solution containing electrolytes, and the subsequent swelling, in humid or dry atmosphere, at different temperatures, or in contact with water or aqueous solutions containing salts. Result discrepancies were explored and discussed.

It was shown how SAXS data from synchrotron measurements of pre-treated samples immersed in solution allow the evaluation of the absolute distance between cellulose crystals in fully hydrated solutions (nanometric scale). At the current state of present setups, this method was the only one that gives us the possibility to investigate the sample while immersed in solution in "static conditions" (i.e. without alterations of any environmental parameter). Spruce compression wood slices of a defined thickness of 100 μm were measured to explore the effects of salt impregnation, and registered values of inter-crystalline distance of 4.04 nm for the untreated sample, and of 4.25 nm for the sample pre-treated with NaI. The analysis could be furthermore implemented as a function of osmotic pressure, both in "static" and "dynamic" mode, via a closed chamber that allows the control of relative humidity.

ESEM techniques allowed us to observe the sample at microscopic scale, to quantify the sensitivity of differently pre-treated materials to environmental condition changes (humidity, temperature). Reported results show that ionic specific effect on swelling properties of wood, already described in a previous work, was qualitatively confirmed. The sample pre-treated with a swelling-inducing salt NaI showed a higher sensitivity to relative humidity changes (3.40% axial strain difference from 100%RH to 25%RH) compared to the one pre-treated with a non-swelling-inducing salt NaBr (3.13%) and to the untreated sample (2.45%). Temperature effects are limited to a maximum strain difference of 0.8% in a ΔT of 15°C, and might be due to an increase of the matrix configurational entropy. To make results more reliable with the state-of-art data, the sample holding system should be implemented to avoid uncontrollable errors due to moving and bending of the sample. For the untreated sample a difference on the axial strain of ca. 2.5% was registered

with respect to the results obtained via a custom built tensile stage, designed to follow in-situ relative swelling of the material during drying, which gave comparable results with respect to literature.

By means of tensile stage measurement the relative swelling of the material during the water/solution sorption was also quantified, and it was shown that with respect to a untreated sample immersed in water, whose strain in wet conditions was taken as reference (i.e. ε_x=0%), impregnation with NaI induces a sensitively higher axial strain ε_x of 3%.

At the current state of development, the techniques show good potential for applications in the field, but the setups could be furthermore improved in order to have more consistent results.

As a continuation of the previous works (*Barbetta et al. 2017a,b*), it was intended to extend the study on the ion specific effects, based on the Hofmeister series, by extending the study from the case of the analysis of the effects of impregnation on the material, to the case of the response of already treated samples to changes in the environmental conditions. For this reason, results obtained with the different techniques for the untreated wood samples have been combined in the form of an experimental Equation of State that quantifies the link between osmotic pressure and wood swelling, reported in terms of distance between cellulose crystal, and compared to the one predicted from modeling. The resulting picture shows consistent trends for the two cases that converge at high humidity, while a tendency to diverge is detected at lower humidity points. Both ESEM and TS experimental setups, as explained, and model input parameters of the calculations could be furthermore implemented to obtain more accurate results, for example recent investigations of the individual forces contributing to swelling given by the single components of the swellable matrix (*Barbetta et al. 2017a*).

The complexity of wood in terms of composition and molecular and hierarchical structure has challenged scientists belonging to different communities for a long time. A comprehensive understanding of the tissues requires the description of the materials at multiple length scales and needs an underlying molecular model. With this contribution, a combination of experimental techniques and a physico-chemical model are proposed, which allow for describing the changes at the nanometric/molecular levels accompanying wood swelling. Despite the results not being fully consistent at all the considered scales, it was shown how to reconcile different languages and conventions used in different communities to obtain a common description of the material.

3.5 Supporting information

3.5.1 Conversion graphs

Correlation between relative humidity and osmotic pressure, between intercrystalline distance and moisture content, and between crystalline cellulose volume fraction and extra swelling due to the presence of salts

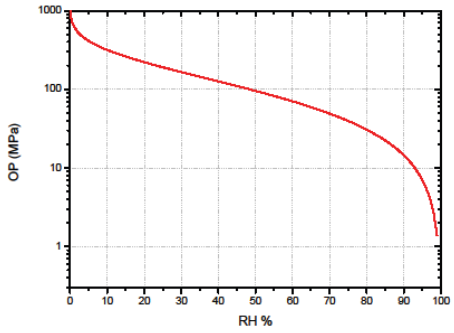

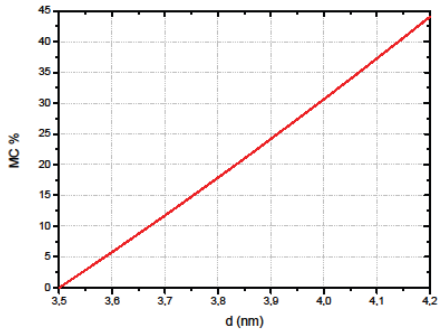

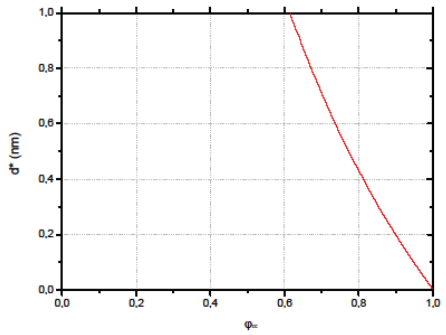

References

(Altaner et al. 2006) C. Altaner, D.C. Apperley, M.C. Jarvis *Spatial relationships between polymers in Sitka spruce: proton spin-diffusion studies*, 2006 Holzforschung 60, 665

(*Alves et al. 2016*) L. Alves, B. Medronho, F.E. Antunes, B. Lindman *Dissolution state of cellulose in aqueous systems- 2 acidic solvents*, 2016 Carb. Pol. 20, 151, 707

(*Baer and Mundy 2013)* M.D. Baer, C.J. Mundy *An ab initio approach to understanding the specific ion effect*, 2013 Farad. Discuss. 160, 89

(*Barbetta et al. 2017a*) A. Barbetta. P. Fratzl, T. Zemb, L. Bertinetti *Impregnation and swelling of wood with salts: ion specific kinetics and thermodynamics effect*, 2016 Adv. Mater. Interfaces 1600437

(*Barbetta et al. 2017b*) A. Barbetta, L. Bertinetti, T. Zemb *Composition dependent Equation of State of cellulose based plant tissues in the presence of electrolytes*, 2017 Colloid Sufaces A Physicochem. Eng. Asp. 532, 314

(*Beckers et al. 1998*) E. Beckers, M. de Meijer, H. Militz, M. Stevens *Performance of finishes on wood that is chemically modified by acetylation*, 1998 J. Coat. Technol. 70, 878, 59

(*Bernabei and Salvatici 2016*) M. Bernabei, M.C. Salvatici *In situ ESEM observations of spruce wood (Picea abies Karst.) during heat treatment*, 2016 Wood Sci. Technol. 50, 715

(*Bertinetti et al. 2013*) L. Bertinetti, F.D. Fischer, P. Fratzl *Physicochemical basis for water-actuated movement and stress generation in nonliving plant tissues*, 2013 Phys. Rev. Lett. 11, 238001

(*Bertinetti et al. 2015*) L. Bertinetti, A. Masic, R. Schuetz, A. Barbetta, B. Seidt, W. Wagermaier, P. Fratzl *Osmotically driven tensile stress in collagen-based mineralized tissues*, 2015 J. Mech. Behav. Biomed. Mater. 52, 14

(*Bertinetti et al. 2016*) L. Bertinetti, P. Fratzl, T. Zemb *Chemical, colloidal and mechanical contributions to the state of water in wood cell walls*, 2016 New J. Phys. 18, 083048

(*Chang et al. 2012*) S. Chang, F. Quignard, F. Di Renzo, B. Clair *Solvent polarity and internal stresses control the swelling behavious of green wood during dehyration in organic solution*, 2012 Bioresurces 7, 2418

(*Eder et al. 2008*) M. Eder, S. Stanzl-Tschegg, I. Burgert *The fracture behavior of single wood fibers is governed by geometrical constraints: in situ ESEM studies on three fiber types*, 2008 Wood. Sci. Technol. 42, 679

(*Elbaum et al. 2008*) R. Elbaum, S. Gorb, P. Fratzl *Structures in the cell wall that enable hygroscopic movement of wheat awns*, 2008 J. Struct. Biol. 164, 101

(*Elustondo et al. 2010*) D.M. Elustondo, L. Oliveira, S. Avramidis *New methodology to optimize sorting in wood drying*, 2010 Maderas. Cienc. Tecnol. 12, 2, 79

(*Fengel and Wegener 2003*) F. Fengel, G. Wegener *Wood - chemistry, ultrastructure, reactions*, 2003 Verlag Kessel

(*Fernandes et al. 2011*) A.N. Fernandes, L.H. Thomas, C.M. Altaner, P. Callow, V.T. Firsyth, D.C. Apperley, C.K. Kennedy, M.C. Jarvis *Nanostructure of cellulose microfibrils in spruce wood*, 2011 PNAS 108, 47, E1195

(*Fratzl and Barth 2009*) F. Fratzl, F.G. Barth *Biomaterial systems for mechanosensing and actuation*, 2009 Nature 462, 442

(*Fratzl and Weinkamer 2007*) P. Fratzl, R. Weinkamer *Nature's hiercachical materials*, 2007 Prog. Mater. Sci. 52, 1263

(*Fratzl et al. 2009*) P. Fratzl, R. Elbaum, I. Burgert *Cellulose fibrils direct plant organ movements*, 2009 Farad. Discuss. 139, 275

(*Gorisek and Torelli 1999*) Z. Gorisek, N. Torelli *Microfibril angle in juvenile, adult and compression wood of spruce and silver fir*, 1999 Phyton 39, 3, 129

(*Heymann et al. 1937*) E. Heymann, H.G. Bleakley, A.R. Docking *Studies on the lyotropic series. I The adsorption of salts on methylcellulose*, 1937 J. Phys. Chem. 42, 3, 353

(*Heymann and McKillop 1938*) E. Heymann G.C. McKillop, *Studies on the lyotropic series. II The adsorption of salts on cellulose*, 1937 J. Phys. Chem. 45, 2, 195

(*Hill et al. 2009*) C.A.S. Hill, A. Norton, G. Newman *The water vapor sorption behavior of natural fibers*, 2009 J. Appl. Polym. Sci. 112, 1524

(*Jakob et al. 1996*) H.F. Jakob, S.E. Tschegg, P. Fratzl *Hydration dependence of the wood-cell wall structure in Picea abies*, 1996 Macromolecules 29, 8435

(*Jendrasiak and Mendible 1976*) G.L. Jendrasiak, J.C. Mendible *The effect of the phase transition on the hydration and electrical conductivity of phospholipids*, 1976 Biochim. Biophys. Acta 424, 133

(*Kazi et al. 1998*) K.M.F. Kazi, P. Jollez, E. Chornet *Preimpregnation: an important step for biomass refining processes*, 1998 Biomass Bioenergy 15, 2, 125

(*LeNeveu et al. 1977*) D.M. LeNeveu, R.P. Rand, V.A. Parsegian, D. Gingell *Measurement and modification of forces between lecithin bilayers*, 1977 BIoph. J. 18, 209

(*Mantanis 2017*) G.I. Mantanis *Chemical modification of wood by acetylation of furfurylation: a review of the present scaled-up technologies*, 2017 BIoresources 12, 2, 4478

(*Mathias et al. 1991*) L.J. Mathias, S. Lee, J.R. Wright, S.C. Warren *Improvement of wood properties by impregnation with multifunctional monomers*, 1991 J. Appl. Polym. Sci. 42, 55

(*Medronho and Lindman 2014*) B. Medronho, B. Lindman *Competing forces during cellulose dissolution: from solvents to mechanisms*, 2014 COCIS 19, 1, 32

(*Medronho et al. 2012*) B. Medronho, A. Romano, M. Graça Miguel,L. Stigsson, B. Lindman *Rationalizin cellulose (in)solubility: reviewing basic physicochemical aspects and role of hydrophilic interactions*, 2012 Cellulose 19, 581

(*Murata et al. 2013*) K. Murata, Y. Watanabe, T. Nakano *Effect of thermal treatment on fracture properties and adsorption properties of spruce wood*, 2013 Materials 6, 4186

(*Onuki et al. 2011*) A. Onuki, R. Okamoto, T. Araki *Phase transitions in soft matter induced by selective solvation*, 2011 Bull. Chem. Soc. Jpn. 84, 6, 569

(*Parsegian and Zemb 2011*) V.A. Parsegian, T. Zemb *Hydration forces: observations, explations, expectations, questions*, 2011 COCIS 16, 618

(*Podgornik and Parsegian 1997*) R. Podgornik, V.A. Parsegian *On a possible microscopic mechanism underlying the vapor pressure paradox*, 1997 Biophys. J. 72, 942

(*Podgornik et al. 1977*) R. Podgornik, H.H. Strey, V.A. Parsegian *Colloidal DNA*, 1977 Biophys 18, 209

(*Poulanne and Halonen 2010*) E. Poulanne, M. Halonen *Theoretical aspects of water-holding in meat*, 2010 Meat Sci. 86, 151

(*Rahim and Huque 1966*) K.A. Rahim, M.M. Huque *Swelling of cellulose in salt solutions and its relation to the radii of ions*, 1966 J. Text. I. 57, 8, T374

(*Rand and Parsegian 1989*) R.P. Rand, V.A. Parsegian *Hydration forces between phospholipid bilayers*, 1989 Biochim. Biophys. Acta 988, 351

(*Redman et al. 2016*) A.L. Redmanm H. Bailleres, I. Turner, P. Perré *Characterisation of wood-water relationships and transverse anatomy and their relationship to drying degrade*, 2016 Wood Sci. Technol. 50, 739

(*Rowell 2014*) R.M. Rowell *Acetylation of wood - a review*, 2014 Int. J. Lignocellulosic products 1, 1

(*Salmén 2004*) L. Salmén *Micromechanical understanding of the cell-wall structure*, 2004 Biologies 327, 873

(*Schindelin et al. 2012*) J. Schindelin, I. Arganda-Carreras, E. Frise, V. Kaynig, M. Longair, T. Pietzsch, S. Preibisch, C. Rueden, S. Saafels, B. Schmid, J.Y. Tinevez, D.J. White, V. Hartenstein, K. Eliceiri, P. Tomancak, A. Cardona *Fiji: an open-source platform for biological-image analysis*, 2012 Nat. Methods 9, 676

(*Singh et al. 2015*) P. Singh, H. Duarte, L. Alves, F. Antunes, N. Le Moigne, J. Dormanns, B. Duchemin, M.P. Staiger, B. Medronho *From cellulose dissolution and regeneration to added value applications - synergism between molecular understanding and material development*, 2015 Cellulose - Fundamental aspects and current trends, Intech

(*Tristram-Nagle et al. 1998*) S. Tristram-Nagle, H.I. Petrache, R.M. Suter, J.F. Nagle *Effect of substrate roughness on D spacing supports theoretical resolution of vapor pressure paradox*, 1998 Biophys. J. 74, 1421

(*Turkulin et al. 20014a*) H. Turkulin, L. Holzer, K. Richter *Application of the ESEM technique in wood research. Part I. Optimization of imaging parameters and working conditions*, 2004 Wood Fiber Sci. 37, 4, 552

(*Turkulin et al. 20014b*) H. Turkulin, L. Holzer, K. Richter *Application of the ESEM technique in wood research. Part II. Comparison of operational models*, 2004 Wood Fiber Sci. 37, 4, 565

(*Volkova et al. 2012*) N. Volkova, V. Ibrahim, R. Hatti-Kaul, L. Wadsö *Water sorption isotherms of Kraft lignin and its composites*, 2012 Carbohyd. Polym. 87, 1817

(*Wallström and Lindberg 2000*) L. Wallström, K.A.H. Lindberg *The diffusion, size and location of added silver grains in the cell walls of Swedish pine, Pinus sylvestris*, 2000 Wood Sci. Technol. 34, 403

(*Weinkamer and Fratzl 2011*) R. Weinkamer, P. Fratzl *Mechanical adaptation of biological materials - the example of bone and wood*, 2011 Mat. Sci. Eng. 31, 1161

(*Whitney et al. 1998*) S.E.C. Whitney, J.E. Brigham, A.H. Darke, J.S. Grant Reid, M.J. Gidley *Structural aspects of the interaction of mannan-based polysaccharides with bacterial cellulose*, 1998 Carbohyd. Res. 307, 299

Acknowledgements

The authors thank Klaus Bienert and Marco Bott, Max Planck Institute of Colloids and Interfaces, for technical support and development of the in situ mechanical testing devices, Stefan Siegel and Chenghao Li for their support during the X-ray measurements at the µ-spot beamline (BESSY II, Helmholtz–Zentrum für Materialien und Energie, Berlin, Germany). The excellence laboratory LABEX-Chemisyst ANR is acknowledged for the French-German PhD Stipendium. T.Z. acknowledges the Humboldt fundation for support. The financial support by DFG through Leibniz Award to P.F. is also aknowledged. This work was fully undertaken within the scope of the French–German agreement L.I.A. RECYCLING between CNRS/INC and MPG/MPIKG. The authors thank Helmuth Möhwald for numerous helpful discussions.

4. Composition dependent Equation of State of cellulose based plant tissues in the presence of electrolytes

A. Barbetta, L. Bertinetti, T. Zemb, 2017 Colloids Surf. A Physicochem Eng. Asp.

DOI: 10.1016/j.colsurfa.2017.04.075

Cell walls of so-called "wood-materials" are constituted by a complex, highly anisotropic and hierarchically organized nanocomposite, characterized by stiff crystalline cellulose nano-fibers, parallel to each other, and embedded in a softer and less anisotropic matrix of hemicelluloses, lignin and water. This matrix is hygroscopic, and therefore swells with increasing humidity. Consequently, wood cells undergo large dimensional changes. A minimal model of wood secondary cell walls to predict water absorption has recently been developed by Bertinetti and co-workers (Bertinetti et al. 2016) in the form of an Equation of State (EOS) that represents equivalently the water sorption versus relative humidity, as considered in chemical engineering, or the relation between osmotic pressure and volume of solutes, in the physical chemistry equation of state approach initiated by Jean Perrin. We extend hereby this model to the presence of electrolytes adsorbed in the gel part wood cell wall and compare compression wood cell walls to the extreme case of coir.

4.1 Introduction

Wood cell wall is a nanocomposite material (*Fratzl and Weinkamer 2007, Dunlop and Fratzl 2010*). It is constituted by parallel stiff crystalline cellulose fibers (ca. 50%), embedded in a soft matrix composed by hemicelluloses (20-35%), lignin (10-25%) and water (*Altaner et al. 2006*). This matrix is hygroscopic, and undergoes dimensional changes (*i.e.* anisotropic swelling) upon water uptake, or upon increasing relative humidity. This swelling behavior can be expressed in terms of Equation of State (EOS) as it has been recently established (*Bertinetti et al- 2006*). Equations of state can be expressed either using quantities typical of chemical and materials engineering, *i.e.* the water content versus relative humidity, or in quantities used in physical chemistry, *i.e.* the osmotic pressure, seen as a chemical potential of water divided by the molar volume versus a distance (*Wolfe and Bryant 1992*), or a volume (*Parsegian et al. 1986*), as introduced by Jean Perrin using monodisperse emulsions of latex in his Nobel prize winning work, early in the XXth century (*Perrin 1913*).

As the EOS, depending on the field, can be expressed using several different units, in **4.5.1** (Supporting information) we present the relationships between the physical quantities needed to convert the EOSs in the different languages:

- the universal relation between relative humidity and osmotic pressure;
- the relation between water uptake and inter-crystalline distance d in the case of compression wood cell walls and for a specific cellulose crystal size;
- the relation between spacing d^* and the water volume fraction (water volume versus total volume) as well as the crystalline cellulose volume fraction knowing that wood cell wall is comprised of four main components of known volumes (crystalline cellulose, soluble cellulose, lignin and water).

The aim of the present work is to extend that Equation of State to the case of cellulose-based materials containing crystalline cellulose in the presence of electrolytes. The chosen reference model system is spruce compression wood either as is for the standard EOS, or impregnated for a long period with a concentrated electrolytes solution to extend the EOS taking into account electrostatic forces.

An important “excess” swelling is sometimes observed if wood is impregnated with a solution containing electrolytes. This is a specific effect: larger strains are induced by so-called "antagonistic salts" (*Onuki et al. 2011*), made by one ion that can easily lose its hydration sphere ("chaotrope") and adsorb at the interface between cell walls constituents, and a counter-ion that stays in the space between them, in its hydrated form ("kosmotrope"). The case of maximal swelling has been considered in a previous work (*Barbetta et al. 2016*), and indicates the asymptotic limit of the EOS at zero osmotic stress.

Efficient swelling agents are for example NaI and $CaBr_2$: axial strains along the fibers direction ε_x of respectively ca. 3% and 2.5% are measured with a tensile stage on thin spruce compression wood foils (150 µm thick) when changing the sample environment from water to the salt solution.

Specific effects also occur in the case of samples pre-treated with salt solutions impregnation and afterwards exposed to decreasing relative humidity, RH, (*i.e.* increasing the osmotic pressure, OP), as shown recently using Environmental Scanning Electron Microscopy (ESEM, *Barbetta et al. submitted*). Dehydration experiments were performed via ESEM in controlled RH conditions: the processing of the recorded images allowed to track clear details in material structure and evaluate the relative changes in their distance during drying. Results showed an axial strain ε_x of -3% from 100% RH to 25% RH in the case of samples pretreated with a NaI solution, compared with an ε_x of -2.45% in the same RH range in the case of non pre-treated samples. Although these effects can be measured only in relative terms with most of the classical techniques used in the field, with an appropriate knowledge of material's structure, by means of scattering techniques it is possible to reinterpret these data in terms of absolute values: with small angle X-ray scattering (SAXS), for example, it is possible to evaluate the absolute distance between adjacent cellulose crystals, which has been shown to be 4.25 nm and 4.04 nm, respectively for the samples pretreated with NaI and the ones that were not pretreated.

Previously to the abovementioned combined microscopy and X-ray micro-investigations (*Paris et al. 2007*), values of wood moisture content were obtained via different techniques, such as gravimetric methods, based on measures of the weight difference between wet and oven dried samples (*Hergt and Christensen 1965*), or using distillation devices, in which liquids immiscible with water that are good solvents for wood volatile components avoid experimental errors due to evaporation (*Kollmann and Höckele 1962*). Lately, more modern instruments that give faster and

more automatic responses were applied for calculations of MC, such as NMR (*Nanassy 1973*) or electrical moisture meters (*Stamm 1927*).

Starting from experiment performed with these techniques, more than 70 different general models have been developed in chemical engineering as parametric expressions to fit sorption isotherm data, and have been applied to water uptake by wood (*Limousin et al. 2007*). Most common models are either based on considering water adsorption at a surface or considering sorption as a solution phenomenon. Although the hypotheses underlying their formulation is different, they are mathematically equivalent (*Boquet et al. 1980*).

Examples of the first type are BET (*Brunauer et al. 1938*) and Dent (*Dent 1980*) models, whose constituent equations are derived by considering the equilibrium of condensation and evaporation of water on wood cell wall sorption sites (*i.e.* hydroxyls) with different binding energies for each binding layer.

In the most popular approach of the second kind, as in the Hailwood-Horrobin parametric model (*Hailwood and Horrobin 1946*), sorbed water is considered to combine with soluble polymeric units to form a hydrate and to form a solid solution in the cell walls. Therefore, the two equilibria that are taken into account are the ones of dissolved water, with water vapor and with water molecules bounded to the polymers. The mathematical expressions for these three models are recalled in **4.5.2** (Supporting information).

In order to evaluate the quality and the reliability of the models, predicted and measured heats of sorption can be compared. Results discrepancy is around 50% (*Simpson 1973*). Despite the fact that fitting the results with non-linear regression techniques could drastically reduces the difference (*Simpson 1973*), the gap between theory and experiments looks still remarkable at this point, especially considering that none of the models takes into account wood materials' specific structure and composition.

Moreover, at the current level a limiting factor for the theory is that matrix components' individual contributions to swelling are not yet distinguishable. Our aim in this work is to compare EOS of compression wood with the ones obtained for another cellulosic natural materials with different composition: lignin-rich poorly swelling coir fibers extracted from coconut, that are largely used since centuries in hot and wet conditions, and that are composed by cellulose (ca. 50%) and lignin (ca. 45%).

4.2 Materials and methods

4.2.1 Compression wood

Compression wood samples from Spruce tree (*Picea abies*) were cut in 100 µm slices, in the parallel direction with respect to fibers orientation, with a Leica-rm2255 microtome, stored in freezer at -20°C, to preserve their natural conditions, and unfrozen in a fridge at 4°C the day before the experiments.

4.2.2 Coir

Coir fibres, extracted from the husk of coconut (*Cocos nucifera*), were obtained from from Hayleys (Sri Lanka), that produces them for fiber mattresses, and stored in dry ambient conditions.

4.2.3 Force balance method for the case of swelling in the absence of impregnating electrolytes

Rationalization of the process of water uptake by wood starts from a geometric minimal model of wood cell walls, at nanometric scale, in which the hexagonal cellulose crystals are considered as coated by a thin layer of a homogeneous matrix, as the distribution of its components in the polymeric gel are not yet fully understood (*Bertinetti et al. 2016*).

In any Equation of State approach molecular and macroscopic forces simultaneously contributing to wood spatial deformations (either by favoring or limiting swelling) are individually evaluated and then summed up in the form of a force balance, in which derivatives of chemical, colloidal and mechanical energies are calculated (*Bertinetti et al. 2013*). The force balance developed so far for cell walls includes: enthalpy of chemical binding between cellulose fibers and matrix components, dependent on the number of contact points, free energy of hydration repelling cellulose crystals separated by a layer of water, configurational entropy of the matrix, van der Waals force between crystals, and elastic energy generated by anisotropic swelling of the material.

The validity of the EOS can be extended to the case of wood impregnation with electrolytes, used as swelling agents, by considering also in the force balance an extra electrostatic term. If an electrolyte penetrates the gel in between the crystallites, and it is in equilibrium with excess brine, no extra term has to be considered, since electrolyte activity is the same inside the wood cell wall and outside, *i.e.* in the bathing fluid as well as in the large macroscopic channels present in wood

cell wall (*Merk et al. 2016*). However, if the anion or the cation is adsorbed or complexated on the surface of the hydrophobic crystalline material, charge separation occurs: electrostatic repulsion between charged crystals is screened by the diffuse layer of counter-ions and any other "background" salt present (*Belloni 1998*).

4.3 Results and discussion

4.3.1 Modification of the Equation of State induced by impregnated salts

The mathematical derivation of the osmotic pressure $\Pi(D)$ considers two adjacent cellulose crystals, coated by a matrix layer, as two infinite parallel plans, separated by a water layer of a certain thickness D, in osmotic equilibrium with a salt solution, used as reservoir. At this level, all ions are considered to be monovalent. In the "weak overlap approximation" case (*i.e.* $D \gg \lambda$, where λ is the Debye length), the layers diffusing in the proximity of the two plans weakly superpose, and the interaction is connected to the electrostatic properties in the proximity of an isolated plan. Analytical expression of the simultaneous equations to calculate the osmotic pressure is reported in **4.5.3** (Supporting information).

The relationship between binding constant of the ions to the available sorption sites and the free energy of binding is based on a simple equation (**Eq 4.1**):

$$K = \Sigma\delta e^{-\Delta G_s/RT} \qquad \textbf{Eq 4.1}$$

In this expression, K is the binding constant of the binding ion, assumed to be by three orders of magnitude higher than the one of the non-binding one, Σ is the surface area of the binding sites, taken as 1 nm^2, δ is the diameter of the dominant binding ion, expressed in nm, and ΔG_s is the binding energy in J/mol. **Fig 4.3.1** shows the calculated Equation of State for three different ionic radii, corresponding to the one used in previous work (0.200 nm, approximately corresponding to the radius of I^-), and the ones of OH^- (0.133 nm) and of Mg^{2+} (0.072 nm). This last one was chosen because, according to the theory, in the case of salts composed by monovalent anions and divalent cations (e.g. $MgBr_2$, $CaBr_2$, ecc..), these last one are supposed to adsorb on the matrix

structure via bidentate complexation. However, we stress out that, for model simplicity, all ions are treated as monovalent (*i.e.* valence of ion $Z_i = \pm 1$ in the calculations).

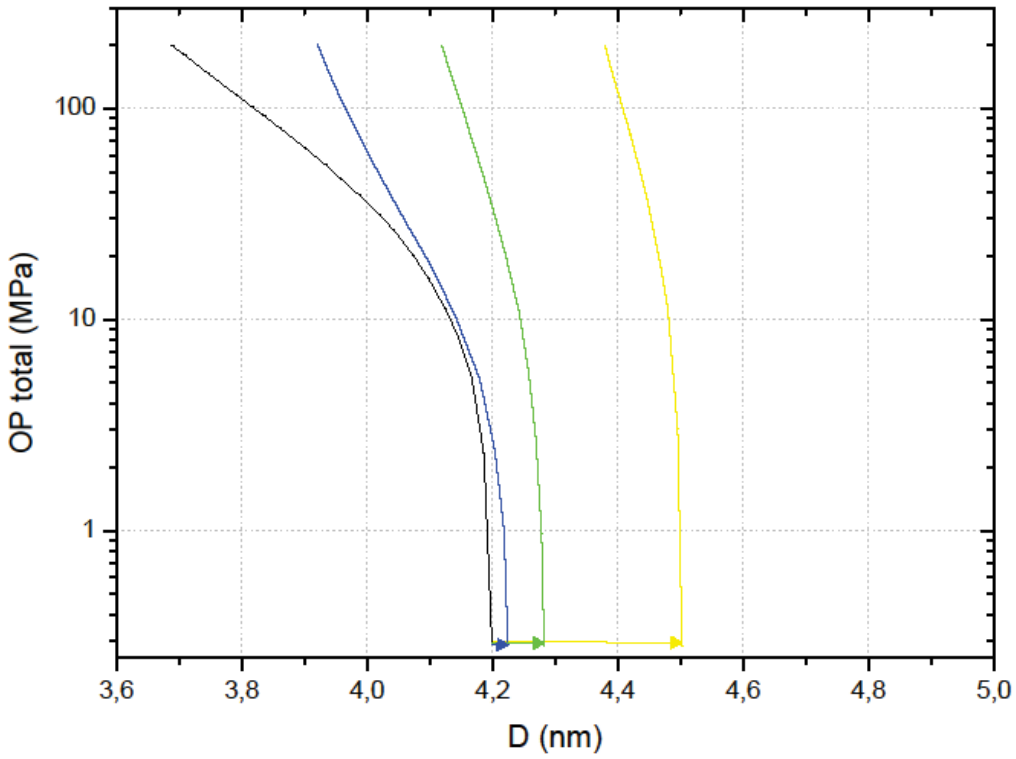

***Fig 4.3.1**: Calculated wood Equation of State, including electrostatic term due to the presence of impregnated salts, for three different ionic radii , corresponding to Mg^{2+} (blue), OH^- (green) and I^- (yellow), compared with the calculate EOS without salt impregnation (black). Arrows indicate the maximum swelling D_{max}.*

At a given binding constant (K = 0.035 M^{-1}), the charge separation created by selective sorption of one of the two ions leads to higher repulsive forces with increasing ionic sizes, and therefore to higher values of the maximum swelling D_{max}, calculated at 100% relative humidity. Moreover, the sensitivity to shrinkage with decreasing relative humidity (*i.e.* increasing Π), looks higher for smaller ions. Results of variations of free energy of adsorption (in the model, this means a tuning of the binding constant) at a fixed ionic radius for $\delta = 0.2$ nm are reported in **Fig 4.3.2**:

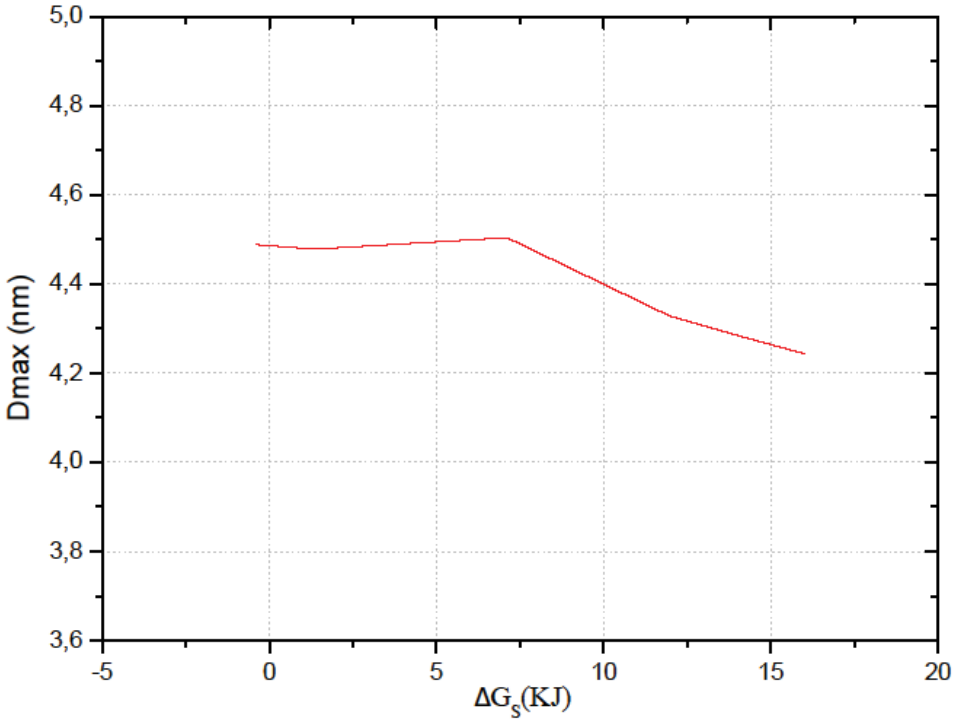

***Fig 4.3.2**: Calculated wood maximum swelling (i.e. swelling at 100% RH) in nm, as a function of free energy of binding of the cation binding to the crystalline cellulose considering the hydrated ionic radius of the chaotropic ion considered.*

Results show an evident increase of the maximum swelling D_{max} at small values of binding constant (higher ΔG_s), until the point at which charges are saturated and it reaches its maximum value: D_{max}= 4.50 nm at K = 0.035 M^{-1}. At higher values (*i.e.* with decreasing free energy of binding), charge screening leads to a slight shrinkage, with a resulting ΔD_{max} of -0.02 nm in a range of K of more than one order of magnitude. Results of the theoretical curve can be compared with experimental results published in literature (*Barbetta et al. 2016*) for D_{max} in the case of compression wood impregnated with a 4.70 M NaI solution, that indicate weak ion binding with positive values of ΔG_S (8 kJ/mol).

4.3.2 Comparing the swelling observed with results by fitting to parametric sorption models

The EOS based on first principle of colloidal forces can be compared with the EOS calculated from first principles with parametric water sorption isotherms such as general BET, or models adapted

to cellulosic materials such as the very popular ones initially proposed by Dent, Hailwood-Horrobin. In BET and Dent models sorption is considered as a surface phenomenon, in which water is sorbed on wood cell wall sorption sites, and supposed forming different "layers" in the crystalline cellulose. Dent model can be considered as modification of generic BET equations, in which secondary layers have a specific binding energy and constant which is assumed not to be the same as liquid water, as in the BET model.

On the other hand, in the Hailwood-Horrobin theory sorption is considered as a solution phenomenon: sorbed water forms an "hydrate" with the wood, and a solid solution is formed in the cell wall. In this case, the two equilibria defining the model equation are the ones of the dissolved water with the environmental water vapor and with the hydrated water.

Wood EOS, predicted from the model, is hereby compared from result obtained from classical sorption theories, such as BET, Dent and Hailwood-Horrobin (H-H). Derivation of the used equations is explained in details in **4.5.2** (Supporting information). **Fig 4.3.3a** compares the Equation of State derived from modeling with the classical aforementioned models. The three models strongly depend on three input parameters: the moisture content in hydrated conditions, and on the equilibrium constants of water condensation and evaporation. Used parameters for BET, Dent and H-H equations are also reported in the Supporting information (**Table 4.1**). BET curve strongly differs from the model curve, while Dent and H-H, which mathematically correspond, give more consistent results. It is important to point out that these theories have limited applicability, as swelling is not taken into account. Nevertheless, non-linear regression techniques can be used to fit these results to the modeling curve, as shown in **Fig 4.3.3b**. BET model looks clearly inadequate, while the curve representing Dent and H-H sorption models perfectly superpose to the modeling curve. Output parameters of the fit give a binding constant for the primary sorbed water layer K_1' (Dent theory) of 2.4 M^{-1} , that approximately corresponds to one half of the one found in literature for spruce wood (*Bertinetti et al. 2016*), while the constant for secondary water layers, K_2', do not change significantly. On the other hand, the value of the moisture content in hydrated conditions, M_0', is increased from 8.7% to 12.8%.

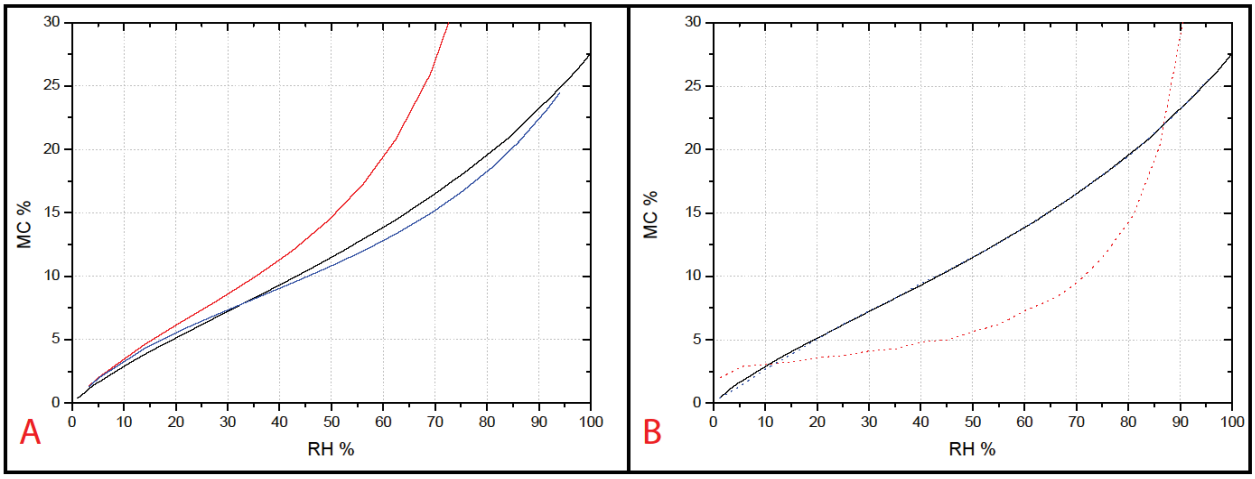

***Fig 4.3.3**: Wood Equation of State, in terms of moisture content MC as a function of relative humidity RH. a) comparison between modeling curve (black) and classical sorption models: BET (red) and Dent/Hailwood-Horrobin (blue) b) results of fitting the classical curves (BET: dotted red, Dent/Hailwood-Horrobin: dotted blue) to the one calculated from the model (black).*

4.3.3 Variations of the EOS with material composition

Experimental gravimetric EOS was obtained for wood via micro-gravimetric measurements, and compared to the one previously calculated by the model. Similarly to the case of results obtained from experiments performed via a tensile stage operating at controlled humidity, the model at its current state predicts higher water uptake than the observed one. This over-estimation was previously quantified, and data are consistent with the lower limit of the model, that has been obtained by multiplying all the attractive terms by a factor of 1.5, and dividing all the repulsive terms by the same factor. Acquired sorption data for coir fibers are also reported, with the interest of understanding how the components of the matrix, which were so far considered as undistinguishable, individually contribute to water sorption process (**Fig 4.3.4**). It must be noted that, for limits of the experimental setup, the materials' weight at the lowest humidity reached (2.7 RH%) was taken as the value of dry reference to calculate the moisture content from DSC raw data.

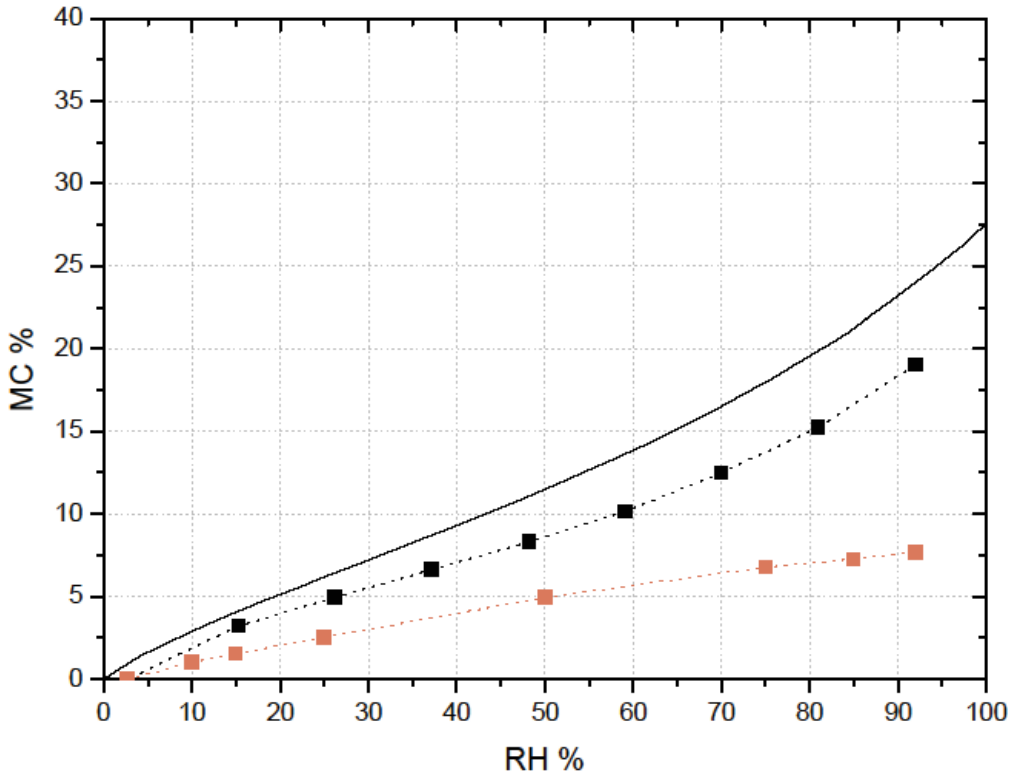

***Fig 4.3.4**: Equations of State, in terms of moisture content MC as a function of relative humidity RH: wood EOS calculated from modeling (black line), wood EOS calculated from modeling at its lower limit (grey), wood sorption data from DSC dehydration experiment (black squares) and coir sorption data from DSC dehydration experiment (light brown). The same experimental EOS are reported in **4.5.1** (Supporting information) in the form OP vs d.*

The sorption behavior of coir material (light brown) show a slight increase of fibers' weight, with a maximum moisture content value of 7% at high humidity, approximately corresponding to one third of the one of compression wood in the same conditions, meaning a limited availability for water uptake.

In order to evaluate the effects of the impregnation with a swelling agent, dehydration experiments were repeated on compression wood and coir samples pre-treated with a 4.7 NaI solution. Results are shown in **Fig 4.5.5a**. In both wood and coir fibers, salt impregnation implies a clear enhancing of water uptake process. This is more evident in the case of wood, where an

increase of 10% on the moisture content at the highest humidity is observed with respect to the untreated sample. In the case of coir, the effect of impregnation is limited to an extra 4%. The study of the effects of NaI impregnation on coir fibers is of primary interest in order to understand the role of each component of wood cell walls material during water uptake. On **Fig 4.5.5b** experimental results of wetting and impregnation tests, performed with a tensile stage on coir fibers, are reported: sample in dry conditions was at first immersed in milli-Q water, then in a 4.7 M NaI, and finally washed again with water. This protocol was already used for similar experiments on compression wood samples. Similarly to the case of wood, wetting process induces an axial elongation ε_x of ca. 3%. The observed time needed for reaching the equilibrium is quite fast in the case of coir (ca. 3 hours). After one cycle of impregnation and washing, the final registered ε_x is less than 0.2%, approximately 1/10 of what was registered in the case of compression wood. Limited swelling indicates a weak electrolyte adsorption, meaning that hemicelluloses, abundant in wood cell wall materials but present only in traces in coir fibers) play a dominant role in the process.

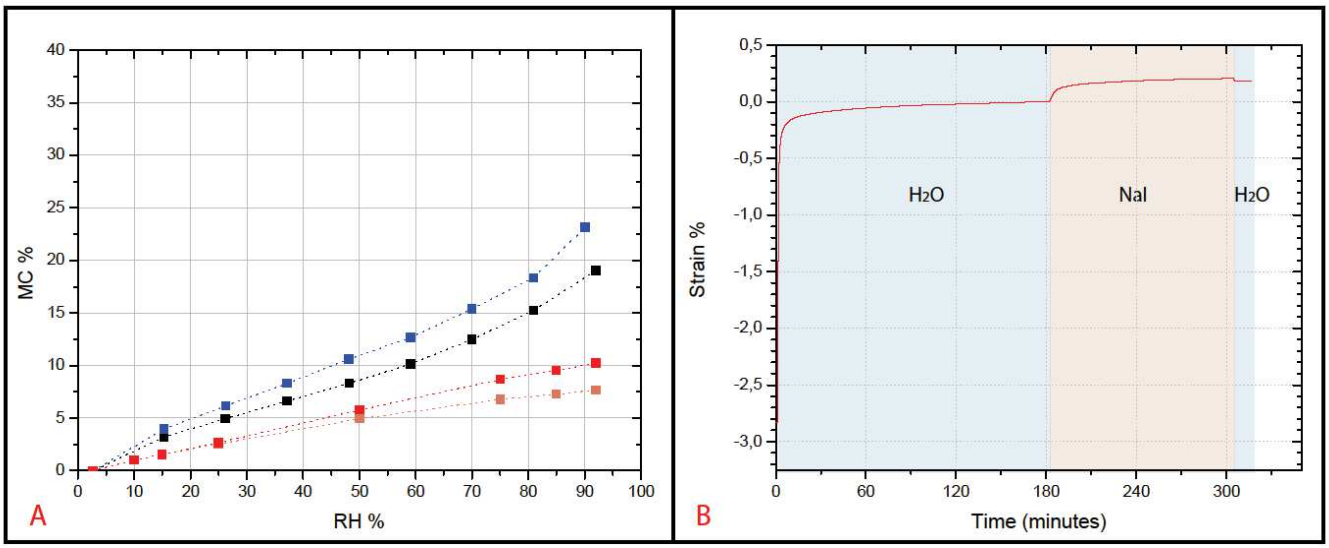

***Fig 4.3.5**: a) EOS expressed in terms of moisture content MC as a function of relative humidity RH, obtained from DSC dehydration experiments, for wood (black), wood pre-treated with a 4.70 M NaI solution (blue), coir (orange), coir pre-treated with a 4.70 M NaI solution (red). The same experimental EOS are reported in **4.5.1** (Supporting information) in the form OP vs d. b) Swelling profile of coir fibers sample, after wetting, impregnation with 4.0 NaI solution, and washing.*

4.4 Conclusion

The validity of the model describing water uptake by wood cell wall material has been extended in the present work to the case of the presence of monovalent ions in the reservoir solution.

An electrostatic term due to salt impregnation has been calculated and added to the force balance, using the swelling agent NaI 4.70M as antagonistic salt, with a chaotropic anion adsorbing on the crystalline cellulose. Free energy of binding of the anion is typically of the order of 8 kJ/mol. Results have been reported in the form of an Equation of State (EOS), showing material's swelling and shrinkage, in terms of absolute distance between adjacent cellulose crystal fibers, as a function of environmental relative humidity. The model shows good response to variation of the equilibrium constant (*i.e.* free energy of adsorption) and hydrodynamic size of the binding ion. Higher ionic radii imply higher structure swelling, while higher binding constants lead to charge screening and therefore to a slight shrinkage.

The peculiarity of the presented model is to take material's structure as a starting point, with respect to the existing sorption models, based on experimental sorption isotherm parameters. Calculated Equations of State derived from three of these "classical" models has been derived from literature, and compared to the modeling curve: although BET result are clearly divergent, Dent and Hailwood-Horrobin data set (which are mathematically equivalent) show only a slight discrepancy at higher humidity values, and their constitutive equation parameters can be fitted to the modeling curve, until they are superposed, by halving the binding constant and increasing the moisture content at fully hydrated status of few percentage points.

It must be pointed out that, at the current state of the model, a detectable difference can still be noted in comparison with experimental results. We showed that experimental gravimetric EOS is comparable to the one derived from lower limit of the model, obtained by overestimating the attractive terms, opposing to swelling, and underestimating the repulsive ones.

In the model, wood has been considered as constituted by inert cellulose fibers embedded in a homogeneous swellable matrix. As this is normally composed of hemicelluloses and lignin, future developing of the modeling concern the evaluation of the individual contributes of the matrix components to swelling. With this goal, experimental gravimetric EOS have been studied for coir

material. Coir is made of cellulose and lignin, and present a considerable electrolytic content. Coir water uptake look limited, with a maximum measured moisture content of ca. 6% at high humidity. Moreover, tensile test experiments were performed to evaluated coir fibers elongation during water and NaI solution uptake: while the 3% axial strain registered while passing from dry to wet sample is equal to that of compression wood, immersion in concentrated salt solution results in a negligible swelling. This favors the idea of a dominant role of hemicelluloses during electrolytes adsorption.

4.5 Supporting information

4.5.1 Conversion graphs

The following graphs show:

1- The correlation between relative humidity and osmotic pressure

2- The correlation between inter-crystalline distance and moisture content

3- The correlation between crystalline cellulose volume fraction and extra swelling due to the presence of salts

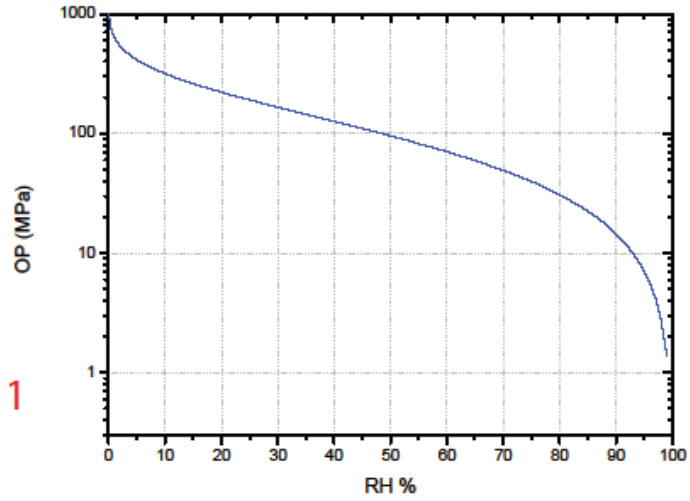
OP (MPa)
1000
100
10
1
0
10
20
30
40
50
60
70
80
90
100
RH %

1

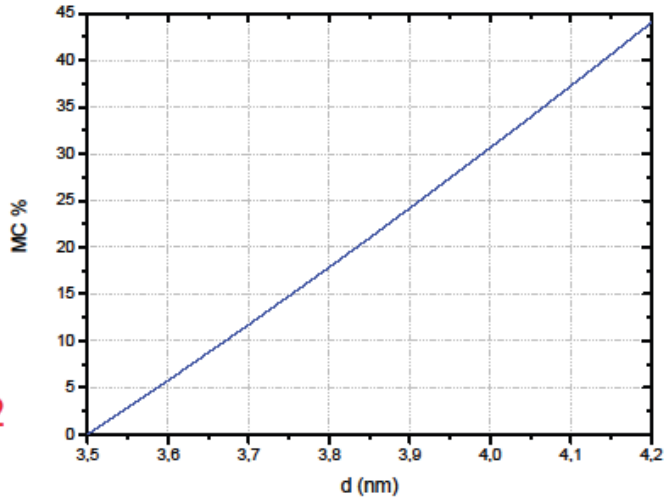
MC %
45
40
35
30
25
20
15
10
5
0
3,5
3,6
3,7
3,8
3,9
4,0
4,1
4,2
d (nm)

2

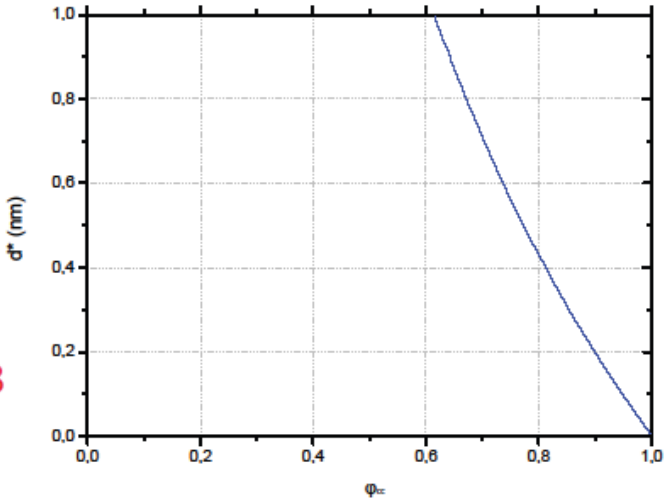
d* (nm)
1,0
0,8
0,6
0,4
0,2
0,0
0,0
0,2
0,4
0,6
0,8
1,0
φ∞

3

Experimental EOS are reported in the form showing osmotic pressure OP as a function of the distance between cellulose crystals, for the case of coir (brown), pre-treated coir with 4.70 M NaI solution (red), compression wood (blue) and pre-treated compression wood with a 4.70 M NaI solution (blue).

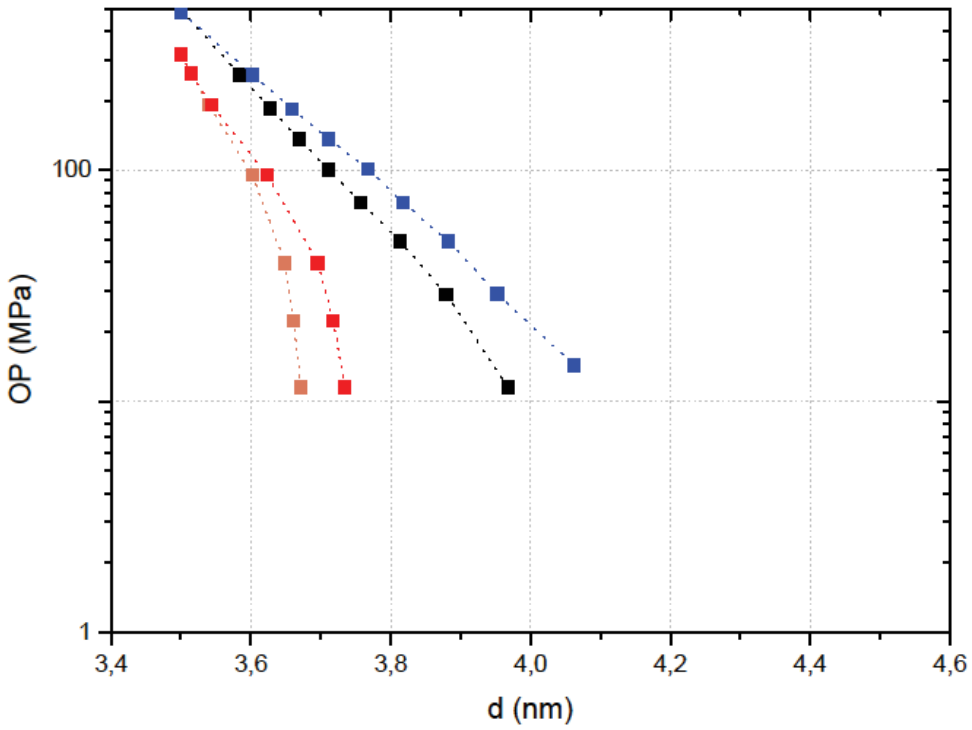

4.5.2 Mathematical expression of classical sorption theories equations

BET and Dent equation are defined from the equilibrium of condensation and evaporation of water from sorption sites, at each layer. The difference between the two models is in the fact that the first one approximates the thermodynamic properties of the water in the secondary layers to the one of liquid water, while in the second one specific binding constants are introduced. In terms of moisture content and relative humidity, the two resulting equations can be rearranged as follows (**Eq 4.2** and **Eq. 4.3**):

BET: $MC = \frac{M_0' K_1' x}{(1-x)(1+K_1' x-x)}$ **Eq 4.2**

Dent: $MC = \frac{M_0' K_1' x}{(1-K_2' x)(1+(K_1'-K_2')x)}$ **Eq 4.3**

where x represents the relative humidity, reported in a scale from 0 to 1, K_1' is equivalent to the saturated vapor pressure, multiplied by the ratio of the attachment rate constant of the vapor molecules per unit vapor pressure to the escape rate constant for the water molecules at the primary sorption. K_2' is similarly defined for secondary sorption sites. M_0' corresponds to the moisture content in the condition of complete monolayer coverage of all the available sorption sites.

The mathematical expression of the Hailwood-Horrobin model (H-H) is reported in **Eq 4.4**:

H-H: $MC = \frac{M_0 K_2 (K_1 + 1) x}{(1 + K_1 K_2 x)(1 - K_2 x)}$ **Eq 4.4**

where the term M_0 indicates the moisture content corresponding to the condition of complete polymer hydration (*i.e.* one molecule of water attached to each hydratable polymer unit). The two constants K_1 and K_2 represent the equilibrium of the formation of hydrates between dissolved water and the polymeric units, and the one between the hydrated water and the water vapor, respectively.

Calculated parameters for BET, Dent and H-H equations are listed in **Table 4.1**, for spruce wood at ca. 30°C.

M_0	M_0'	K_1	K_1'	K_2	K_2'
8.70	8.70	6.23	5.15	0.712	0.712

Table 4.1: *Calculated parameters for the sorption BET, Dent and H-H equations, for the case of spruce wood.*

4.5.3 Analytical derivation of the electrostatic term

Analytic expression of osmotic pressure is reported in **Eq 4.5**:

$\Pi = 64 k T c_s' \gamma^2 e^{-\kappa D}$ **Eq 4.5**

where c_s' is the total concentration of salt in the reservoir, intended as the sum of all the concentrations of the present ions, $\kappa = \lambda^{-1}$ is the screening constant, defined in **Eq 4.6**:

$$\kappa = \sqrt{8\pi L_B c_s'} \qquad \textbf{Eq 4.6}$$

In this equation, L_B represents Bjerrum length, which has a value of ca. 0.7 nm, in water at 25°C. Its analytical form is described in **Eq 4.7**:

$$L_B = \frac{e^2}{4\pi\varepsilon_0\varepsilon kT} \qquad \textbf{Eq 4.7}$$

In **Eq 4.5**, $\gamma = \tanh(\frac{\phi_s}{4})$ is a coefficient related to the surface electrostatic potential ϕ_s, defined from **Eq 4.8** (Grahame equation):

$$\sin(\frac{\phi_s}{2}) = \frac{2\pi L_B \Sigma_s}{\kappa} \qquad \textbf{Eq 4.8}$$

where Σ_s is the surface charge density.

Each ion *i* can adsorb on surface sites via a chemical reaction, following the law of mass action, expressed in **Eq 4.9**:

$$K_i = \frac{[site{-}i]}{[site]c_{i(surface)}} \qquad \textbf{Eq 4.9}$$

In this expression, three terms are present: the surface concentration of sites occupied by an *i* ion, that of the unoccupied sorption sites, and the volumetric concentration of ions *i* in contact with the plan where the reaction takes place. In **Eq 4.10**, the term $c_{i(surface)}$ is explained, and the law of mass action is written as a function of the occupation rate α_i if each *i* ion:

$$K_i = \frac{\alpha_i}{(1-\sum_j \alpha_j)\, c_i' e^{-Z_i\phi_s}} \qquad \textbf{Eq 4.10}$$

where the valence Z_i can be either +1 or -1.

The surface charge density is derived by summing all the *i* contributions, as shown in **Eq 4.11**:

$$\Sigma_S = \Sigma_0(Z_0 + \sum_j \alpha_j Z_j) \qquad \textbf{Eq 4.11}$$

Iterated solution of the three simultaneous equations (**Eq 4.8**, **Eq 4.10** and **Eq 4.11**) furnishes all the required parameters, including the coefficient γ that is needed to calculate Π.

References

(*Altaner et al. 2006*) C. Altaner, D.C. Apperley, M.C. Jarvis *Spatial relationships between polymers in Sitka spruce: proton spin-diffusion studies*, 2006 Holzforschung 60, 665

(*Barbetta et al. 2016*) A. Barbetta, P. Fratzl, T. Zemb, L. Bertinetti *Impregnation and swelling of wood with salts: ion specific kinetics and thermodynamics effects*, 2016 Adv. Mater. Interfaces 1600437

(*Barbetta et al. submitted*) A. Barbetta, L. Bertinetti, J. Lautru, R. Podor, T. Zemb *Nano-, meso- and macro- swelling characterization of impregnated compression wood cell walls*, submitted

(*Belloni 1998*) L. Belloni *Ionic condensation and charge renormalization in colloidal suspension*, 1998 Colloids Surf. A 140, 1, 227

(*Bertinetti et al. 2013*) L. Bertinetti, F.D. Fischer, P. Fratzl *Physicochemical basis for water-actuated movement and stress generation in nonliving plant tissues*, 2013 PRL 111, 238001

(*Bertinetti et al. 2016*) L. Bertinetti, P. Fratzl, T. Zemb *Chemical, colloidal and mechanical contributions to the state of water in wood cell walls*, 2016 New J. Phys. 18, 083048

(*Boquet et al. 1980*) R. Boquet, J. Chirife, H.A. Iglesias *Technical note: on the equivalence of isotherm equations*, 1980 J. Fd. Technolog. 15, 345

(*Brunauer et al. 1938*) S. Brunauer, P.H. Emmett, E. Teller *Adsorption of gases in multimolecular layers* 1938 J. Am. Chem. Soc. 60, 2, 309

(*Dent 1980*) R. W. Dent *A sorption theory for gas mixtures* 1980, Polym. Eng. Sci. 20, 4, 286

(*Dunlop and Fratzl 2010*) J.W.C. Dunlop, P. Fratzl *Biological composites*, 2010 Annu. Rev. Mate. Res. 40, 1

(*Fratzl and Weinkamer 2007*) P. Fratzl, R. Weinkamer *Nature's hierarchical materials*, 2007 Prog. Mater. Sci. 52, 1263

(*Hailwood and Horrobin 1946*) A.J. Hailwood, S. Horrobin *Absorption of water by polymers. Analysis in terms of a simple model*, 1946 Trans. Faraday Soc. 42B, 84

(*Hergt and Christensen 1965*) H.F.A Hergt, G.N. Christensen *Variable retention of water by dry wood*, 1965 J. Appl. Polym. Sci. 9, 2345

(*Kollmann and Höckele 1962*) F.F.P. Kollmann, G. Höckele *Kritischer Vergleich einiger Bestimmungsverfahren der Holzfeuchtigkeit*, 1962 Holz Roh-Werkst 20, 461

(*Limousin et al. 2007*) G. Limousin, J.P. Gaudet, L. Charlet, S. Szenknect, V. Barthès, M. Krimissa *Sorption isotherms: a review on physical bases, modeling and measuremtns*, 2007 Appl. Geochem. 22, 249

(*Merk et al. 2016*) V. Merk, M. Chanana, S. Gaan, I. Burgert *Mineralization by Calcium carbonate insertion for improved flame retardancy*, 2016 Holzforschung 70, 9, 867

(*Nanassy 1973*) A.J. Nanassy *Use of wide-line NMR for measurement of moisture content in wood*, 1973 Wood Sci. 5, 187

(*Onuki et al. 2011*) A. Onuki, R. Okamoto, T. Araki *Phase transitions in soft matter induced by selective solvation*, 2011 Bull. Chem. Soc. Jpn. 84, 6, 569

(*Paris et al. 2007*) O. Paris, C. Li, S. Siegel, G. Weseloh, F. Emmerling, H. Riesemeir, A. Erko, P. Fratzl *A new experimental station for simultaneous X-ray microbeam scanning for small- and wide-angle scattering and fluorescence at BESSY II*, 2007 J. Appl. Cryst. 40, s466

(*Parsegian et al. 1986*) V.A. Parsegian, R.P. Rand, N.L. Fuller, D.C. Rau *Osmotic stress for the direct measurement of intermolecular forces*, 1992 NATO ASI Subseries

(*Perrin 1913*) J. Perrin *Les atomes*, 1913 Flammarions, re-edited 1991

(*Simpson 1973*) W.T. Simpson *Predicting equilibrium moisture content of wood by mathematical models*, 1973 Wood Fiber Sci. 5, 1, 41

(*Stamm 1927*) A.J. Stamm *The electrical resistance of wood as a measure of its moisture content*, 1973 Wood Sci. 5, 187

(*Wolfe and Bryant 1992*) J. Wolfe, G. Bryant *Physical principles of membrane damage due to dehydration and freezing*, 1986 Method. Enzymol. 127, 400

Acknowledgements

This work was supported by a PhD Grant for the Labex “Chemisyst” ANR 2011-05 centered in Montpellier, and was performed with the CNS/INC and MPG/MPIKG agreement L.I.A. “RECYCLING” 2013-2017. The authors acknowledge input for the calculation of electrostatic term of Luc Belloni as well as inputs of Helmut Möhwald, supervisor of the associated French-German PhD.

5. Conclusions and outlook

In this work, we investigated the effects of the adsorption within wood materials of solutions containing monovalent and divalent electrolytes. For this purpose, several techniques were used in parallel to follow material's changes due to solution uptake at different scales, in controlled environmental conditions (*i.e.* temperature, water chemical potential, ionic strength): at the nanometric scale, via small angle X-ray scattering (SAXS), at the microscopic level, via Environmental Scanning Electron Microscopy (ESEM), and at macroscopic size, via mechanical tensile devices.

The experiments at macroscopic scale were performed with a tensile stage, and consisted in immersing compression wood foils in solutions of different salts, in iso-stress and iso-osmolar conditions, in order to be able to quantitatively compare the results. Experiments have been described in Chapter 2 (see **2.2** and **2.4**). This instrumental setup allows the user to follow the in-situ dynamics of adsorption by constantly monitoring and quantifying the axial dimensional changes of the sample during the experiment.

The results show that all salts tested induce a positive strain, of the order of few percentage points at maximum. Its amount strongly depends on salt composition. The strongest swelling is induced in the presence of salts made by one chaotropic and one kosmotropic ion (such as Sodium iodide NaI): in these cases, charge separation occurs, as the monovalent chaotropes (*Kunz et al. 2004*) can lose their hydration sphere and, once ejected from the bulk water, they then are supposed to specifically adsorb on the hemicelluloses structure, thus creating a surface charge of the crystalline cellulose fibres. This adsorption creates a net electrical field in which electrostatic forces induce some condensed effective counter-ions (most of the times kosmotropes) that remain strongly hydrated. The net charge is the effective charge and the rest of the counter-ions are located in the diffuse cloud, approximated herein as a simple Poisson-Boltzmann distribution.

Conversely, in the case of salts with divalent cations (such as $CaBr_2$) the swelling is induced by their weak binding to the OH groups at the cellulose crystal surface via bidentate complexation, which induces a positive charge. Among the salts studied, NaI induces the highest strain: 3% axial strain, in the direction parallel to the fiber orientation, is registered in the case of salts treated with a 4.70 M NaI solution (see Chapter 2, **Fig 2.2.3**).

The range of interest and applicability of our experimental research was then furthermore extended to a wider range of environmental conditions by studying the swelling of wood, pre-treated or not with electrolytic aqueous solutions, in contact with humid atmosphere with different relative humidity. The results can be presented in the form of an experimental Equation of State (EOS) for impregnated and non-impregnated wood. In the form of an EOS (*Podgornik et al. 1998*), the swelling of the material is reported as a function of the osmotic pressure. For this reason, SAXS experiments, which allow the evaluation of the absolute distance between adjacent crystalline cellulose fibers, were performed in conditions of maximum swelling (*i.e.* 100% RH, thanks to a custom-built frame for measuring samples in solution). The inter-crystalline distance increases from 3.5 nm to ca. 4.0 nm due to wetting, and to 4.25 nm when the sample is immersed in sodium iodide solution. The EOS is obtained by correlating these results with ESEM tests, which give the possibility to quantify the elongation of the samples during dehydration and rehydration cycles. It must be pointed out that these results were influenced by different difficulties in setting up the system, mostly related to beam damage effects and to uncontrolled bending of the sample in the ESEM chamber (up to 2.5% error in terms of axial strain). Nonetheless, ion specific effects were confirmed, and the samples pre-treated with the swelling agent NaI proved to have higher sensitivity to increasing osmotic pressure (0.25 nm shrinkage from 100% to 25% RH) than the non-treated ones (0.1 nm shrinkage in the same humidity range). Results are resumed in **Table 5.1** and **Table 5.2**, showing respectevly how the different techniques can be used according to the experimental condition of the samples, and the parameters measured for the case of comrpession wood with each of the consided setups.

	MICROSCOPIC	MACROSCOPIC
SOLUTION STATIC	SAXS	X
SOLUTION DYNAMICS	X	TS
RH STATIC	SAXS	X
RH DYNAMIC	SAXS	ESEM TS

Table 5.1: *Synergic use of SAXS, ESEM and TS according to the experimental conditions (sample immersed in water or exposed to different RH, during adsorption or of pre-treated samples).*

	UNTREATED	NaI
SAXS	4.04 nm	4.25 nm
TS	0 % (reference)	3.0 %
ESEM	-2.5% (100%->25% RH)	-3.4% (100%->25% RH)
TS (RH)	-5.0% (100%->25% RH)	X

Table 5.1: *Results obtained in terms of absolute distance (nm) or axial strain (%) for un-treated or pre-treated samples, with the different techniques.*

The theoretical framework of the work included the implementation of an Equation of State, calculated for water uptake on wood, with an electrostatic term due to the presence of electrolytes in solution. Starting from structural and compositional considerations, a model to predict water adsorption at the molecular level has been developed. According to this model, stiff hexagonal cellulose crystals, parallel to each other, are embedded in a swellable matrix. At the current state of the work, the individual components of the matrix, lignin and hemicelluloses, are not yet distinguished as such, therefore the gel in between the crystalline cellulose is considered as homogeneous. With this assumption, the multi-scale force balance already includes microscopic

terms (cross-linking between cellulose and matrix), as well as mesoscopic (hydration force and matrix configurational entropy) and macroscopic ones (mechanical terms due to anisotropy). The electrostatic term has been added to the balance by considering adjacent crystals as infinite planes, separated by a thin layer of the matrix of a known thickness, in osmotic equilibrium with the salt solution reservoir. The equilibrium between chaotropic ions and adsorbing sites follows the Poisson-Boltzmann distribution, and the free energy of adsorption depends on the binding constant of the binding ion and on its hydrodynamic size. The estimated free energy of adsorption is on the order of 8 kJ/mol for 4.70 M NaI solution, with a binding constant K of 0.035 M^{-1}, as obtained by comparing the model outputs with the observed swelling. This has been derived from the equation linking the binding constant of the ions to the available sorption sites: $K = \Sigma\delta e^{-\Delta G_S/RT}$ (Chapter 4, **Eq 4.1**, where Σ and δ are respectively indicating the surface area of the binding sites and the diameter of the binding ion).

In order to test the validity of this model, experimental gravimetric equations of state were obtained for compression wood samples with a Differential Scanning Calorimetry (DSC) setup. The results showed that our model currently overestimates the factors opposing to swelling, so that experimental data are consistent with its lower limit. It can be accounted for by multiplication of all the attractive terms in the force balance by a factor of 1.5, and division of all the repulsive terms by 1.5.

After these series of experiments, all made with the same type of compression wood, we decided to test the predicting power of the model with electrostatics embedded. Indeed, this model seems compatible with recent results obtained by using NaOH for swelling and dissolving cellulose microcrystals in the absence of any lignin (*Hagman et al. 2017*). As a matter of fact, microcrystalline cellulose is insoluble in common polar solvents, as well as in non-polar and intermediate solvents, and NaOH can dissolve it only within limited pH and temperature ranges. When dissolved, the solution is composed by dissolved and essentially free cellulose chains, except for a small percentage of clusters, bound together in crystalline patches.

In a second step, we preformed some preliminary studies on the contributions of the single components of the swellable matrix on other cellulosic materials, *i.e.* lignin-rich coir fibers extracted from the husk of coconut. However, results on water and solution uptake by coir fibers are limited. Gravimetric experiments showed an increase of 6% in moisture content (MC) at high humidity for the case of coir (see Chapter 4, **Fig 4.3.5** and **4.5.1**, Supporting information). Tensile

experiments on coir fibers immersed in NaI solution confirmed a negligible swelling of the material, suggesting a dominant role of hemicelluloses in water uptake, to be further investigated.

In the following paragraphs, we present preliminary results of an analysis that could give complementary information towards a better understanding of how the water uptake is regulated by hemicelluloses (**5.1**), and concerning the effects of having a mixture of solvents to boost swelling by enhancing salt activity (**5.2**).

5.1 Mistletoe

The knowledge of the dependence of wood materials' swelling (*i.e.* calculated and experimental Equation of State) from their composition can be extended of other cellulosic materials, with different composition, as thr already mentioned case of coir fibres. Fibres from mistletoe are a good example for this case, being composed only of cellulose and hemicelluloses.

Berries from the European mistletoe (*Viscum album L.*), growing on poplar hardwood were harvested and stored in dry ambient conditions. Fibers were pulled out manually from the berries, stretched and dried under ambient conditions. Typical fiber diameters range from ca. 50 to 150 µm (*Gedalovich and Kuijt 1987*). They are composed of ca. 45% cellulose and ca. 53% hemicelluloses (*Azuma et al. 2000, Azuma and Sakamoto 2003*). ICP analysis of mistletoe berries was performed in order to quantify the presence of electrolytes in the material (**Table 5.2**). Results show a high concentration of monovalent (K^+ ca. 0.51 M) and divalent ions (Ca^{2+} 0.27 M, Mn^{2+} 0.16 M). Taking into account the water content, the ionic strengths of the monovalent Potassium and the divalent Calcium and Manganese cations are higher than the one resulting from the same analysis on compression wood (Na^+ 0.09 M and Ca^{2+} 0.02 M for the untreated wood, Na^+ 0.39 M and Ca^{2+} 0.02 M for the wood impregnated with 4.70 M NaI solution).

	MISTLETOE	COMPRESSION WOOD	COMPRESSION WOOD TREATED WITH NaI
K^+	0.51 M		
Ca^{2+}	0.27 M	0.02 M	0.02 M
Mn^{2+}	0.16 M		
Na^+		0.09 M	0.039 M

Table 5.2: *Ionic content of mistletoe, untreated compression wood, and compression wood treated with a 4.70 M NaI solution. The values are obtained from ICP analysis.*

Gravimetric EOS is reported in **Fig 5.1.1**, together with the data of untreated and pre-treated compression wood samples. Water uptake follows an exponential trend, rather than having the typical sigmoid shape of wood material, with a sensitive increase of the moisture content, starting from intermediate humidity, to a value of ca. 41% at 85% RH, leading to amounts of adsorbed water that are significantly higher than the ones obtained in the case of wood.

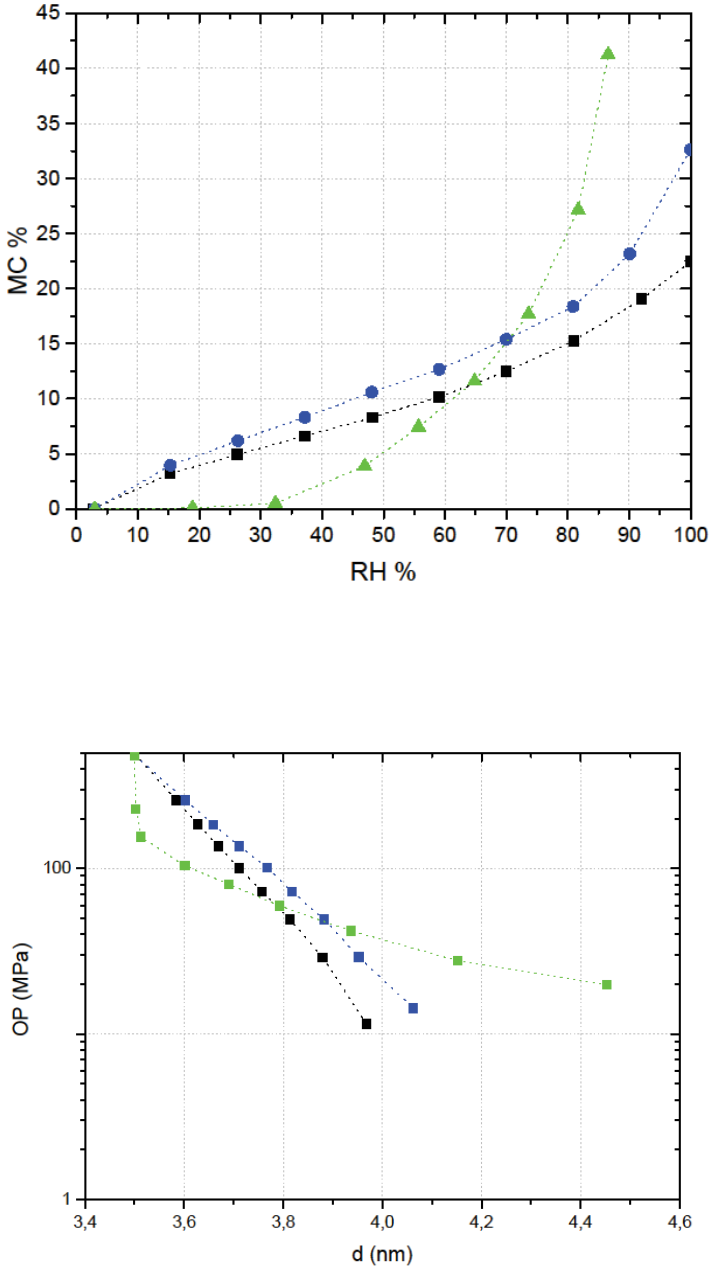

Figure 5.1.1: *Experimental Equations of State, obtained from DSC dehydration experiments, for untreated compression wood (black), wood pre-treated with a 4.70 M NaI solution (blue), and mistletoe fibers (green). a): moisture content MC as a function of relative humidity RH. b): osmotic pressure OP as a function of inter-crystalline distance d.*

These results were compared with the calculations obtained by adapting the model developed for wood to the case of mistletoe. In this case, all the same parameters used as input in the wood model are taken into account, but the only term considered in the force balance is the configurational entropy of the hemicelluloses of the matrix. Moreover, in the present state of this description, the electrostatic term, due to the intrinsic presence of electrolytes in the material, is not yet calculated. Results are shown in **Fig. 5.1.2**.

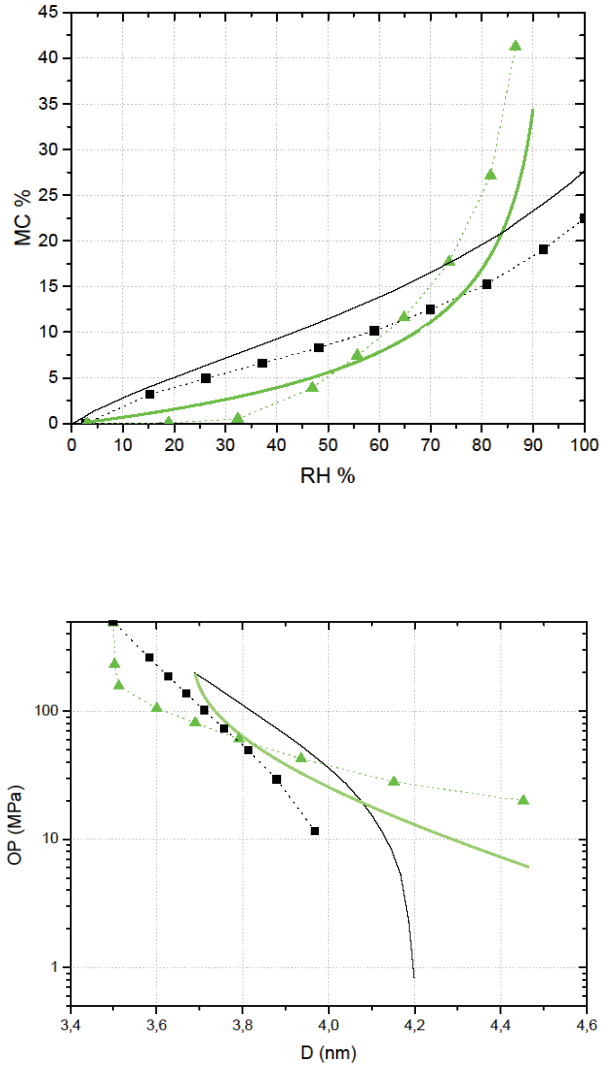

***Figure 5.1.2**: Case of mistletoe: Calculated (continuous lines) and experimental (dotted lines) Equations of State, obtained from DSC dehydration experiments, for untreated compression wood (black) and mistletoe fibers (green). a): moisture content MC as a function of relative humidity RH. b): osmotic pressure OP as a function of inter-crystalline distance d.*

The trends indicate a reasonable agreement between the calculated and the experimental curves. If compared to the calculated curve for the case of wood, these results suggest a relevant influence of the matrix configuration of material's water uptake from humid air. In particular, the absence of the mechanical term, which is opposing to swelling, reflects the absence of the stiff lignin constituent of the matrix, and explain the divergency of MC at high humidity values. As a matter of facts, these results are comparable to the case of wood calculated by selectively excluding the elastic term (*Bertinetti et al. 2016*). From the fit of the initial quasi-linear curve obtained at low humidity for the case of mistletoe, we can derive from the slope of the log-line OP vs MC profile a value for the apparent Debye screening length of 1.78 nm. This corresponds to a ionic concentration of 0.03 M ca, that is by one order of magnitude lower than the results obtained for mistletoe, *i.e.* the calculated Debye screening length at the current state of the model is over-estimating the electrostatic interactions between the mistletoe fibrillar plans, which lack of the structural contribute of the lignin and therefore tends to dissolve at high humidities.

5.2 Choline hydroxide

5.2.1 Choline hydroxide in homogeneous solvents

It has been shown that choline hydroxide, a strong non-toxic base made of renewable sources is abundantly available. The salt is composed of extremely antagonistic ions, which normally induce high swelling, and for this reason, and possible new industrial applications of efficient and rapid swelling pre-treatment of wood, we decided to test the properties of choline.

In the model, a radius of 0.33 nm has been considered from literature for the choline cation (*Levitt and Decker 1988*). The input free energy of adsorption from the reservoir was chosen to be 8 kJ mol^{-1}, which is the one of the case of NaI (see **2.2.1**). This value is associated to a binding constant of the dominant ion K=0.02 M^{-1} (**2.2.1**, **Eq 2.1**). Results are shown in **Fig 5.2.1**, coupled with tests obtained by tuning the binding constant to 0.05 M^{-1} (corresponding to a free energy of adsorption of ca. 6 kJ mol^{-1}) and 0.075 M^{-1} (corresponding to a free energy of adsorption of ca. 5 kJ mol^{-1}).

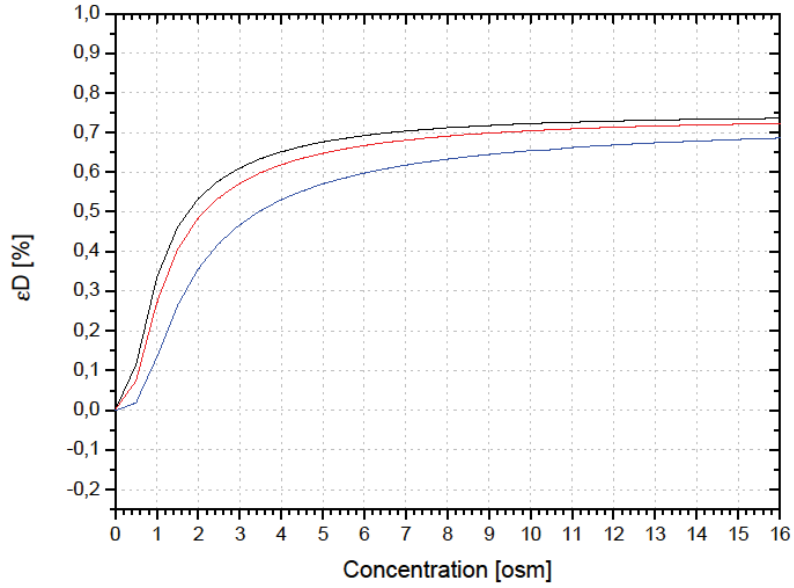

Fig 5.2.1: *The inter-crystalline strain of wood with choline hydroxide, ε_D, is reported as a function of the solution concentration, as obtained from modeling, for three different binding constants: K= 0.02 M^{-1} (black), K=0.05 M^{-1} (red) and K=0.075 M^{-1} (blue).*

Consistently to the experimental results, for which a 1.3% inter-crystalline strain has been measured (choline aqueous solution of 30% in weight, see **Fig 5.2.3**), the predicted swelling is limited, with respect to the case of the most effective salt, NaI, for which a value of ε_D of ca. 5% was observed at 15 osm concentration. This can be attributed to the ion size, which can induce steric problems, so that the ions are not able to penetrate within the matrix structure. In this sense, a way to facilitate choline penetration involves the use of ethanol to facilitate lignin dissolution. Therefore, the use of mixed structured solvent has also been investigated.

5.2.2. Choline hydroxide in structured solvents

Electrostatic swelling of wood can be enhanced when salts are impregnated from an ultra-flexible micro-emulsion. Micro-emulsions derive from a ternary mixture, composed of two immiscible fluids and an added hydrotropic co-solvent (*e.g.* short-chain alcohol, *Zemb et al. 2016*). They are thermodynamically stable, transparent and macroscopically homogeneous. On mesoscopic scale, well-defined microstructures around the phase boundary are present, detectable via scattering

experiments (*Klossek et al. 2012, Diat et al. 2013*). Water-rich and solvent-rich domains coexist, separated by a thin interfacial layer.

The presence of additives induces different remarkable effects in the micro-emulsion structures, as it has been studied for the case of the ternary system water/ethanol/1-octanol in the pre-Ouzo domain. The so-called Ouzo effect is observed in this type of formulation: it consists in the formation of fine and stable emulsions, when water is added to a mixture of ethanol and a hydrophobic component. The pre-Ouzo domain is the monophasic and clear phase, close to the phase separation border, that occurs before a sufficient amount of water is added to ethanol to reach the Ouzo region. The addiction of salts induces two main processes: a salting-out effect that drives ethanol molecules to the interface, implying an increase of the size of the nano-structures (*i.e.* it induces the maximum stability of larger aggregates), and the charging of the interfaces in the case of antagonistic salts, in which the chaotrope is adsorbed onto the interface and charges it, with a resulting electrostatic stabilization of the aggregates (*Marcus et al. 2015*).

In order to quantify how swelling of wood after impregnation with structured solvents near the single phase/two phase boundary are influenced by structuration occurring at nanoscale, mechanical tensile experiments with the strong antagonistic base choline hydroxide have been performed, after that the pre-Ouzo region was identified via x-Ray scattering experiments.

For the preparation of the solutions choline hydroxide in 45 wt % aqueous solution was provided by Taminco, 2-octanol (purity ≥97%) was purchased from Sigma-Aldrich, and anhydrous ethanol (purity ≥99%) was provided by Carlo Erba. For the phase diagram preparation, a series of binary mixtures containing hydrotrope/aqueous phase or hydrotrope/2-octanol was mixed in screwable tubes at fixed weight ratios. During thermostatic control at T=25°C, 2-octanol or choline hydroxide in aqueous phase was added until the clear mixtures became cloudy. A vortexer was used for mixing. The mass of the added compound was determined and the weight percent of each compound was plotted in a ternary phase diagram.

Fig 5.2.2 shows a typical strain change for a wood sample immersed in an aqueous solution at first, and then into an electrolyte solution.

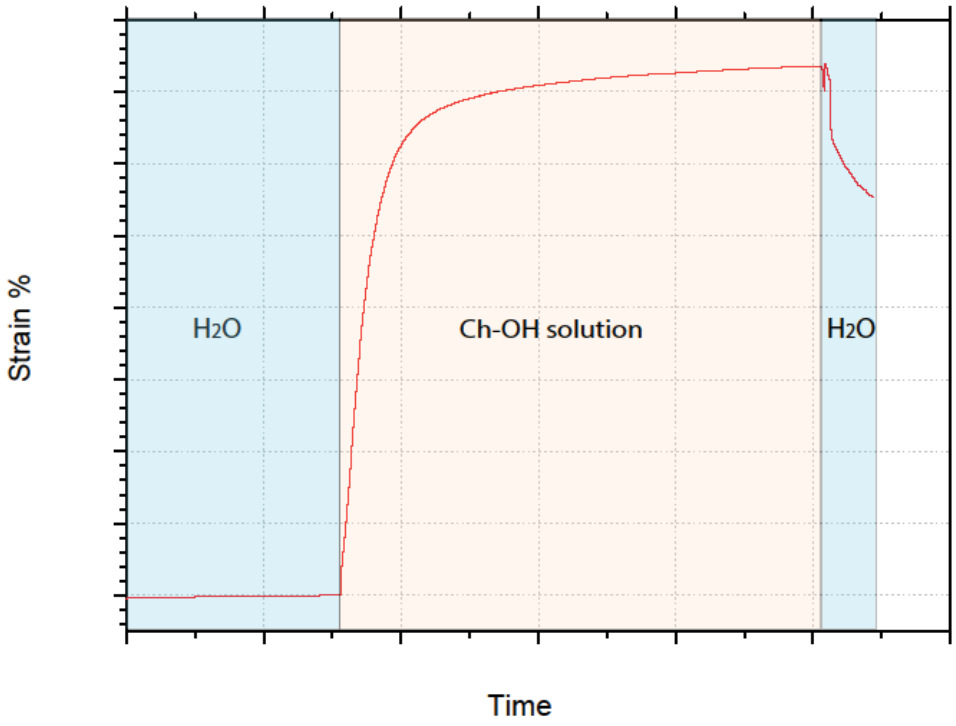

***Fig 5.2.2**: Typical experimental strain change of a wood sample immersed in milliQ water (left blue area), then in a choline hydroxide solution (red area), then washed again with milliQ water (right blue area).*

Results show a positive strain for each investigated sample, as it is typical for monovalent ions. After 3 hours, the solutions were replaced with water and a partial shrinkage is observed after washing. **Fig 5.2.3** shows the results of tensile strain measurements performed on different samples, after one cycle of impregnation.

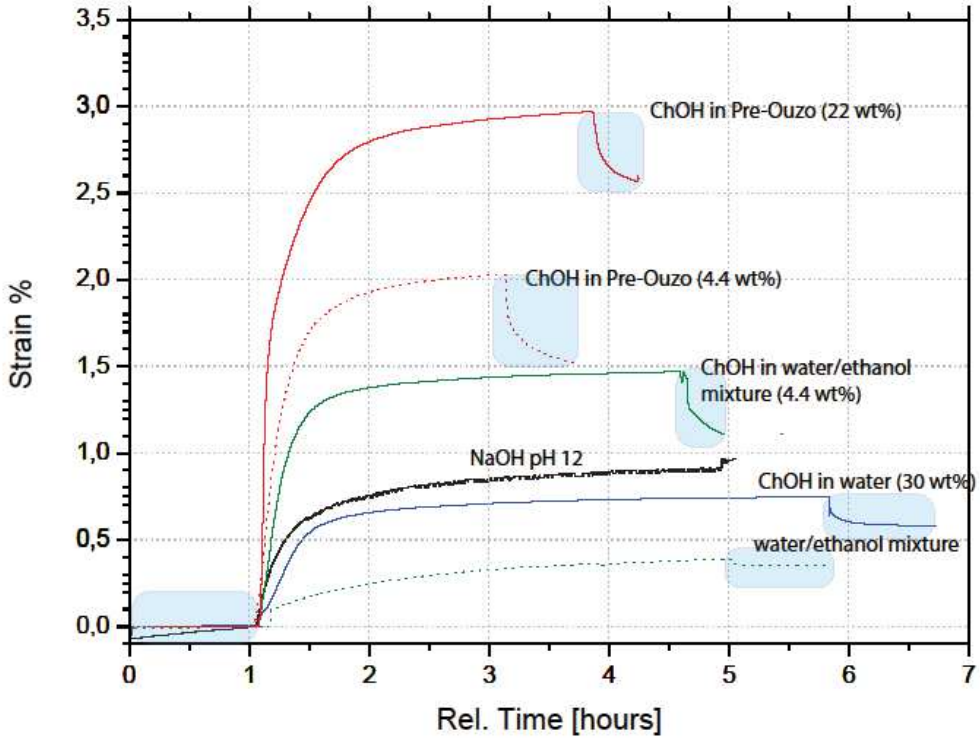

***Fig 5.2.3**: Mean axial strain after immersion of compression wood foils into electrolyte solutions, as a function of time, after one cycle of impregnation. ChOH in Pre-Ouzo 22 wt% (continuous red), ChOH in Pre-Ouzo 4.4 wt% (dotted red), ChOH in water/ethanol mixture 4.4 wt% (continuous green), NaOH pH 12 (black), ChOH in water 30 wt% (continuous blue), water/ethanol mixture (dotted green).*

Results after one cycle of impregnation show that an aqueous solution of choline hydroxide in 30 weight percent (blue) produces a limited swelling of ca. 0.8% in terms of axial strain, considerably less than a binary mixture of ethanol and water containing 4.4 wt% of choline hydroxide (green), that produces 1.5% axial strain, and less than a solution in the pre-Ouzo regime (red continuous) that produces 3.0 % axial strain, despite the fact that these two solutions contain less quantity of choline hydroxide.

Swelling ability in the pre-Ouzo regime is also confirmed, even if less evident, when the salt content is reduced to 4.4 wt% (red dotted); in this case, 2.0% axial strain is registered. Measuring a 10 mM solution of NaOH (black) confirmed that also in this case swelling can not only be caused by a pH effect. The swelling ability of the choline solution increases when passing from a pure

water to a binary ethanol/water mixture and to a ternary water-ethanol/2-octanol mixture (3% axial strain).

The reasons for this trend seem to be that in the binary system water-ethanol clathrate-like structures can be found (*Tomza and Czarnecki 2015*). In the ternary cases dynamic clusters are present, in which water-rich and solvent-rich domains are separated by a hydrotrope that accumulates at the interface (*Schoettl et al. 2014*). This suggests that in both cases the structuration at nano-scale enhances the salt activity and favors transfer from the bulk solution into the lignin-hemicelluloses matrix.

5.3 Conclusions

Up to now, the path delineated in this work aims to provide a first attempt to quantify the effects of salt impregnation on wood, with the control of a single physical quantity, which is the free energy of adsorption of the binding ion.

The novelty of the approach we developed results from the fact that adding to the force balance the entropic and colloidal terms to the chemical and mechanical ones, which have always been taken into account, provides a better link between the theory and the experimental multi-scale observations, including the colloidal meso-scale (*Singh et al. 2015, Alves et al. 2016*).

Further implementations are obviously required to extend the validity of the model and improve its consistency with experimental evidences. These include a more detailed evaluation of the matrix components, as already considered in the case of the analysis of coir fibres and mistletoe (**5.1**), a deeper analysis of more complex salts (**5.2**) and of mixtures of different solvents (*Chang et al. 2012*), that could enhance the swelling properties of the electrolytes.

References

(***Alves et al. 2016***) L. Alves, B. Medronho, F.E. Antunes, B. Lindman *Dissolution state of cellulose in aqueous system- 2. Acidic solvents*, 2016 Carb. Pol. 20,151,707

(***Azuma and Sakamoto 2003***) J. Azuma, N. Kim, L. Heux, R. Vuong, H. Chanzy *The cellulose system in viscin from mistletoe berries*, 2000 Cellulose 7, 3

(***Azuma et al. 2000***) J. Azuma, M. Sakamoto *Cellulosic hydrocolloid system present in seed of plants*, 2003 Trends Glycosci. Glycotechnol. 15, 81, 1

(***Bertinetti et al. 2016***) L. Bertinetti, T. Zemb, P. Fratzl *Chemical, colloidal and mechanical contributions to the state of water in wood cell walls*, 2016 New. J. Phys. 18, 083048

(***Chang et al. 2012***) S. Chang, F. Quignard, F. Di Renzo, B. Clair *Solvent polarity and internal stresses control the swelling behaviour of green wood during dehydration in organic solution*, 2012 Bioresources 7, 2, 2418

(***Diat et al. 2013***) O. Diat, M.L. Klossek, D. Touraud, B. Deme, I. Grillo, W. Kunz, T. Zemb *T.Octanol-rich and water-rich domains in dynamic equilibrium in the pre-Ouzo region of ternary systems containing a hydrotrope*, 2013, J. Appl. Crystallogr. 46, 1665

(***Gedalovich and Kuijt 1987***) E. Gedalovich, J. Kuijt *An ultrastructural study of the viscin tissue of Phthirusa pyrifolia (H.B.K.) Eichler (Loranthaceae)*, 1987 Protoplasma 137, 145

(***Hagman et al. 2017***) J. Hagman, L. Gentile, C.M. Jessen, M. Behrens, K.E. Bergqvist, U. Olsson *On the dissolution state of cellulose in cold alkali solutions*, 2017 Cellulose 24,2003

(***Klossek et al. 2012***) M.L. Klossek, D. Touraud, T. Zemb, W. Kunz *Structure and solubility in surfactant-free microemulsions*, 2012 Chem. Phys. Chem. 13, 4116

(***Kunz et al. 2004***) W. Kunz, P. Lo Nostro, B.W. Ninham *The present state of affairs with Hofmeister effects*, 2004 COCIS 9, 1

(***Levitt and Decker 1988***) D.G. Levitt, E.R. Decker *Electrostatic radius of the gramicidin channel determined from voltage dependence of H^+ ion conductance*, 1988 Biophys. 53,33

(*Marcus et al. 2015*) J. Marcus, D. Touraud, S. Prévost, O. Diat, T. Zemb, W. Kunz *Influence of additives on the structure of surfactant-free microemulsions*, 2015 Phys. Chem. Chem. Phys. 17,32528

(*Podgornik et al. 1998*) R. Podgornik, H.H. Strey, V.A. Parsegian *Colloidal DNA*, 1998 COCIS 3, 534

(*Schoettl et al. 2014*) S. Schoettl, J. Marcus, O. Diat, D. Touraud, W. Kunz, T. Zemb, D. Horinek *Emergence of surfactant-free micelles from ternary solutions*, 2014 Chem. Sci. 5, 2949

(*Singh et al. 2015*) P. Singh, H. Duarte, L. Alves, F. Antunes, N. Le Moigne, J. Dormanns, B. Duchemin, M.P. Staiger, B. Medronho *From cellulose dissolution and regeneration to added value applications - synergism between moleculare understanding and material development*, 2015 Cellulose - Fundamental aspects and current trends. InTech

(*Tomza and Czarnecki 2015*) P. Tomza, M.A. Czarnecki *Microheterogeneity in binary mixtures of propyl alcohols with water: NIR spectroscopic, two-dimensional correlation and multivariate curve resolution study*, 2015 J. Mol. Liq. 209, 115

(*Zemb and 2016*) T. Zemb, M. Klossek, T. Lopian, J. Marcus, S. Schoettl, D. Horinek, S.F. Prevost, D. Touraud, O.Diat, S. Marcelja et al. *How to explain microemulsions formed by solvent mixtures without conventional surfactants*, 2016 Proc. Natl. Acad. Sci. USA 113, 16, 4260

Glossary

Cellulose

Criystalline cellulose is the stiff component of the plant cell wall. Cellulose is a linear-polymer glucan with a uniform chain structure that consists of anhydroglucopyranose units (AGU), bound by β-(1→4) glycosidic linkages. Two adjacent units are linke with elimination of one water molecul between their hydroxilic groups at carbon 1 and carbon 4. The repeating unit of the cellulose chain, called cellobios unit, has a length of 1.03 nm. The two hydroxyl groups at the ends have different behavior: the C1-OH is an aldehyde hydrate group deriving from the ring formation by an intramoleculare hemiacetal linkage, and it has reducing properties, while the C4-OH is an alcoholic group with non-reducing properties. The cellulose chain is elongated and the glucose units are arranged in one plane. Its degree of polymerization (*i.e.* the number of monomeric units) is ca. 8000 in the case of spruce. The stabilization of these long chains occurs with the formation of supramolecular structures, originated in the presence of hydroxyls groups by hydrogen intra- and intermolecular hydrogen bonds. These bonds give the chains a certain stiffness and order the chains into a fibrillar structure.

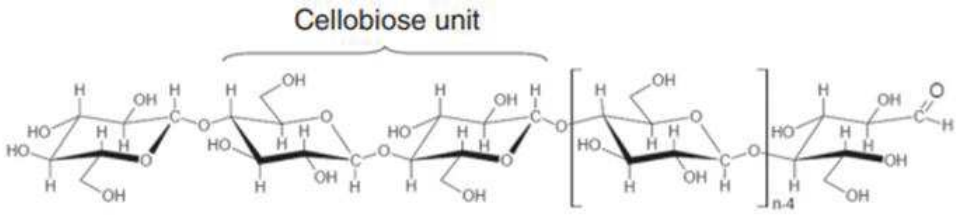

Structure of a cellulose chain (B. Medronho, B. Lindman *Competing forces during cellulose dissolution: from solvents to mechanisms*, 2014 COCIS 19, 1, 32)

Chaotrope

A chaotrope, or chaotropic ion, is a weakly hydrated (*i.e.* hydrophobic) large ion, or ionic group, of low charge density, that disrupts the hydrogen bonding network between water molecules.

Compression wood

Compression wood is a type of reaction tissue: the shape of wood cells is influenced by mechanical forces: trees react to strain forces acting on stems (*e.g.* wind) and branches (*e.g.* their own weight) by forming reaction wood in the zones of compression or tension. Compression wood differes from normal wood in anatomical, chemical and physical properties. The angle of the fibrils (see **MFA**) in the secondary layer of compression tracheids is ca. 45° with respect to the fibre axis.

Equation of state (EOS)

In physics and thermodynamics, an equation of state is a thermodynamic equation relating state variables which describe the state of matter under a given set of physical conditions, such as pressure, volume, temperature, or internal energy. It is a constitutive equation which provides a mathemaical relationship between state functions associated with the matter. For colloidal solutions containing any type of surfactant inducing the formation of locally flat interfaces, two equations of state describe the system: the "perpendicular" EOS is the one associated to swelling (*i.e.* OP vs spacing), and the "parallel" EOS relating the in-plane area per molecule to the free energy.

Hemicelluloses

Hemicelluloses are cellulose-binding polysaccharides, which together with cellulose form a network that is strong yet resilient. Matrix polysaccharides are integrated to the wall network by physical interactions, enzymatic ligations and crosslinking reactions. The hemicellulose diffe from cellulose by a composition of various sugar units, shorte molecular chains, and branching of the chain molecules. The main chain of hemicelluloses of primary cell walls consist either of only one unit (homopolymer, *e.g.* xylans) or two or more units (heteropolymer, *e.g.* glucomannans).

Hydration force

Hydration force is a strong short-range repulsive force associated with ordering of water at an interfaces, that acts between polar surfaces separated by a thin layer of water. it decays quasi-

exponentially with the surfaces' spacing, and the decay constants are comparable to the size of water molecules. Primary hydration force is linked to enthalpic adsorption energy (*i.e.* binding) of successive water layers to any interface and to entropy increase when moving away from the interface, while secondary hydration is associated to weaker interactions with larger decay lengths, being linked to the competition between water adsorbed around solutes and water adsorbed at the interface.

Kosmotrope

A kosmotrope, or kosmotropic ion, is a strongly hydrated (*i.e.* hydrophilic) small ion, or ionic group, of high charge density, that contributes to the stability and structure of water-water interactions.

Lignin

Together with cellulose, lignin is the most abundant polymeric organic substance in plants. Chemically, lignins are relatively hydrophobic and aromatic cross-linked phenolic polymers. They are not formed by a regular mechanism, but by a random coupling of lignols to a non-linear polymer: from a morphological point of view, the growing lignin molecules are forced to fill up the spaces between the preformed polysaccharidic fibrillar elements of the cell wall. The incorporation of the hydrophobic lignin causes a de-swelling of the cell walls.

Micro-fibrillar angle (MFA)

Cellulose fibrils wind around the tube-like wood cells at an angle called the micro-fibrillar angle (MFA). Tipically, the cell wall consist of several layers (S1, S2, ..) where the S2 is the thickest. While the cellulose microfibrils in the S1 layer run at almost 90° to the cell axis, in the S2 layer they are more parallel to it, and microfibrillar angles rang from 0° to 45°. The MFA determines to a large extent the elasticity and stifness of wood (the steeper the winding angle, the stiffer the wood).

Moisture content (MC)

Wood exchanges moisture with the surrounding air and the amount of moisture gain or loss depends on the relative humidity (see **RH**) and temperature of the air, and the existing moisture in the wood. Moisture content (MC) is described by the ratio of mass of moisture to mass of dry wood substance: $MC = {}^{m_{wet} - m_{dry}}/_{m_{dry}}$.

Osmolarity and Osmotic coefficient

Osmolarity, or osmotic concentration, is a measure of a solute concentration, expressed as the number of osmoles of solute per litre (Osm/L), and therefore accountig for the osmotically active concentration of the solute. The osmolarity of a solution is calculated from the following expression: $Osmolarity = \sum_i \varphi_i n_i C_i$. C is the molar concentration of the solute, n is the number of ions into which a molecule dissociates. φ is the osmotic coefficient, which ranges from 0 to 1 and accounts for the degree of non-ideality of the solution (referenced to Raoult's law).

Osmotic pressure (OP)

Namely, osmotic pressure (OP) is defined as the minimum pressure which needs to be applied to a solution to prevent the inward flow of its pure solvent across a semipermeable membrane, *i.e.* it is a measure of the tendency of a solution to take in pure solvent. From a thermodynamic standpoint, osmotic pressure is the derivative of the free energy against molar volume, and it indicates the chemical activity of the solvent. Osmotic pressure can be calculated from Van't Hoff equation: $OP = i\varphi CRT$ where i is the dimensionless van't Hoff index that addresses solute that non-ideally dissociates (by definition, it is the ratio between the actual concentration of particles produced when the substance is dissolved and the concentration of a substance as calculated from its mass) and φ is the osmotic coefficient.

Relative humidity (RH)

Relative humidity (RH) is defined as the ratio of the partial pressure of water vapor to the equilibrium vapor pressure of water, at a given temperature, *i.e.* is it a measure of the activity of water. It is related to the osmotic pressure by derivation from Raoult-Lewis law: $OP = -\frac{RT \ln\left(\frac{RH}{100}\right)}{V_{mol}}$, where V_{mol} is the molar volume of water.

List of symbols

$\boldsymbol{\alpha}$ [%] Occupation rate of ions to the available adsorbing sites. Calculate to be 10% in the case of NaI.

(Eq 2.11, *Eq 2.*12, *Par 2.5.3*, *Par 4.5.3*)

$\boldsymbol{d}$ [nm] Center to center distance between adjacent cellulose crystal.

(Par 3.3.2)

$\boldsymbol{\delta}$ [nm] Hydrodynamic radium of the adsorbing ion. Set to 0.5 nm independently of ion thickess. Tuned to 0.200 nm, 0.133 nm, 0.072 nm for the cases of I^-, OH^-, and Mg^{2+} respectively.

(Eq 1.2, *Par 2.2.1*, *Par 4.3.1*)

$\boldsymbol{\delta^*}$ [nm] Extra swelling due to salt impregnation, expressed as the difference between the intercrystalline distance after impregnation and after wetting.

(Par 2.2.1, *Par 2.5.5*)

$\boldsymbol{D_{max}}$ [nm] Maximum swelling, measured in fully hydrated conditions, and expressed in terms of absolute distance.

(Par 4.3.1)

ΔG_s [kJ mol^{-1}] Free energy of adsorption of ions to the binding sites. For the case of NaI, calculated to be 8KJ mol^{-1} ≈ 3.2 kT.

(Eq 1.2, *Par 2.2.1*, *Par 4.3.1*)

ε_D [%] Inter-crystalline strain calculated from ε_x considering a MFA of 45° (*e.g.* ε_x=3.0% corresponds to ε_D=5.3%).

(Par 2.2.1, *Par 3.3.2*)

ε_x [%] Axial strain calculated in the parallel direction with respect to fibres orientation.

(Par 2.2.1, *Par 3.3*, *Par 4.3.4*, *Par 5.2*)

ε_y [%] Axial strain calculated in the perpendicular direction with respect to fibres orientation.

(Par 3.3)

K [M^{-1}] Specific binding constant for the equilibrium between adsorbing ions and sorption sites. Calculated to be 0.035 M^{-1} for the case of NaI.

(Eq 1.2, *Par 2.2.1*, *Par 4.3.1*)

K_1' [M^{-1}] Binding constant for the primary sorbed layer according to the Dent theory. Fitting to the model isotherm gives a value of 2.4 M^{-1}.

(Par 4.3.2, *Par 4.5.2*)

$\boldsymbol{K_2'}$ [M^{-1}] Binding constant for the secondary sorbed layer according to the Dent theory.

(Par 4.3.2, *Par 4.5.2*)

$\boldsymbol{L_B}$ [nm] Bjerrum length: is the separation at which the electrostatic interaction between two elemenatry charges is comparable in magnitude to the termal energy scale kT. For water at rioom temperature, $L_B \approx 0.7$ nm.

(Eq 2.4, *Par 4.5.3*)

$\boldsymbol{M_0'}$ [%] Moisture content in fully hydrated conditions according to the Dent theory. Fitting to the model isotherm gives a value of 12.8%.

(Par 4.3.2, *Par 4.5.2*)

$\boldsymbol{\Sigma}$ [nm^2] Surface area of a sorption site. Set to 1 nm^2 for the calculations

(Eq 1.2, *Par 2.2.1*, *Par 4.3.1*)

$\boldsymbol{\Sigma_s}$ [C m^{-1}] Surface charge density.

(Eq 2.7, *Eq 2.*12, *Par 4.5.3*)

$\boldsymbol{\varphi_s}$ [J C^{-1}] Electrostatic potential at the sorption surface plane.

(Eq 2.6, *Par 4.5.3*)